SEARS FOUNDATION FOR MARINE RESEARCH
BINGHAM OCEANOGRAPHIC LABORATORY, YALE UNIVERSITY

JOURNAL OF
MARINE RESEARCH

VOLUME XII 1953 NUMBER 1

POLAROGRAPHIC DETERMINATION OF NITRATE IN SEA WATER[1]

By

DAVID TUNG-WHEI CHOW AND REX J. ROBINSON

Chemical and Oceanographic Laboratories
University of Washington, Seattle 5, Wash.

ABSTRACT

A new and accurate method for the determination of nitrate in sea water, based on the polarographic reduction of nitrate in the presence of uranyl ions, is presented.

Sulfate ions depress the reduction current by a definite proportion, depending on the chlorinity of the water sample; for chlorinities in the range of 14 to 19 °/₀₀, this effect is rather constant. Fluoride interferes strongly with the reduction of nitrate, but aluminum or zirconyl salts may satisfactorily eliminate this effect. Other interfering ions and preservatives are also discussed. A procedure for the determination of nitrate in sea water has been proposed and its validity tested.

INTRODUCTION

Nitrate, though present in very small amounts, plays an important role in the sea. It is considered one of the nutrient salts upon which biological activity in the sea depends, and ecological studies involving nutrient salts necessitate extensive surveys and numerous analyses. A method for obtaining such data needs to be as simple, rapid, sensitive and accurate as possible, but to date such a method for nitrate has been lacking and ecological studies involving nitrate analyses of sea water have been discouraged. Reported data on nitrate have been obtained mainly by the use of Harvey's (1929) colorimetric

[1] This work was supported in part by the Office of Naval Research under contract No. N8onr–520/III with the University of Washington.

"reduced strychnine" method, which has been investigated and revised by Zwicker and Robinson (1944); but at best this method is not convenient and the reliability of the results may be questioned, though they appear to be reasonably accurate.

In the present investigation a new method of determining nitrate in sea water by polarographic reduction of nitrate with uranyl ions has been developed. The catalytic effect of uranyl was first reported by Kolthoff, Harris and Matsuyama (1944). Also, polarographic determination of nitrate with molybdate as the catalyst has been reported by Johnson and Robinson (1952), but this method lacked the sensitivity demanded for the determination of small amounts of nitrate in sea water.

APPARATUS

The polarographic data were obtained with a Heyrovsky Micropolarograph, Model X, calibrated by the method of Kolthoff and Lingane (1946). An H-shaped electrolytic cell (Lingane and Laitinen, 1939), with a saturated calomel reference electrode as one arm connected by a potassium chloride bridge, was used. The capillary characteristic, $m^{2/3}t^{1/6}$, was 1.30 $mg^{2/3}sec^{-1/2}$. The electrolytic cell was immersed in a thermostat adjusted to 25.0 ± 0.1° C by a "merc-to-merc" thermo-regulator and a "merc-to-merc" relay control box (Precision Scientific Co.).

REAGENTS

All chemicals used in this investigation were of reagent grade, and the various solutions were prepared with distilled water.

1. Uranyl Acetate Solution. 0.8484 g uranyl acetate crystals, $UO_2(CH_3COO)_2 \cdot 2H_2O$, was dissolved in water to one liter. The concentration of the uranyl ion in this solution was 2.00×10^{-3} M.

2. Aluminum Chloride-Hydrochloric Acid Reagent. 32.2 g aluminum chloride crystals, $AlCl_3 \cdot 6H_2O$, and 83.3 ml of 12 N hydrochloric acid were added to water and diluted to one liter. This reagent was 1 M in hydrochloric acid and 0.13 M in aluminum chloride.

3. Fluoride-free Synthetic Sea Water. This was prepared according to Robinson and Spoor (1936) by dissolving the following in a liter of water: 23.38 g NaCl, 3.9066 g anhydrous Na_2SO_4, 0.7455 g KCl, 10.676 g $MgCl_2 \cdot 6H_2O$, and 1.47 g $CaCl_2 \cdot 2H_2O$. This synthetic sea water had a chlorinity of 19 °/₀₀, and the concentrations of the various salts were as follows: 0.40 M in NaCl, 0.0273 M in Na_2SO_4, 0.0525 M in $MgCl_2 \cdot 6H_2O$, 0.01 M in KCl, and 0.01 M in $CaCl_2 \cdot 2H_2O$. Synthetic sea water samples with lesser chlorinities were made by diluting this solution with appropriate amounts of distilled water.

4. Synthetic Sea Water Containing Fluoride. This was made by dissolving in the above solution 0.0029 g NaF per liter. The resulting concentration of fluoride ion was 7×10^{-5} M.

5. Standard Nitrate Solution. 0.00200 M $NaNO_3$ solution was used as the standard for nitrate.

EXPERIMENTAL

Polarograms were obtained after the dissolved oxygen in the various solutions had been driven off with nitrogen gas. The current due to nitrate was obtained by measuring the current at -1.2 v. vs. S. C. E. and subtracting the current of an uranium blank. All potentials reported in this work have been referred to the saturated calomel electrode, S. C. E.

I. Polarographic Reduction of Nitrate in Fluoride-free Synthetic Sea Water in the Presence of Uranyl Ions

Kolthoff, et al. (1944), in their investigations of the polarography of uranium, found two waves in acid solution which indicated reductions of uranium VI to uranium V and uranium V to uranium III. They also found that, in the presence of uranyl ions, nitrate was reduced to nitrogen gas at potentials where the second uranium wave occurred. They offered the explanation that the uranium III formed at the cathode acted as an "activator" for the reduction of nitrate. A typical polarogram was shown in their paper. They also reported a linear relationship between the reduction current and the nitrate concentration when the uranyl concentration was above a certain limiting value which varied according to the nitrate concentration.

On the basis of the work by Kolthoff, et al., a uranyl concentration of 1×10^{-4} M would be needed for application of this method, since the nitrate content in sea water ranges from zero to about 70 μg-at/L. The reduction current should then be directly proportional to the nitrate concentration for the range involved.

Preliminary investigations were made with solutions containing various amounts of nitrate in 0.2 M sodium chloride and in fluoride-free synthetic sea water. To a 100 ml portion of each solution were added 5 ml of uranyl solution and 1.5 ml of 1 M hydrochloric acid; the polarogram was then taken. The results, shown in Tables I and II and in Fig. 1, indicate that the current is proportional to the nitrate concentration in either medium. The data obtained with nitrate in 0.2 M sodium chloride solutions agree very well with those reported by Kolthoff, et al. It should be noted that the current in synthetic sea water is somewhat less than that in the sodium chloride medium

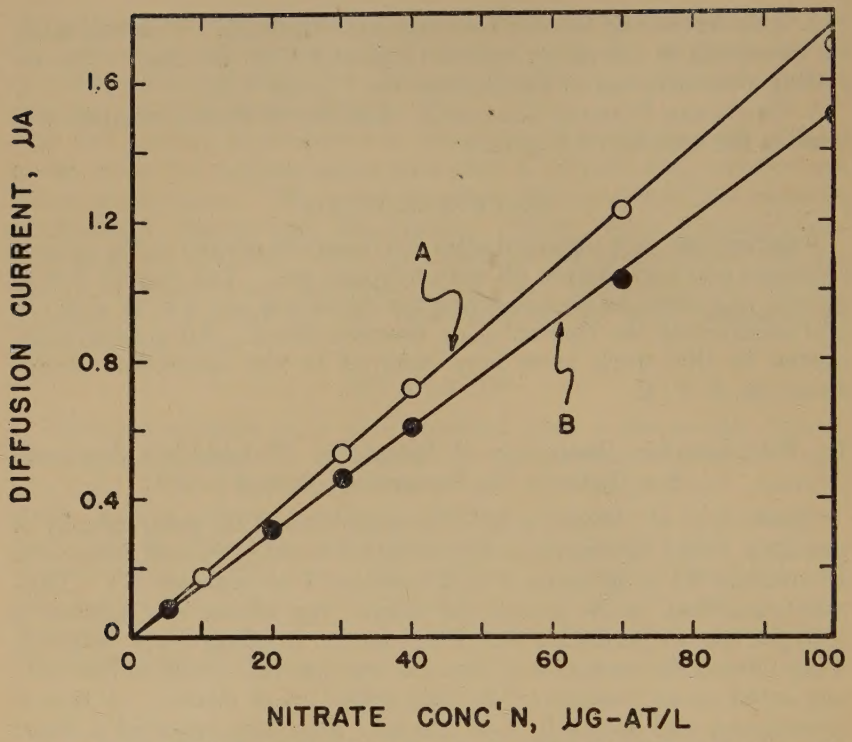

FIGURE 1. Calibration curve for nitrate in presence of uranyl in sodium chloride and in synthetic sea water solutions. Curve A: 0.015 M hydrochloric acid, 0.2 M sodium chloride, 1×10^{-4} M uranyl acetate. Curve B: 0.015 M hydrochloric acid, synthetic sea water, Cl °/₀₀ =19, 1×10^{-4} M uranyl acetate. Current measured at −1.2 v. vs. S.C.E.

due to the effect of sulfate. It was also found that the half-wave potential of the second uranium wave was shifted from −0.95 v. to −1.04 v. vs. S. C. E. in the presence of sulfate.

The effect of sulfate on the reduction current of nitrate was investigated further in synthetic sea water media of varying chlorinities. Since there is a definite ratio between chlorinity and sulfate concentration in sea water, the amount of sulfate was varied accordingly. It was found that chlorinity variations in the range of 14 to 19 °/₀₀ had very little effect on the current. When the chlorinity became less than 14 °/₀₀, the current increased as the chlorinity decreased. Since the chlorinity in natural sea water is normally between 14 and 19 °/₀₀, it seemed feasible to obtain calibration data by using a synthetic sea water with chlorinity of 19 °/₀₀. The nitrate concentration in natural sea water may be obtained by using the calibration curve (lower curve

in Fig. 1) or by using the following equation derived from the Ilkovic equation (Ilkovic, 1934):

$$i = (1.17 \times 10^{-2})\ (m^{2/3}t^{1/6})\ (C),$$

where i is the observed diffusion current due to nitrate in microamperes, $m^{2/3}t^{1/6}$ the capillary characteristic, and C the concentration of nitrate in the sample in microgram-atoms per liter. The constant of 1.17×10^{-2} has been obtained by taking the ratio of current in microamperes to the product of the capillary characteristics and the nitrate concentration in microgram-atoms per liter as given in the last column in Table II.

TABLE I. Diffusion Current of Nitrate in Sodium Chloride Solutions. 0.015 M Hydrochloric Acid, 0.2 M Sodium Chloride, 1×10^{-4} M Uranyl Acetate; $M^{2/3}\ T^{1/6} = 1.30\ Mg^{2/3}\ Sec^{-1/2}$; Residual Current at −1.2 V. vs. S. C. E. = 0.734 Microamperes

Nitrate Conc'n. μg-*at/L*	*Diffusion Current for Nitrate,* μa	$K' = i/C$ $\mu a/\mu g$-*at/L* ($\times 10^2$)	$K = i/Cm^{2/3}t^{1/6}$ ($\times 10^3$)
2.0	0.037	1.85	1.42
6.0	0.110	1.67	1.28
10.0	0.175	1.75	1.35
20.0	0.356	1.78	1.37
30.0	0.527	1.76	1.35
40.0	0.718	1.79	1.38
70.0	1.242	1.77	1.36
100.0	1.699	1.70	1.31
	Average value	1.76	1.35

The effect of hydrogen-ion concentration on the current was also studied. In neutral solutions neither the second uranium wave nor the nitrate wave occurred. When the hydrogen-ion concentration was too high, the reduction of hydrogen took place at about − 1.2 v. vs. S. C. E., thus making the method impractical. The hydrogen-ion concentration range of 0.005 to 0.02 M gave the best results, the current remaining constant in this range for a given amount of nitrate. The desired hydrogen-ion concentration was obtained with 1.5 ml of 1 M hydrochloric acid per 100 ml of sample.

II. Polarographic Reduction of Nitrate in Synthetic Sea Water Containing Fluoride

When this method was first applied to natural sea water, only uranyl and hydrochloric acid reagents were added, but the nitrate wave was distorted so that the current could not be measured due to the lack of

the flat diffusion current region. Also, the half-wave potential was shifted toward the more negative side, being approximately − 1.1 v. vs. S. C. E., while the first uranium wave was unaffected. It was found that the distortion of the nitrate wave was due to fluoride ions in the sea water. Since the first uranium wave was not affected, it seemed likely that the uranium III ions, formed at the dropping mercury electrode, must have been reacting with fluoride ions. Thus the catalytic behavior of uranium upon the reduction of nitrate was greatly reduced, causing the wave to become ill-defined and the wave height to be much lowered.

TABLE II. Diffusion Current of Nitrate in Synthetic Sea Water Solutions. 0.015 M Hydrochloric Acid, Synthetic Sea Water, Cl °/₀₀ = 19, 1×10^{-4} M Uranyl Acetate; $M^{2/3}\ T^{1/6} = 1.30$ $Mg^{2/3}Sec^{-1/2}$; Residual Current at −1.2 V. vs. S. C. E. = 0.734 Microamperes

Nitrate Conc'n. $\mu g\text{-}at/L$	*Diffusion Current for Nitrate,* μa	$K' = i/C$ $\mu a/\mu g\text{-}at/L$ ($\times 10^2$)	$K = i/Cm^{2/3}t^{1/6}$ ($\times 10^2$)
1.0	0.022	(2.2)	(1.69)
2.0	0.029	1.45	1.12
4.0	0.060	1.50	1.15
5.0	0.081	1.62	1.25
6.0	0.093	1.55	1.19
10.0	0.154	1.54	1.19
20.0	0.304	1.52	1.17
30.0	0.458	1.53	1.18
40.0	0.602	1.51	1.16
70.0	1.026	1.47	1.13
100.0	1.495	1.50	1.15
	Average value	1.52	1.17

If this method were to be applied successfully to sea water analyses, then it would be necessary to remove interference by fluoride ion. Conversion of the fluoride to a stable complex ion appeared to be the simplest means, although it seemed conceivable that precipitation methods might be used successfully. The efficiencies of a number of cations that complex with fluoride were studied in a fluoride-containing synthetic sea water medium. Ferric ions, tried first, were unsatisfactory. When the concentration of ferric ion was small, the effect of fluoride was not eliminated completely, and when the concentration was greater than that needed for complexing the fluoride ions, the ferric ions themselves were reduced, thus masking the nitrate wave. Aluminum and zirconium salts, tried next, gave satisfactory results.

When the fluoride was complexed with either of them, the nitrate wave was restored and the wave height became the same as that obtained in the absence of fluoride. The minimum amounts of aluminum chloride and zirconyl chloride necessary to prevent the interference of fluoride in sea water, Cl = 19 °/₀₀, were 8×10^{-4} M and 4×10^{-5} M respectively. An excess of these reagents did not affect the reduction current. Aluminum chloride was selected because of its lower price and availability. In practice an aluminum concentration of 2×10^{-3} M has assured the complete complex formation of all fluoride ions.

III. Polarographic Determination of Nitrate in Actual Sea Water

A. *Discussion of Interferences.* Nitrite, reduced in the same manner as nitrate, also interferes, but its current is only about three-fifths of that due to nitrate (Keilin and Otvos, 1946). In sea water the nitrite concentration, readily determined by the usual colorimetric method (Robinson and Thompson, 1948), is usually less than 0.4 μg-at/L, which is too small to exert an appreciable effect. If and when the nitrite content in sea water is greater than 10 μg-at/L, which is very rare, a correction should be made.

Phosphate, if present in sufficient amount, interferes by precipitating the uranyl ions. In ordinary sea water the amount of phosphate was so small that no interference was observed.

Theoretically, ferric ions should interfere with this determination, since they give a reduction current starting at zero applied potential. But in sea water no current due to ferric ions was observed, apparently because they were in some complexed form.

As discussed previously, sulfate decreases the nitrate current. In the sulfate concentration range for chlorinity values of 14 to 19 °/₀₀, the current was decreased by a definite proportion for the different nitrate concentrations observed, being approximately 86% of the current obtained in the absence of sulfate, as seen in Tables I and II. Within this chlorinity range, the given calibration curve (lower curve in Fig. 1) or the equation on page 5 may be used for the determination of nitrate. But when the chlorinity is less than 14 °/₀₀, different calibration curves should be used. For sea water with a low chlorinity, it is suggested that calibration curves at different chlorinities be used or that sulfate be precipitated out with strontium salts. In the latter case, the interference of sulfate is completely eliminated; the concentration of nitrate may be obtained from the upper curve in Fig. 1 or by using the Ilkovic equation, simplified to the following form:

$$i = (1.35 \times 10^{-2})\ (m^{2/3}t^{1/6})\ (C)\ ,$$

where i is the observed diffusion current due to nitrate in microamperes, $m^{2/3}t^{1/6}$ the capillary characteristics, and C the concentration of nitrate in the sample in microgram-atoms per liter.

In addition to the above interferences, water samples stored in polyethylene plastic bottles gave a rapidly increasing current at the applied potential of about − 1.1 v. vs. S. C. E., thus masking the nitrate wave completely. Possibly this was due to the fact that reducible substances in the plastic material had dissolved in sea water and affected the current. Hence, plastic bottles could not be used for the storage of water samples, but glass bottles were suitable.

B. *Preservation of Water Samples.* Since plankton utilize nitrate as a nutrient and since bacteria may break down organic nitrogen compounds to form nitrate ions, the analyses should be made immediately in order to ascertain the true amount of nitrate in sea water samples at the time they are collected. But since this method is impractical for use on shipboard, preservatives must be added to the samples to prevent the above actions from taking place until the analyses can be made.

Mercuric chloride solution, though frequently used, is not desirable for polarographic analysis of sea water because mercuric salts give a reduction current starting at zero applied potential. Although the currents due to nitrate and mercuric ions are additive and could be corrected by the addition of definite amounts of mercuric salts, they greatly reduce the sensitivity of this method.

Chloroform, frequently used as a preservative, is satisfactory for use in this determination. Dissolved chloroform is driven off by nitrogen gas when freeing the water samples from dissolved oxygen, and any chloroform remaining in the solution does not interfere because it is not reduced at the dropping mercury electrode. Samples to which chloroform had been added several days before gave the same nitrate results as those taken just before its addition. The addition of 1 to 2 ml of chloroform to each 300 ml of sample was satisfactory.

C. *Proposed Procedure for the Determination of Nitrate in Sea Water.* In view of the previous discussions, the following procedure for the polarographic determination of nitrate in sea water is proposed:

As soon as the water sample is taken, add 2 ml of chloroform to each 300 ml of sample and store in glass bottles in a dark and cool place. Analysis should be performed at the earliest possible time.

Measure 100 ml of water sample into the electrolytic cell with a pipet and add 5 ml of uranyl acetate solution and 1.5 ml of the aluminum chloride-hydrochloric acid reagent. Remove the dissolved

oxygen by washing with nitrogen gas and take the polarograms immediately. Measure the current at − 1.2 v. vs. S. C. E. and obtain the nitrate concentration from a previously determined calibration curve or from the equation $i = (1.17 \times 10^{-2})\ (m^{2/3}t^{1/6})\ (C)$ after making the correction for the residual current of uranium.

D. *Validity of the Method.* The validity of this method was tested by determining the nitrate contents of sea water samples before and after the addition of known amounts of nitrate. The results are shown in Table III.

TABLE III. TEST OF THE VALIDITY OF THE METHOD

Chlorinity	*Nitrate Concentration, μg-at/L*			
°/₀₀	*Originally Present*	*Added*	*Found*	*Difference*
16.40	0.0	10.0	9.8	−0.2
16.20	5.2	10.0	15.1	−0.1
15.47	12.5	20.0	32.0	−0.5
16.47	14.5	20.0	34.5	0.0
15.95	14.7	40.0	54.7	0.0
14.34	17.0	20.0	37.0	0.0
16.40	18.5	10.0	28.7	+0.2
16.79	22.3	20.0	42.4	+0.1
16.60	23.5	10.0	33.2	−0.3
16.48	23.5	20.0	43.5	0.0
16.71	24.4	20.0	44.7	+0.3
16.62	25.5	20.0	45.5	0.0
16.14	26.5	40.0	66.5	0.0
16.78	27.2	20.0	48.0	+0.8
16.69	28.0	20.0	48.0	0.0
16.44	29.2	40.0	69.0	−0.2
16.89	29.4	10.0	39.4	0.0
16.75	29.4	40.0	70.0	+0.6
16.91	29.8	10.0	39.6	−0.2
16.74	31.0	20.0	50.3	−0.7
19.05	46.1	10.0	56.0	−0.1
19.08	47.2	20.0	67.0	−0.2
			Average deviation	±0.20

The concentrations of nitrate obtained after the addition of known amounts agree very well with the sum of both added and actual nitrate contents in the samples. This indicates that the proposed method determines nitrate accurately and that the calibration curve obtained with synthetic sea water with a chlorinity of 19 °/₀₀ is equally applicable to the analyses of natural sea water samples over the chlorinity range of 14 to 19 °/₀₀.

E. *Results of the Analyses for Nitrate in Sea Water.* Several series of sea water samples were collected from the Pacific Ocean and from East Sound and San Juan Channel in the San Juan Islands; they were analyzed by the stated procedure. The stations chosen gave waters of different types and produced the maximum range of nitrate concentrations which would normally be encountered. The results are shown in Table IV.

TABLE IV. Analyses for Nitrate in Sea Water Samples. East Sound, San Juan Islands, 48° 40.3′ N, 122° 53.7′ W, July 11, 1952

Depth (*m*)	*Nitrate Conc'n* (*μg-at/L*)	*Chlorinity* (°/₀₀)
0	0.0	16.50
5	0.0	16.49
12	0.0	—
18	0.0	16.38
23	0.5	16.66
San Juan Channel, San Juan Islands, 48° 35′ N, 123° 01′ W, July 11, 1952		
0	9.6	—
5	11.7	—
10	14.5	—
20	14.8	—
50	13.5	—
100	13.4	—
Pacific Ocean, 48° 30′ N, 136° 30′ W, July 7, 1952		
0	6.5	17.99
5	5.5	17.99
10	5.5	17.99
20	7.8	17.99
30	3.2	18.01
50	5.3	18.05
100	5.2	18.06
200	22.0	18.65
300	30.5	18.73
500	38.2	18.85
750	41.5	18.93
1000	46.6	19.01
1500	42.2	19.05
2000	47.2	19.08

In East Sound, essentially an enclosed basin, there is little exchange of water with the adjoining bodies; also, East Sound waters are stratified. At the time of sampling, its water supported an abundant diatom population which rapidly depleted the water of nitrate.

The waters of San Juan Channel are rather uniform in distribution because of vertical mixing; the water itself shows the effect of dilution by the Fraser River.

The ocean station offered deep samples that were rich in nitrate and surface samples with reduced nitrate concentrations.

The results shown in Table IV are in general agreement with the previously reported data for nitrate in these waters (Phifer and Thompson, 1937; Sverdrup, Johnson and Fleming, 1946). It may be concluded from these results that the method yields satisfactory results when applied to the analysis of sea waters.

APPLICATIONS

This method may be applied to the determination of nitrate in fresh as well as salt waters. Since interfering ions are not present in an appreciable amount in fresh water, the determination of nitrate may be performed by merely adding to the samples a supporting electrolyte, such as sodium chloride to make a 0.1 M solution, and then following the same procedure as outlined previously. It should be applicable also to other saline waters similar to sea water.

BIBLIOGRAPHY

Harvey, H. W.
1929. Methods of estimating phosphates and nitrates in sea water. Rapp. Cons. Explor. Mer, *53:* 68–74.

Ilkovic, D.
1934. Dependence of limiting currents on the diffusion constants, on the rate of dropping and on the size of drops. Coll. Trav. chim. Tchécosl., *6:* 498–513.

Johnson, M. G. and R. J. Robinson
1952. Analytical applications of the polarography of molybdenum. Anal. chem., *24:* 366–369.

Keilin, B. and J. W. Otvos
1946. The polarographic analysis of nitrite and nitrite-nitrate mixtures. J. Amer. chem. Soc., *68:* 2665–2668.

Kolthoff, I. M., W. E. Harris and G. Matsuyama
1944. A new method for the polarographic determination of nitrate. J. Amer. chem. Soc., *66:* 1782–1786.

Kolthoff, I. M. and J. J. Lingane
1946. Polarography. Interscience Publishers, New York. p. 228.

Lingane, J. J. and H. A. Laitinen
1939. Cell and dropping electrode for polarographic analysis. Industr. Engng. chem., Anal. Ed., *11:* 504–505.

Phifer, L. D. and T. G. Thompson
1937. Seasonal variations in the surface waters of San Juan Channel during the five-year period, January 1931 to December 30, 1935. J. Mar. Res., *1:* 34–59.

Robinson, R. J. and H. J. Spoor
1936. Photometric determination of silicate in sea water. Industr. Engng. Chem., Anal. Ed., *8:* 455–457.

Robinson, R. J. and T. G. Thompson
1948. The determination of nitrites in sea water. J. Mar. Res., *7:* 42–48.
Sverdrup, H. U., M. W. Johnson and R. H. Fleming
1946. The Oceans. Prentice-Hall, Inc., New York. p. 242.
Zwicker, B. M. G. and R. J. Robinson
1944. The photometric determination of nitrate in sea water with a strychnidine reagent. J. Mar. Res., *5:* 214–232.

CONTROL OF SALINITY IN AN ESTUARY BY A TRANSITION[1]

By

HENRY STOMMEL AND HARLOW G. FARMER

Woods Hole Oceanographic Institution
Woods Hole, Massachusetts

ABSTRACT

A theoretical reason is developed to explain why the mouth of a vertically stratified estuary should act as a constraint on the amount of salt water available for mixing in the estuary. Flume experiments designed to test this idea are described. The effect of tides on the control action and application to various estuaries is discussed.

THEORY

There is a curious way in which a control[2] acts to limit the possible amount of mixture. Consider an estuary E (Fig. 1) opening into the ocean O (without tides) through a transition T. If the entire system is sufficiently deep, and if the discharge (q_0 per unit width of the transition) of the river R is not too great, there is a two layer flow through the transition. If there is no mixing between the two fluids, then the lower layer is stagnant and the upper layer at T is entirely fresh.

Suppose that some agency for vertical mixing of the two layers exists in the estuary E and that the amount of mixing is progressively increased. The upper layer is now somewhat brackish, the discharge of both layers through T is increased, and the interface is nearer to the mid-depth. Increased mixing in E decreases the salinity difference of the two layers at T and increases the discharge; but there is a point beyond which increased mixing has no further effect on either the discharges through or the salinities at T.

It is natural to suppose that some estuaries will be overmixed in this sense and that the salinity control will be exercised by the nature of the transition rather than by diffusion, whether it be horizontal, vertical, or otherwise.

The criterion for "overmixing" can be obtained from the equation for a stationary interfacial wave,

[1] Contribution No. 587 of the Woods Hole Oceanographic Institution; work done in this paper was supported by public funds made available by the Office of Naval Research.

[2] The notation and theory is a continuation of an earlier paper in this Journal (Stommel and Farmer, 1952).

Figure 1. Schematic diagram of an estuary, E, connecting the river, R, to the ocean, O, through a transition in width, T.

$$\frac{q_2^2}{(1-\eta)^3} + \frac{\alpha q_1^2}{\eta^3} = g\beta D^3 , \tag{1}$$

from the equation of continuity,

$$q_1 + q_2 = q_0 , \tag{2}$$

and from the equation for the conservation of salt,

$$q_1 s_1 + q_2 s_2 = 0 . \tag{3}$$

To relate salinity and density we may take a simplified equation of state

$$\rho = \rho_0 (1 + a\, s) . \tag{4}$$

Thus

$$\beta \equiv \frac{\rho_2 - \rho_1}{\rho_2} \backsimeq a\,(s_2 - s_1), \quad \alpha \equiv \frac{\rho_1}{\rho_2} \backsimeq 1 - a\,(s_2 - s_1) . \tag{5}$$

The equation (1) may now be written in the following form:

$$\varphi(\eta) = \nu^2\eta^3 + (1-\eta)^3 - (1-\nu)^3\eta^3(1-\eta)^3\mathfrak{F}^{-1} = 0 , \tag{6}$$

where

$$\nu = \frac{s_1}{s_2} , \qquad \mathfrak{F} = q_0^2/\,(gas_2D^3) .$$

This is an approximation of equation (1).

The real roots of $\varphi(\eta) = 0$ between $\eta = 0$ and $\eta = 1$ cease to exist as $\nu \rightarrow 1$, and this point determines the state of overmixing. The value of η at which there is a double root occurs when

$$\frac{\partial \phi}{\partial y} = 0 = 3\{\nu^2\eta^2 - (1-\eta)^2 - (1-\nu)^3(1-\eta)^2\eta^2(1-2\eta)\mathcal{F}^{-1}\}. \quad (7)$$

If we multiply equation (7) by η and substract from (6) we obtain

$$(1-\nu)^3\eta^4 = \mathcal{F}. \quad (8)$$

Elimination of ν gives the following form

$$\mathcal{F}\eta^8 = (\eta^4 - (1-\eta)^4)^3. \quad (9)$$

As $\mathcal{F} \rightarrow 0$, $\eta \rightarrow 1/2$. This means that, for weak river flows in estuaries with large transitions, the overmixing leads to an interface at half depth. In order to investigate approximately the effect of $\mathcal{F} > 0$ we introduce $\epsilon = \eta - 1/2$; ϵ is a small quantity as long as $\mathcal{F}$ is small. Substituting this into equation (9) and retaining only the large terms, we obtain

$$256\epsilon^3 - \mathcal{F}(1 + 16\epsilon) = 0. \quad (10)$$

For small values of $\mathcal{F}$ the roots of this expression are approximately

$$\epsilon = \sqrt[3]{\mathcal{F}/256}. \quad (11)$$

In states of overmixing we can thus evaluate at what values of $\mathcal{F}$ the quantity η deviates significantly from 1/2. The ratio of salinities of the upper and lower layers, ν, is given by

$$\nu = 1 - \sqrt[3]{\mathcal{F}/\eta^4}. \quad (12)$$

EXPERIMENTAL STUDIES IN A FLUME

The experimental flume used in this work has been described elsewhere (Stommel and Farmer, 1952). Vigorous mixing was produced by large rotary beaters.

Two sets of runs were made past a transition to test the theory of overmixing. The transition was a short narrow section of width W_1, the channel opening to full width both upstream and downstream. The length of the narrow section was 42 cm in series G, and 100 cm in series H. In all runs the total depth D was 31.5 cm; q_0 is the river discharge per unit width of the transition, ρ_0 the density of river discharge, ρ_1 the density of the overmixture, and ρ_2 the density of the sea water. ν is defined as

$$\nu = \frac{\rho_1 - \rho_0}{\rho_2 - \rho_0},$$

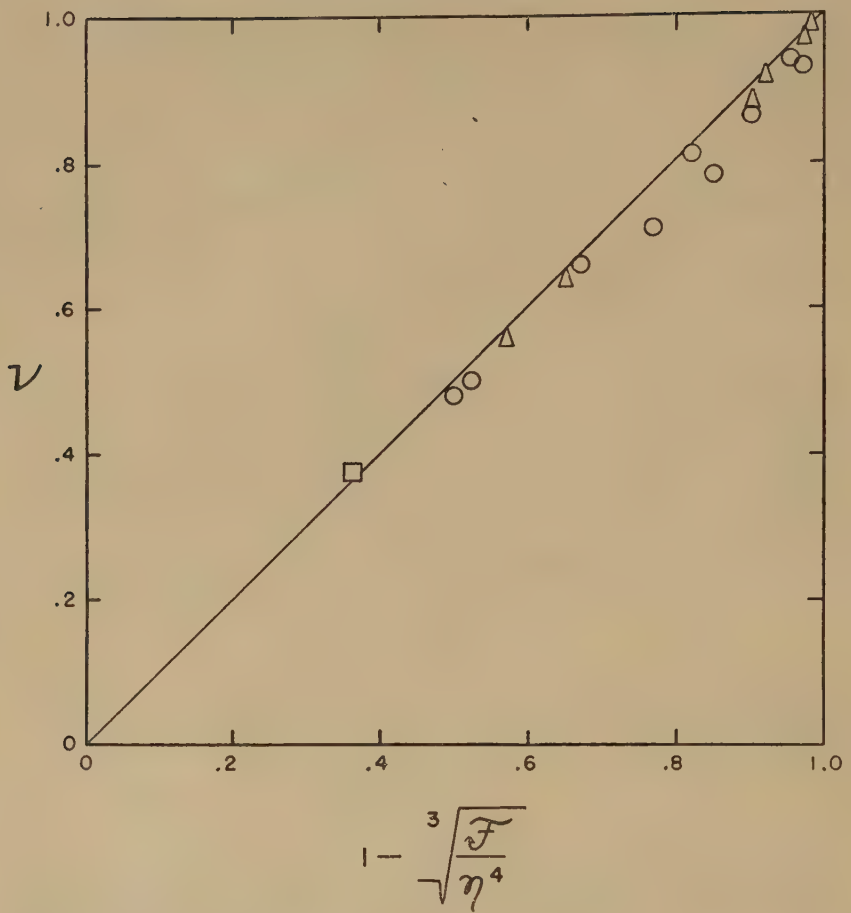

Figure 2. Comparison of observed values of ν and computed value. The meaning of the different points is explained in the text.

and ν_c is computed from the theory. The data are plotted in Fig. 2: the circles are G runs, the triangles are H series, and the square is the only run (G-6) where ε is of sensible order of magnitude.

Four tests were also made with a tide imposed on the overmixed condition; Fig. 3 shows the results of these experiments. In test 2, with the two-minute tidal period, and in test 3, the sea water of density ρ_2 was swept out of the transition for a portion of the tidal cycle and there was a reversal of flow in the upper layer. It is evident that serious disagreement in ρ_1 of the steady and unsteady tests was not experienced until test 4. In this test the surface profile was distorted by a bore and there was no vertical stratification.

TABLE I. Overmixing Experimental Runs

Run	q_0 (cm^2/sec)	W_1 (cm)	ρ_0	ρ_1	ρ_2	ν	ν_c
G–1	43.5	8.7	1.0170	1.0213	1.0259	.48	.50
–3	14.5	8.7	1.0170	1.0233	1.0259	.71	.77
–4	14.5	8.7	1.0000	1.0214	1.0259	.81	.82
–5	1.5	8.7	1.0000	1.0243	1.0259	.94	.95
–6	145.0	8.7	1.0000	1.0097	1.0259	.37	.36
–7	0.7	17.7	1.0000	1.0247	1.0259	.93	.97
–8	7.1	17.7	1.0000	1.0229	1.0255	.86	.90
–9	43.0	17.7	1.0000	1.0171	1.0255	.66	.67
–10	7.1	17.7	1.0170	1.0239	1.0255	.78	.85
–11	43.0	17.7	1.0170	1.0212	1.0255	.50	.52
H–1	0.7	17.5	1.0000	1.0240	1.0248	.97	.97
–2	7.1	17.5	1.0000	1.0221	1.0248	.88	.90
–3	71.0	17.5	1.0000	1.0140	1.0248	.56	.57
–4	0.5	27.8	1.0000	1.0248	1.0250	.99	.98
–5	4.6	27.2	1.0000	1.0230	1.0250	.92	.92
–6	46.0	27.2	1.0000	1.0160	1.0250	.64	.65

OVERMIXING IN ESTUARIES

The only type of estuary to which the concept of overmixing can properly be applied is that in which there is vertical stratification and in which there is evidence of a net flow (averaged over a tidal cycle) downstream in the upper layer and a net flow upstream in the bottom layer. It is important not to attempt to apply this hydraulic condition to vertically mixed estuaries, such as the Raritan River, Delaware Bay, Bristol Channel-Severn estuary, where there appears to be no hydraulic control action at the mouth.

Not all vertically stratified estuaries are likely to be overmixed. Rather obvious examples are Alberni Inlet, which is too deep to be thoroughly mixed by tides, and the Mississippi River passes, in which the tidal action is too small. However, in estuaries where there are tides of several feet or more and where the depth is not more than about ten meters, it is reasonable to suppose that overmixing may occur; that is, the salinity of the estuary upstream of a transition is determined by the control or "throttling" action of the transition on the two layer flow through it, not by the magnitude of large scale horizontal turbulent exchange in the sense of Ketchum (1951) and Arons and Stommel (1951).

Hachey (1939) has summarized the data available on the salinity of the upper layer in St. John Harbor (New Brunswick, Canada). In Fig. 4 the difference in salinity of the upper and lower layers is plotted as a function of river discharge. The straight line is computed from

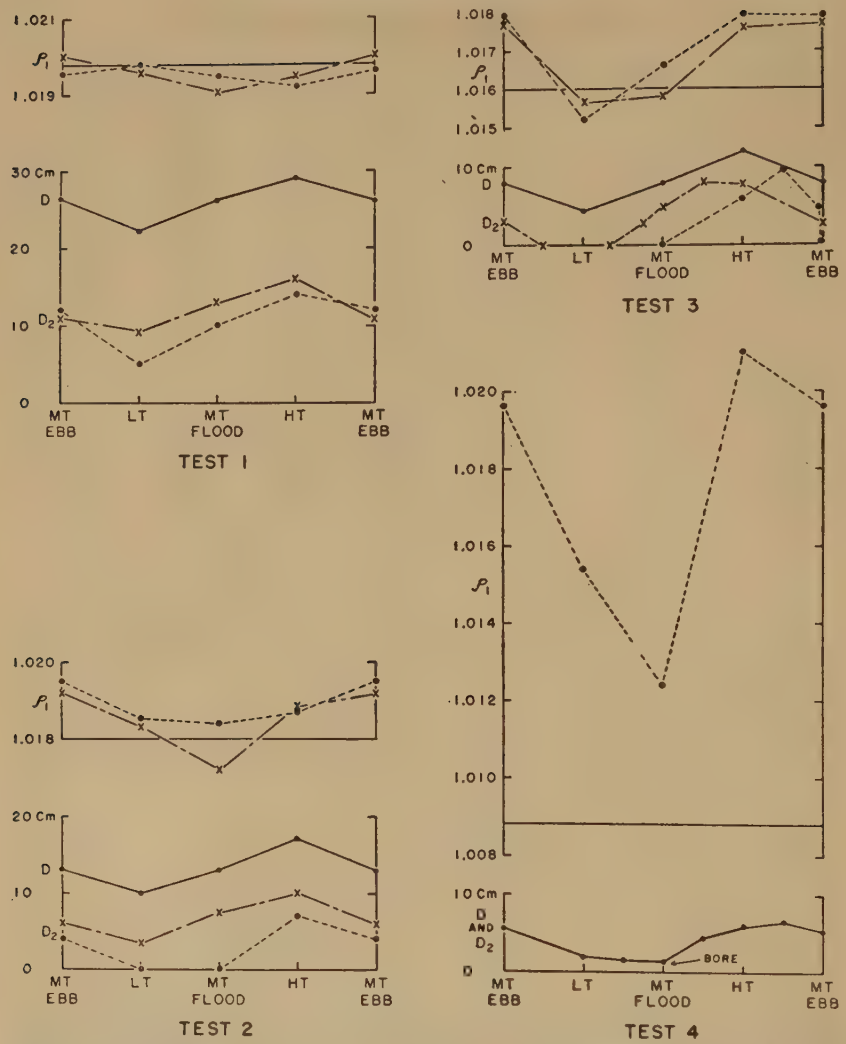

Figure 3. Experimental tests on the influence of tides on overmixing. X's refer to tides of 6-minute period and O's refer to tides of 2-minute period. The solid straight lines indicate the observed ρ_1 without the influence of tides. Data: $\rho_2 = 1.0237$; $\rho_0 = 1.0009$; $q_0 = 7.1$ cm²/sec (test 1); and 3.5 cm²/sec (tests 2, 3, 4); $W_1 = 17.7$ cm.

equation (12) on the supposition that the abrupt widening at the mouth of the harbor acts as a control, that the width of the channel is 2,000 feet, that the depth of the water is 30 feet, and that the mixing action of the reversing-falls upstream is so efficient that overmixing

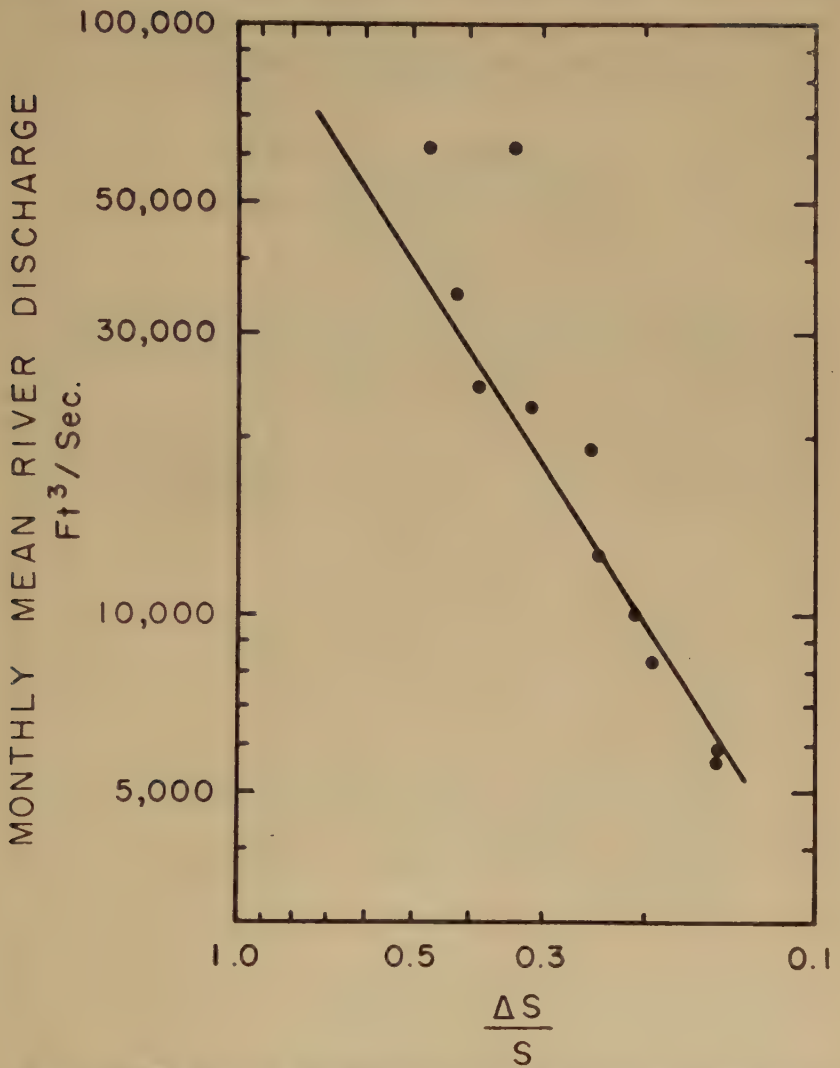

Figure 4. Ratio of vertical salinity difference between the bottom and surface layers in St. John Harbor, plotted against the monthly mean river discharge of the St. John river. The points are from data by Hachey (1939). The straight line is computed from the theory of overmixing.

occurs. Considering the crude nature of both the theory and data, the agreement is fairly good, and it is concluded that St. John Harbor is overmixed.

Data on the dependence of stratification at the mouth of an estuary upon the river discharge are difficult to find in the literature. Very fragmentary data suggest that the following estuaries may be overmixed:

St. Johns River, Jacksonville, Fla.
Columbia River, Oregon
Savannah River, South Carolina
New Waterway, Holland
New York Harbor, N. Y.

It is suggested that future surveys of estuaries where the possibility of overmixing exists include considerable detailed survey work on sections that are likely to exert control action. The observations should give vertical salinity and temperature soundings over a complete tidal cycle for several different stages of river discharge throughout the year. Construction of a graph, such as that shown in Fig. 3, will immediately determine whether or not a condition of overmixing exists in a particular estuary.

REFERENCES

Arons, A. B. and Henry Stommel
1951. A mixing length theory of tidal flushing. Trans. Amer. geophys. Un., *32* (3): 419–421.

Hachey, H. B.
1939. Hydrographic features of the waters of Saint John Harbour. J. Fish. Res. Bd. Canada, *4* (5): 424–440.

Ketchum, B. H.
1951. The exchange of fresh and salt waters in tidal estuaries. J. mar. Res., *10* (1): 18–38.

Stommel, Henry and H. G. Farmer
1952. Abrupt change in width in two-layer open channel flow. J. mar. Res., *11* (2): 205–214.

A SEAWATER SAMPLING BOTTLE[1]

By

R. L. I. FJARLIE

Pacific Oceanographic Group,
Nanaimo, B. C.

ABSTRACT

A new type seawater sampling bottle consisting of a tube with hinged lids and a frame holding three reversing thermometers is described. The bottle is designed to be free flushing, reliable mechanically, and simple to operate. The relative sampling efficiency of Nansen, Knudsen, Ekman and new type bottles is compared.

The earliest seawater sampling bottles, such as those used on the first CHALLENGER Expedition, consisted of a simple tube through which the water flowed more or less freely (flushed) while it was lowered on a sounding line to any desired depth. When in position, it was closed by striking a trigger mechanism with a small weight (messenger) which slid down the line. With the advent of reversing thermometers in 1902, a reversing mechanism was added.

The most successful bottles are the Nansen (Wüst, 1932), Knudsen (Knudsen, 1929) and Ekman (Knudsen, 1923), in which the thermometers are attached to the tube which reverses and closes when the trigger is actuated. In the first two, both ends of the bottles are attached to the sounding line while they are lowered into position; when the messenger strikes the releasing mechanism, the top end falls away from the line by its own weight and reverses. There is a common objection to them in that the sampling tube is not perfectly sealed when the bottle is reversed. Because their flushing characteristics are poor they must be left at the sampling depth for some time to obtain a true sample.

In the Ekman bottle the thermometer and sampling tube assembly are mounted on pivots in a frame that can be attached to the sounding wire at both ends. It has relatively good flushing characteristics, and with care the lids on the tube can be maintained leak-proof. But this bottle, though rugged, is very heavy and tiresome to use.

The ideal water sampler must obtain and preserve a true sample of the water at the sampling depth and bring it on shipboard intact. This requires good flushing characteristics when open and a positive

[1] Plans and specifications may be obtained at cost from the Oceanographer in charge, Pacific Oceanographic Group, Nanaimo, B. C.

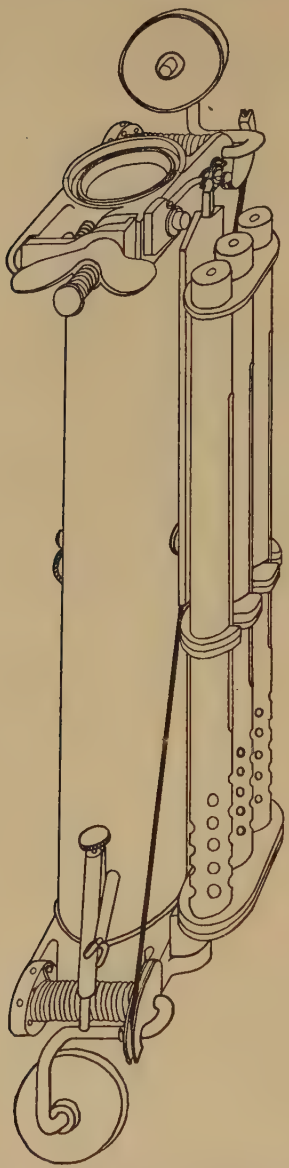

Figure 1. The seawater sampling bottle.

seal when closed. Furthermore, once the thermometers have reversed they should be locked in position to safeguard the temperature readings. The unit should be fastened to the line at both ends to prevent damage against the side of the ship in rough weather, and the thermometer cases should be readily removable so that these instruments may be stored properly (Ekman, 1905; Richter, 1950) between observations at sea.

THE NEW SEAWATER SAMPLING BOTTLE

With the requirements of an ideal water sampler in view, a new bottle has been designed (Fig. 1) to incorporate as many of these features as possible. The design was commenced in 1949 and the prototype of the present bottle was first used in January 1950. Since then the design has been modified six times. It is presented here as a unit which has proved dependable, easy to handle, and capable of obtaining true samples and temperatures.

This sampling bottle consists of a light metal tube with hinged lids on each end which are co-ordinated with a rotating frame that holds three reversing thermometers. The tube is clamped to the sounding line at the top and is hooked at the bottom end, similar to the Ekman bottle. A device below the bottle for releasing a messenger when it closes allows any number of units to be used in series on the line. The major features which have been designed into the bottle permit unrestricted flow of water through it when open, a positive seal when the lids are closed, and complete mechanical reliability.

The free flow of water through the bottle has been facilitated by mounting the operating springs outside on the lid hinges and by providing large openings at the ends of the tube. The only impediment to flow is a ¼ inch diameter axle which passes transversely through the center of the tube to support the reversing thermometer frame.

The tube is sealed by flexibly mounted lids which carry a rubber gasket (Fig. 2). The flexibility of the mount allows the lid to adapt itself to the end of the bottle in case the hinge bar becomes bent in service, and the metal rim which forms the seal with the gasket has been slightly recessed inside the bottle to prevent damage.

A flexible cable forms the link between the lids and the reversing thermometer frame so that when the frame is rotated it also opens both lids against the springs. A lock is provided to prevent accidental opening with consequent loss or contamination of the sample and errors in the thermometer readings. A removable case holding three thermometers locks to the reversing frame with two spring catches.

The bottle has an eye welded to the tube at each end so that it can be hung upright on a hook before the thermometers are read and up-

side down after the sample is drawn and temperatures are recorded. In this way the reversing thermometers can be kept in the approved storage position (Richter, 1950) while they are still on the bottles if it is not convenient to transfer them to a separate rack. In practice, a wooden case fitted with hooks serves as a bottle rack on deck and as a case for shipping.

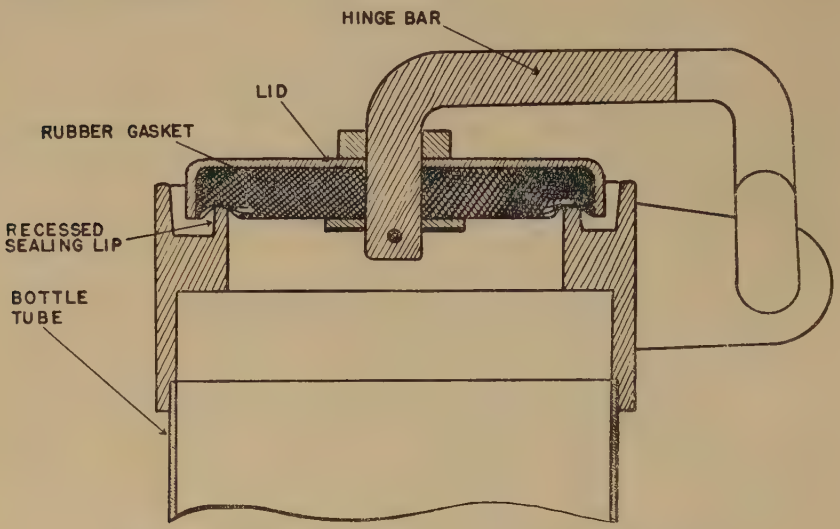

Figure 2. Detail of lid construction on the seawater sampling bottle.

The weight of the new bottle (7.3 lbs.) compares favorably with that of the Nansen bottle (7.7 lbs.) and its weight is the same as that of the Knudsen bottle. It is much lighter than the 17-pound Ekman bottle.

The messenger, a "split" type, is cast in two pieces of manganese bronze which are held together under tension by a heavy piece of rubber. The messenger is pushed onto the line and pulled off, but it has no tendency to fall off or to become jammed.

In use, the bottle is first attached to the sounding line by a spiral hook at the lower end (Fig. 3A) and then clamped at the top (Fig. 3B). The plunger which locks the thermometer frame is released and the lids are opened by rotating the frame 180 degrees until it engages the trigger (Fig. 3C). The messenger is then attached to a spring loaded plunger that bears against the lower hinge bar (Fig. 3D), and finally the messenger is fitted to the line.

Every attempt has been made to reduce the number of motions required. The hook at the lower end is positioned so that the movements used in attaching and detaching the bottle from the line are

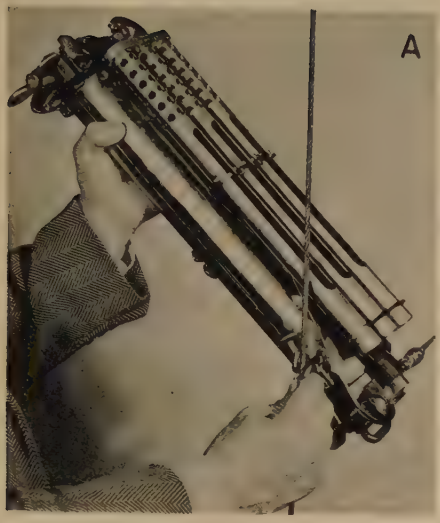

Figure 3. Attaching the bottle to the sounding line.

those which would naturally be used in moving the bottle to or from the wire. The bottle is designed so that it can be held in the left hand while the right hand performs the more complicated motion of screwing up the clamp, which has a large wing nut to attach it securely to the line with reasonable effort. Both lids are opened and the thermometers are reversed in a single motion. The messenger is attached after this action is completed so that the operator does not have to coordinate two moving parts.

FLUSHING EFFICIENCY—A COMPARISON WITH OTHER SEAWATER SAMPLING DEVICES

In a single experiment the relative efficiency of the Nansen, Knudsen, Ekman and Fjarlie bottles was investigated in water having a moderate salinity gradient. Strings consisting of four bottles of each type, attached at two-meter intervals, were hung side by side from a bar suspended from the main cargo boom of H. M. C. S. Cedarwood, the end of which was high enough above the sea to allow all of the bottles to be in the air at once. With bottles open and messengers attached, the four strings were lowered into the water, and at a measured time from immersion of the uppermost bottle, messengers were dropped on each line simultaneously. The bottles were then hauled up and the samples were drawn. This procedure was repeated to obtain samples after a submersion time of 0, ½, 1, 1½, 2, 3, 4, 5, 6, 9, 11 and 15 minutes, the different intervals being observed in random order (Table I).

It is believed that this method of sampling makes it possible to estimate the time required for a bottle to flush completely by comparing the salinity of the samples taken. Ideally, the time required for complete flushing of all bottles is the time from which they are submerged until all bottles at the same depth have identical samples. In this experiment an arbitrary reference salinity for each cast was obtained by choosing the maximum salinity at each depth, regardless of the type of bottle from which it was drawn. If the salinity as shown by one bottle was less than the reference salinity at the same depth, it was assumed that some water of a lower salinity had been trapped in the bottle and had been carried down with it to the sampling position.

To evaluate the relative efficiency of the different bottles, the area between the reference salinity curve and the curve shown by each type of bottle was measured for the various submersion times. It was assumed that, as this area approached zero with longer "soaking," flushing became more complete. Thus, the efficiency is measured by

TABLE I. The Salinity (‰) of Samples Taken Simultaneously in Four Types of Sea Sampling Bottles After Various Intervals of Immersion

Depth (*m*)	*Type of Bottles*			
	Fjarlie	*Nansen*	*Knudsen*	*Ekman*
		0 Minutes Immersion		
0	23.35	23.39	23.33	23.31
2	23.42	23.33	23.35	23.37
4	24.43	23.57	23.64	24.30
6	—	24.69	24.78	25.48
		½ Minute Immersion		
0	23.93	23.90	23.93	23.90
2	24.16	24.00	23.90	23.95
4	—	24.36	24.42	24.78
6	25.62	24.90	25.55	25.64
		1 Minute Immersion		
0	24.40	24.27	24.29	24.29
2	24.29	24.30	24.30	24.29
4	25.30	24.74	25.01	25.28
6	25.68	24.69	25.52	25.68
		1½ Minutes Immersion		
0	23.98	24.50	23.98	24.02
2	24.20	24.14	24.16	24.16
4	24.81	24.61	24.69	24.81
6	25.81	25.52	25.73	25.80
		2 Minutes Immersion		
0	24.36	24.38	24.40	24.40
2	24.51	24.45	23.87	24.47
4	25.35	25.16	25.39	25.41
6	25.59	25.50	25.59	25.57
		3 Minutes Immersion		
0	24.02	24.00	24.02	24.00
2	24.00	24.04	24.00	24.04
4	24.92	24.61	24.92	24.94
6	25.75	25.53	25.73	25.72
		4 Minutes Immersion		
0	23.60	23.69	23.71	23.69
2	23.73	23.71	23.73	23.74
4	24.34	24.05	24.18	24.34
6	25.59	25.48	25.57	25.57

the area between the curves and the time required for them to approach zero. For discussion purposes, the units of area have been called "Salinity Meters" (S. M.).

The data are shown in Table I. The salinity profiles for a submersion time of 0 minutes are shown in Fig. 4, together with the reference profile.

TABLE I.—Continued

Depth (*m*)	*Type of Bottles*			
	Fjarlie	*Nansen*	*Knudsen*	*Ekman*
		5 Minutes Immersion		
0	24.14	24.13	24.11	24.05
2	24.11	24.13	24.11	24.14
4	24.47	24.38	24.31	24.47
6	25.73	25.64	25.72	25.72
		6 Minutes Immersion		
0	24.11	24.18	24.11	24.11
2	24.22	—	24.27	24.27
4	24.76	25.16	24.69	25.10
6	25.82	25.84	25.82	25.84
		9 Minutes Immersion		
0	23.59	23.66	23.62	23.57
2	23.69	23.62	23.71	23.68
4	24.45	24.54	24.61	24.50
6	25.55	25.61	25.62	25.62
		11 Minutes Immersion		
0	24.18	24.07	24.11	24.11
2	24.22	24.25	24.27	24.27
4	24.58	24.54	24.52	24.60
6	25.81	—	25.81	25.80
		15 Minutes Immersion		
0	23.48	23.44	23.38	23.44
2	23.48	23.51	23.50	23.55
4	24.09	25.10	25.37	25.39
6	—	25.64	25.72	25.62

The relative efficiency of the four types of bottles is shown in Fig. 5. The variation in the data, about 0.25 S. M., becomes approximately constant after nine minutes submersion time. The data for the six and 15 minute intervals are not consistent with the remainder of the series and cannot be explained from the records of the experiment.

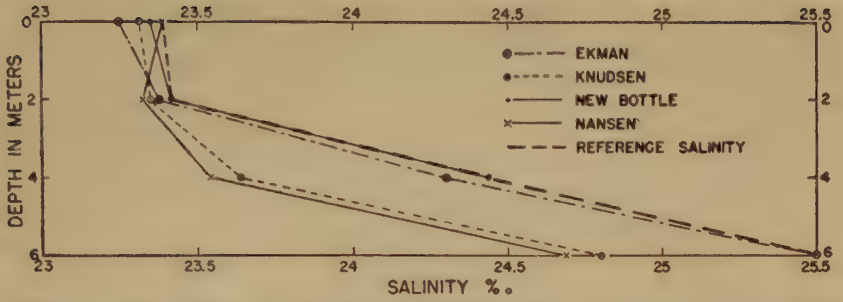

Figure 4. The salinity of samples taken simultaneously in the four types of bottles after zero minutes submersion.

Despite these anomalies, the relative efficiencies are clearly indicated. In these waters, where the salinity (and consequently the density) gradient was moderate, the samples in the new bottle apparently were in equilibrium with the surrounding waters immediately, those taken in the Ekman bottle after one-half minute, the Knudsen samples after two minutes, the Nansen bottle samples after five minutes "soaking."

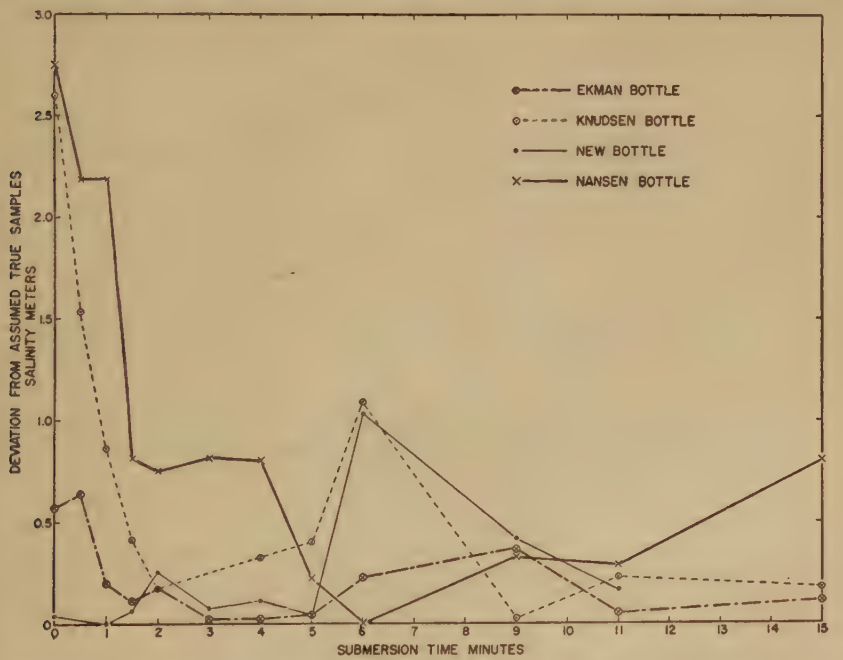

Figure 5. Deviation of the salinity in each type of sample bottle from the reference value. Efficiency varies inversely with the deviation.

When a bottle is being lowered, flushing results from the velocity head in the fluid at the end opening; after the bottle is in position the lighter water, entrapped and carried down in the lowering, will float out and be replaced by the denser surrounding water. During the lowering, when the velocity is greatest, small end-openings and internal obstructions cause a flow resistance which is most effective in retarding the flushing, but it is also effective in retarding the hydrostatic flushing when the bottle is in position.

The data in Fig. 5 show that the efficiency is proportional to the effective size of the end-openings and to freedom of flow through the bottles. While the end caps on the Ekman bottles undoubtedly retard free flow, equilibrium is quickly attained (½ minute) because of the large openings and an unobstructed tube. The end-opening of the Knudsen bottle is of fair size, but it is partially obstructed by the internal spring, which also occupies a large percentage of the cross section area in the narrow bottle. The stopcocks on the Nansen bottle constrict the end-openings so much that flushing requires more than twice the time of any other bottle.

The bottle described here approaches the postulated requirements more closely than any of the bottles designed previously, and it is believed to be an acceptable improvement.

REFERENCES

Ekman, V. W.

1905. On the use of insulated water bottles and reversing thermometers. Publ. Circ. Cons. Explor. Mer., *23:* 27–28.

Knudsen, M.

1923. Some oceanographical instruments. Publ. Circ. Cons. Explor. Mer., *77:* 9–10.

1929. A frameless reversing water bottle. J. Cons. int. Explor. Mer., *4* (2): 192.

Richter, N.

1950. Über die Funktion der Umkippthermometer sowie die Beseitigung von storungen. Richter and Wiese, Berlin. 9 pp.

Wüst, Georg

1932. III. Die bei den serienmessungen angewandten methoden und apparate. 1. Wasserschöpfer, thermometernahmen. Wiss. Ergebn. dtsch. Atlant. Exped. Meteor, 1925–27, *4* (A): 21–30.

THE DETERMINATION OF ORGANIC PHOSPHORUS IN SEA WATER WITH PERCHLORIC ACID OXIDATION[1]

By

ANDREW L. HANSEN and REX J. ROBINSON

Oceanographic and Chemical Laboratories
University of Washington, Seattle 5, Washington

ABSTRACT

A method is proposed for the determination of organic phosphorus in sea water; in this procedure the organic material is oxidized with perchloric acid and the organic phosphorus is converted to phosphate. Oxidation in a perchloric acid medium is superior to sulfuric acid: (a) The perchlorate salts formed upon digestion of sea water are readily water-soluble in contrast to certain sulfates; (b) A small blank correction for impurities must be applied. Interference by arsenic is prevented by volatilization of the arsenic chloride formed by heating the samples with concentrated hydrochloric acid. Total phosphorus is determined colorimetrically, and the organic phosphorus is calculated by deducting the inorganic phosphorus. Preliminary digestion with nitric acid is desirable before samples of high organic content are digested with perchloric acid.

INTRODUCTION

The occurrence and distribution of phosphorus in its various forms in the sea are of interest in connection with the productivity of the sea. Phosphorus occurs in the sea as inorganic phosphate and as organic phosphorus in soluble organic forms and particulate matter. Inorganic phosphate is conveniently determined by a colorimetric method (Robinson and Thompson, 1948; Wooster and Rakestraw, 1951), and a considerable fund of information has been collected regarding its distribution. On the other hand, little information is available on the occurrence and distribution of organic phosphorus because of the difficulty experienced in its determination.

Organic phosphorus as particulate matter has been determined by separation of the particulate matter, oxidation in acid solution, and estimation by the colorimetric method for inorganic phosphate (Redfield, Smith and Ketchum, 1937). What is retained as particulate matter depends on the method of separation and of washing. Knowledge of the particulate organic phosphorus content gives incomplete information regarding the organic phosphorus content of the sea unless the soluble organic phosphorus content is also known.

[1] This work was partly supported by the Office of Naval Research under Contract No. N8onr–520/III with the University of Washington.

Most frequently the total organic phosphorus content, which includes both soluble and particulate organic phosphorus, is obtained by determining total phosphorus and subtracting inorganic phosphate. Total phosphorus is determined by colorimetric estimation after acid oxidation of organic phosphorus to phosphate. A number of procedures have been reported for the oxidation of organic phosphorus in sulfuric acid solution. Kreps and Osadich (1933) oxidized with 3% hydrogen peroxide, Kalle (1933) with potassium persulfate, and Cooper (1934) with 30% hydrogen peroxide. But these methods failed to account for the oxidation of arsenite to arsenate and its subsequent estimation along with phosphate by the colorimetric method. Failure to correct for arsenate introduces considerable error, since arsenic occurs in the sea to the extent of 0.2 to 0.5 μg-at/L, mostly as arsenite (Gorgy, Rakestraw and Fox, 1948), while the organic phosphorus content is only about 0.5 to 0.6 μg-at/L. Kalle (1935) attempted to prevent the interference of arsenate by reducing it to arsenite with thiourea. However, Cooper (1937) was unable to reduce arsenate in sea water with Kalle's method. Redfield, Smith and Ketchum (1937) digested sea water samples with hydrogen peroxide in sulfuric acid solution and reduced the arsenate by heating with sodium bisulfite for a period of eight hours. Harvey (1948) described another modification in which the samples were heated in the autoclave at 130° C in sulfuric acid solution with sodium sulfite to reduce arsenate.

Extensive investigations of various procedures for the determination of total phosphorus by Robinson and co-workers (Jesseph, 1932; Selbo, 1940) have indicated several inherent disadvantages in methods that employ sulfuric acid for the digestion of samples. It is difficult to obtain sulfuric acid that is sufficiently free of interfering impurities. Anhydrous sulfate salts of sodium, calcium, etc. separate on digestion and redissolve in distilled water with difficulty. Small undissolved salt nuclei often remain and cause excessive color development of the colloidal phosphomolybdate blue reduction complex.

Preliminary work by Selbo and Robinson (Selbo, 1940) has indicated that oxidation of organic matter in sea water could be effected by perchloric acid, the use of which results in a number of advantages. (a) The interfering impurities present in perchloric acid are of small magnitude. (b) The organic matter is quickly oxidized by the perchloric acid. (c) Salts, very soluble in water, are obtained upon digestion of the sample. A more complete examination of the method, made by Hansen and Robinson (Hansen, 1950), is reported in this paper. Recently, application of the perchloric acid method for lake waters (Robinson, 1941) has been made to sea water analysis by Rochford (1951).

THE PROPOSED METHOD

Reagents and Standard Solutions

All chemicals used in this investigation were of analytical grade.

Sulfuric Acid: 36 Normal, arsenic-free acid.

Perchloric Acid: 60 or 72% acid.

Hydrochloric Acid: 12 Normal acid.

Sodium Hydroxide: 1 Normal sodium hydroxide solution.

Ammonium Hydroxide: 15 Normal ammonium hydroxide.

Ammonium Molybdate-Sulfuric Acid Reagent: Dissolve 10 g of ammonium molybdate, $(NH_4)_6Mo_7O_{24} \cdot 4H_2O$, in 100 ml of distilled water. Add this solution to 300 ml of 18 N sulfuric acid. Keep reagent in an amber glass-stoppered bottle and protect from light to prevent photochemical reactions from occurring.

Stannous Chloride Solution I. Dissolve 2.15 g of stannous chloride, $SnCl_2 \cdot 2H_2O$, in 20 ml of 12 N hydrochloric acid and dilute to 100 ml with freshly boiled distilled water. Store the solution in an amber glass-stoppered bottle and add a piece of mossy tin to counteract air oxidation. The solution was stable for about a month.

Stannous Chloride Solution II. Dilute 5 ml of Solution I to 25 ml with freshly boiled distilled water. Add a small piece of mossy tin to stabilize the solution. Prepare a fresh solution each day.

Standard Phosphate Solution I. Dissolve 0.340 g of anhydrous potassium dihydrogen phosphate, KH_2PO_4, in distilled water and make up to 1 liter. Add 0.2 ml of chloroform to retard possible bacterial action. One ml of this solution contained 2.50 μg-at phosphate-phosphorus.

Standard Phosphate Solution IIa for Inorganic Phosphate. Dilute 10 ml of Standard Solution I to 1 liter with a sodium chloride solution having a chlorinity similar to that of the sea water being tested. Add 0.2 ml of chloroform to retard bacterial action. One ml of this solution contained 0.0250 μg-at phosphate-phosphorus.

Standard Phosphate Solution IIb for Inorganic Phosphate. Dilute 40 ml of Standard Solution I to 1 liter by means of the sodium chloride solution and add 0.2 ml of chloroform. One ml of this solution contained 0.100 μg-at phosphate-phosphorus.

Standard Phosphate Solutions IIa and IIb for Organic Phosphorus. Because no salt-effect correction is necessary for samples digested with perchloric acid, these standards were prepared in the same way as Standard Phosphate Solutions IIa and IIb for inorganic phosphate, except that they were diluted with distilled water rather than with sodium chloride. The phosphate-phosphorus concentrations of the standards remained the same in both cases.

Apparatus

The colorimetric estimations were made for the most part with a Model AC Fisher Electrophotometer, using filter A, of 625 mμ average wavelength, and glass cells with optical paths of 5 cm. Some of the estimations were made with the Electric Eye Photometer developed by Ford (1950).

Analytical Procedures

Inorganic Phosphate. Mix thoroughly 0.5 ml of ammonium molybdate reagent and 0.20 ml of Stannous Solution II with a 50 ml sea water sample as soon after collection as possible. Allow seven minutes for color development, then measure the resulting color in the Electrophotometer, using distilled water as the reference solution. Obtain the phosphate value from a calibration curve prepared with standard phosphate solutions.

Total Phosphorus. Treat 50 ml samples of sea water with 3 ml of 60% perchloric acid in a 125 ml Erlenmeyer flask. This volume of perchloric acid is equivalent to the salts of a typical sea water sample with a salinity of 30°/$_{oo}$ plus an excess of 0.2 ml for oxidation purposes. After evaporation on a hot plate to fumes of perchloric acid, place a cover glass on the flask and heat the sample for about 5 minutes just below the fuming temperature of perchloric acid. In order to drive off the arsenic present, add 3 ml of 12 N hydrochloric acid and fume off rapidly. Let cool and add 30 ml of distilled water to dissolve the salts. Neutralize the excess acid with a normal sodium hydroxide solution, using phenolphthalein as the indicator. Add dilute perchloric acid drop by drop until the solution is slightly acidic. Dilute the solution to 50 ml and mix thoroughly with 0.50 ml of ammonium molybdate solution and 0.30 ml of Stannous Chloride Solution II. After maximum color development, estimate the color in the Electrophotometer, using distilled water as the reference solution. Obtain the phosphate value from a calibration curve prepared with standard phosphate solutions.

Prepare blank solutions by treating a sodium chloride solution of the same chlorinity as sea water with perchloric acid in the manner just described.

Notes on the Procedures. Frequently it has been noted (Lundell and Hoffman, 1945) that under certain conditions perchloric acid reacts violently with organic material. This hazard is eliminated by the initial oxidation of the more easily oxidizable material by using nitric acid before perchloric acid is added. The amount of organic material in a typical sea water sample is relatively small, hence there is no hazard when it is oxidized with perchloric acid, but if samples of ab-

normally high organic content such as plankton or mud are being analyzed, it is advisable to digest with a small amount of nitric acid first. Water samples from East Sound, San Juan Islands, which contained as much as 2 μg-at organic phosphorus per liter, were digested directly with perchloric acid without trouble. However, as a precaution, plankton samples obtained by filtration were treated with small portions of nitric acid before oxidation with perchloric acid, and all such experiments proceeded without violence. *It should be emphasized that, before using perchloric acid, one should be familiar with its hazards and with the precautions to be followed to insure its safe use* (*Kuney, 1947*).

INVESTIGATION OF THE METHOD OF ANALYSIS

Testing the Method of Analysis

The method just described was tried on known amounts of sodium glycero-phosphate in a sodium chloride solution, Cl = 17‰. A satisfactory recovery of the phosphorus was obtained.

The organic phosphorus content of a sea water sample was determined by the perchloric procedure and by the sulfuric acid-hydrogen peroxide procedure. The excess perchloric acid was neutralized with sodium hydroxide and the excess sulfuric acid with ammonium hydroxide, as in the procedure described by Redfield, et al. (1937). The results are recorded in Table I. The total phosphorus concentrations in each case were corrected for a blank.

TABLE I. Determination of Organic Phosphorus in Sea Water

Phosphate Concentrations (μg-at/L)			
Sulfuric Acid Procedure		*Perchloric Acid Procedure*	
*Total P**	*Organic P*	*Total P***	*Organic P*
2.11	0.53	2.36	0.78
1.89	0.31	2.49	0.91
2.08	0.50	2.47	0.88
2.48	0.90	2.54	0.96
2.36	0.78	2.36	0.78
2.32	0.74	2.53	0.95
2.21 av.	0.63 av.	2.46 av.	0.88 av.

Inorganic phosphate concentration 1.58 μg-at/L.

* Corrected for a blank of 1.09 μg-at/L.

** Corrected for a blank of 0.36 μg-at/L.

The blank for the sulfuric acid procedure was considerably greater than that for the perchloric acid procedure. Thus the more than 3 ml of concentrated sulfuric acid and 8 ml of ammonium hydroxide

gave a blank of 1.09 μg-at phosphorus per liter, the 3 ml of perchloric acid and several drops of sodium hydroxide solution a blank of 0.36 μg-at/L. Various attempts to purify the sulfuric acid and ammonium hydroxide did not reduce the magnitude of the blank.

As shown in Table I, the results for total phosphorus (and also for organic phosphorus) by the perchloric acid method were somewhat larger than those obtained by the sulfuric acid procedure. It is not known whether this is due to greater efficiency of oxidation by the perchloric acid or to error arising from the establishment and application of the quite large blank for the sulfuric acid method. However, in general it may be said that results obtained by a method that utilizes a large blank are apt to suffer in accuracy.

The organic phosphorus was calculated by deducting the inorganic phosphate, which amounted to 1.58 μg-at/L, from the total phosphorus value. An organic phosphorus content of 0.63 μg-at/L was obtained by the sulfuric acid method, 0.88 μg-at/L by the perchloric acid procedure. Provision for reduction of arsenate was not included in either method, hence the final concentrations found represented the sum of phosphate, arsenate and oxidized arsenite.

Time of Color Development and Stability of Color

It was determined that, after the addition of reagents, maximum color intensity developed in 3 minutes in distilled water or in sea water digested with perchloric acid; this color was stable for about 8 minutes before fading began. On the other hand, in undigested sea water samples full color developed in about 6 minutes and was stable for 27 minutes before fading began.

Effect of Perchlorate upon Color Intensity

For some time it has been known that, for a given amount of phosphate, less color is developed in the estimation of phosphate in an undigested sea water sample than in distilled water. This is known as the salt effect. When sea water is digested with sulfuric acid or perchloride acid, hydrogen chloride is evolved and salts of sulfate or perchlorate remain. However, no salt effect was noted (Table II) when phosphate was estimated in a sulfate or perchlorate medium and its color compared with that developed in the distilled water medium. This is in accordance with Cooper's (1938) explanation that the salt effect is due to the formation of certain yellow molybdenyl halides.

Arsenite Interference

It is generally thought that arsenic is present in sea water mainly as arsenite with inappreciable amounts of arsenate. However Armstrong and Harvey (1950), as a result of experiments which they per-

TABLE II. Effect of Various Salts on Color Development

Medium g/50 ml	*Phosphate Concentration (μg-at/L)* *Added*	*Found*
2 g NaCl	1.20	1.00
2 g Na_2SO_4	1.20	1.20
	2.20	2.20
2 g $NaNO_3$	1.60	1.50
2 g $NaClO_4$	1.60	1.60

formed, suggested that arsenate may be the predominating form. According to Zinzadze (1935), arsenate but not arsenite forms a blue reduction product with the reagents for the phosphate determination, and thus it would be estimated along with phosphate. However, if arsenite is oxidized to arsenate in the oxidization of organic phosphorus, there would be interference in the estimation of total phosphorus. Experimentally it was demonstrated by the authors that this is the case (Table III). Sea water samples with added arsenite were digested

TABLE III. Oxidation of Arsenite with Perchloric Acid in a Sea Water Medium

Arsenite Concentration (μg-at/L)	*Found as Arsenate*	
Added	*Fumed 5 min.*	*Fumed 1 hr.*
2.00	0.22	0.96
	0.10	1.08
	0.10	2.03
	0.19	2.00
	0.17	1.62

with perchloric acid and estimated colorimetrically. From these values was subtracted the total phosphorus of the sea water, which contained no added arsenite. The total phosphorus value also included arsenic which was present in the sea water and which had been oxidized to arsenate as well as phosphorus. The results indicated that the added arsenite had been oxidized, but it was not determined quantitatively.

It was also noted that arsenite causes a blue color with the phosphate reagents even though it is not thought to form a complex. Fig. 1 shows the extent of the color development by arsenite in different media. Almost as much color is developed by arsenite in distilled water or in a medium containing the digested sea water salts as is developed by an equivalent amount of phosphate, while in a chloride medium considerably less color is formed. Thus arsenite in sea water would cause an error of comparatively small magnitude.

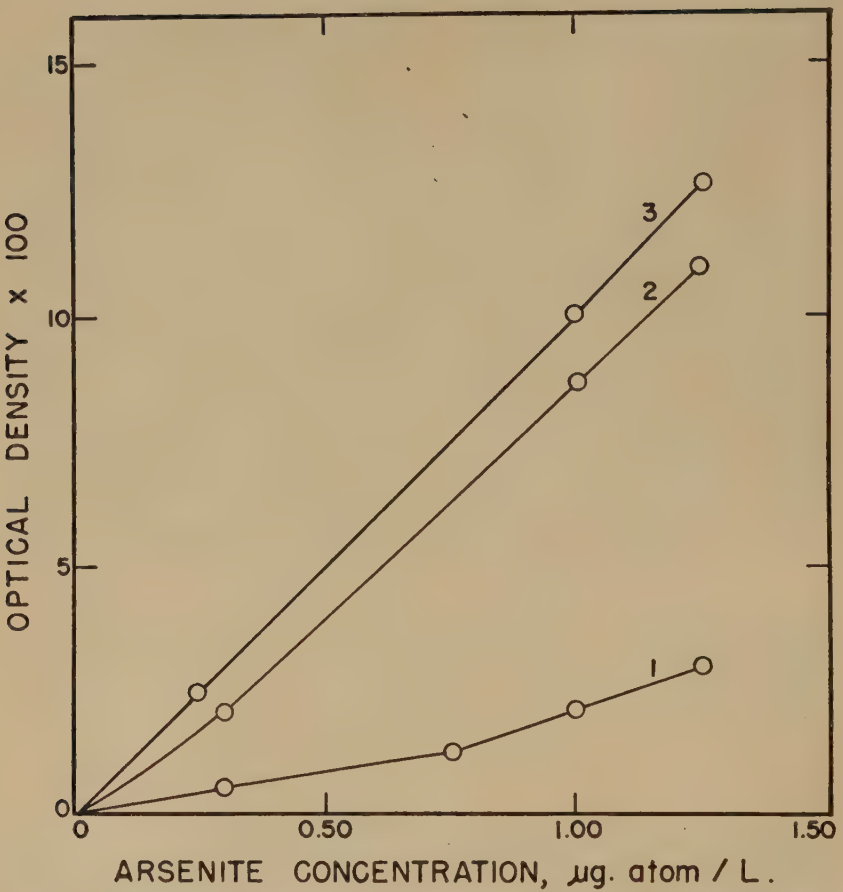

Figure 1. Arsenite interference in various media at $Cl^- = 17$ °/₀₀. 1. Arsenite in sodium chloride solution. 2. Arsenite in distilled water or in digested sea water. 3. Calibration curve for phosphate in sodium chloride solution.

It was found that the color developed by arsenite depends upon the chloride concentration. This is demonstrated by the results shown in Fig. 2. An arsenite concentration of 12 µg-at/L, which is 20–50 times its probable concentration in sea water, was used to accentuate the effect at various chloride concentrations. Considerably less color was developed by arsenite at the higher chlorinities. Thus, in undigested sea water arsenite interference can ordinarily be neglected, but it should be considered when samples without chloride are being analyzed.

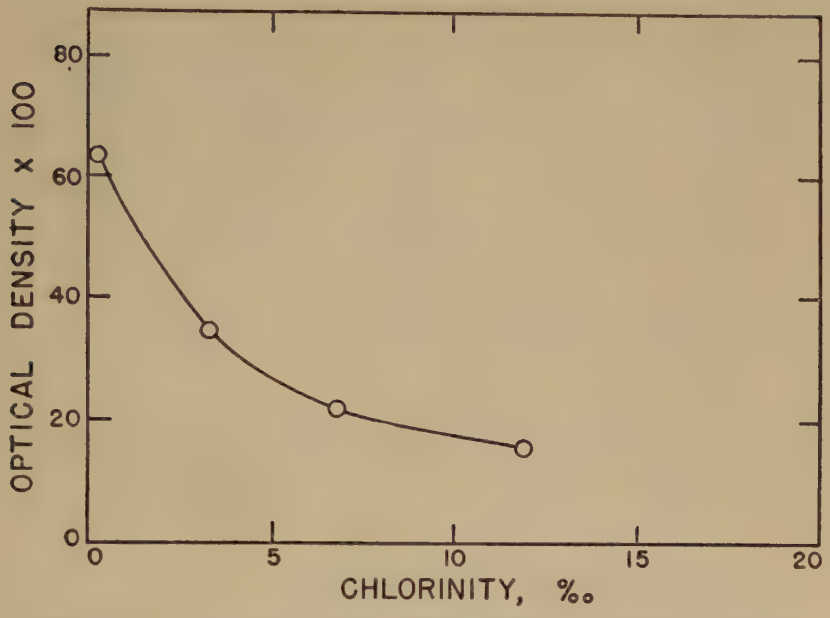

Figure 2. Arsenite color development with variation in chlorine concentration.

Elimination of Arsenic

In an attempt to eliminate interference by arsenic, a reduction procedure with sulfite was tried. It was found that, in a sea water sample digested with perchloric acid, arsenate was apparently reduced to arsenite after heating for one hour at 90° C in the presence of 0.4 g of sodium bisulfite. The method was not satisfactory, however, as the results were erratic.

In order to completely eliminate all forms of arsenic, a volatilization procedure was developed. After the sea water samples were digested for 5 minutes with perchloric acid, 3 ml of concentrated hydrochloric acid were added and rapidly fumed off. This procedure was effective when tried with samples to which known amounts of arsenite had been added. The arsenic was probably driven off in the form of arsenic trichloride.

Analysis of Sea Water Samples

The values given in Table IV were obtained when sea water samples collected in Dabob Bay were analyzed by the recommended procedure. The inorganic phosphate concentration increased with depth, as is usually the case with stratified waters. The organic phosphorus values showed no definite correlation with depth. The results in

TABLE IV. Determination of Organic Phosphorus in Sea Water

Depth (*m*)	*Temp.* (°*C*)	*Salinity* (°/₀₀)	*Phosphorus, μg-at/L* *Inorganic*	*Organic*
S	18.63	25.46	0.66	0.36
20	8.96	29.07	2.00	0.36
50	8.46	29.51	2.19	0.57
75	8.06	29.60	2.19	0.59
100	—	29.72	2.50	0.32
140	7.51	29.97	2.74	0.48
175	7.49	30.10	3.07	0.45

Location: Dabob Bay, Puget Sound, Lat. 48° 45.0′ N, Long. 122° 49.7′ N.
Time: July 20, 1950.
Tide: Ebb.

Table IV are given to illustrate the applicability of the method rather than the occurrence and distribution of organic phosphorus in sea water, which will be discussed more fully in a later paper.

SUMMARY AND CONCLUSIONS

1. Organic phosphorus in sea water has been determined after oxidation of the organic material with perchloric acid. With samples of high organic content, preliminary digestion with nitric acid should precede the perchloric acid digestion.

2. Perchloric acid is superior to sulfuric acid as a digestion medium; its salts are more readily water soluble and its blank smaller.

3. Neither perchlorate nor sulfate give a salt effect in the colorimetric determination of phosphate.

4. In the colorimetric determination of phosphate the speed of color development in a medium containing perchlorate is the same as that in distilled water, both of which have faster rates of development than a medium containing chloride.

5. Arsenite in a chloride medium yields but a slight color intensity with the phosphate reagents; in a distilled water medium its color intensity is almost equal that of an equivalent amount of phosphate.

6. Arsenic can be prevented from interfering in the determination of organic phosphorus by treatment of the samples with concentrated hydrochloric acid and volatilization of the arsenic.

LITERATURE CITED

Armstrong, F. A. J. and H. W. Harvey
1950. The cycle of phosphorus in the waters of the English Channel. J. Mar. biol. Ass. U. K., *29:* 145–162.

Cooper, L. H. N.
1934. The determination of phosphorus and nitrogen in plankton. J. Mar. biol. Ass. U. K., *19:* 755–759.
1937. Organic phosphorus in sea water. J. Mar. biol. Ass. U. K., *21:* 673–678.
1938. Salt error in determinations of phosphate in sea water. J. Mar. biol. Ass. U. K., *23:* 171–195.

Ford, W. L.
1950. Seagoing Photoelectric Colorimeter. Anal. Chem., *22:* 1431–1435.

Gorgy, Samy, N. W. Rakestraw and D. L. Fox
1948. Arsenic in the sea. J. Mar. Res., *7:* 22–32.

Hansen, A. L.
1950. Determination of organic phosphorus in sea water. University of Washington M. S. thesis.

Harvey, H. W.
1948. The estimation of phosphate and of total phosphorus in sea waters. J. Mar. biol. Ass. U. K., *23:* 337–359.

Jesseph, D. C.
1932. Determination of organic phosphorus in sea water. University of Washington B. S. thesis.

Kalle, K.
1933. Phosphate und Gesamphosphor in Beziehung zu Temperatur, Salzegehalt und Plankton an der Oberflache der islandischen Kustengewasser. Ber. dtsch. Komm. Meeresforsch., *6:* 273–299.
1935. Meereskundliche chemische Untersuchungen mit Hilfe des Zeisschen Pulfrich-photometers. V. Die Bestimmung des Gesamt Phosphorgehaltes, des Plantonphosphorgehaltes und Trubungsmessungen. Ann. Hydrogr. Berl., *63:* 195–204.

Kreps, E. and M. Osadich
1933. The organic phosphorus in the sea. Int. Rev. Hydrobiol., *29:* 221–228.

Lundell, G. E. F. and J. I. Hoffman
1945. Outlines of Methods of Chemical Analysis. John Wiley and Sons, Inc., pp. 46–47.

Kuney, J. H.
1947. Perchloric acid, friend or foe? Chem. Engng. News, *25:* 1658–1659.

Redfield, A. C., H. P. Smith and B. H. Ketchum
1937. The cycle of organic phosphorus in the Gulf of Maine. Biol. Bull. Woods Hole, *73:* 421–443.

Robinson, R. J.
1941. Perchloric acid oxidation of organic phosphorus in lake waters. Ind. Engng. Chem., Anal. Ed. *13:* 465–466.

Robinson, R. J. and T. G. Thompson
1948. The determination of phosphates in sea water. J. Mar. Res., *7:* 33–39.

Rochford, D. J.
1951. Studies in Australian estuarine hydrology. Aust. J. Mar. Freshwater Res., *2* (1): 1–116.

Selbo, M. L.
1940. Determination of total phosphorus in sea water. University of Washington B. S. thesis.
Wooster, W. S. and N. W. Rakestraw
1951. The estimation of dissolved phosphate in sea water. J. Mar. Res., *10:* 91–100.
Zinzadze, C.
1935. Colorimetric methods for the determination of phosphorus. Ind. Engng. Chem., Anal. Ed. *7:* 230.

A THEORY OF FOG FORMATION

By

ROBERT G. FLEAGLE

University of Washington[1]

ABSTRACT

It is shown that just above a cold black-body surface the effect of radiation is to warm the air, whereas just above a warm surface the effect of radiation is to cool the air. Above a height of the order of one meter the signs of the radiative temperature change are reversed. Since, as Emmons and Montgomery (1947) have pointed out, fog formation usually requires net radiation from the air, it follows that, above a cold surface, fog forms only above a certain critical height whereas above a warm surface fog forms below a critical height. Other processes which produce condensation appear to be less important.

INTRODUCTION

It has been pointed out by Emmons and Montgomery (1947) that turbulence is equally effective in conducting moisture and heat from a nearly saturated atmosphere to a colder surface. They conclude that supersaturation and condensation can be achieved only "when there is further cooling by radiation directly from the air or when saturation is not required."

Intuition suggests that the air immediately above a cold black-body surface must be heated by radiation from the warmer atmosphere, whereas the warmer air farther from the cold surface may be cooled by interchange of radiation with the surface. Thus, it appears that fog cannot form immediately above a cold surface but that it may form at a distance above the surface. Conversely, it appears that fog may form in contact with a warm surface. It is the purpose of this paper to verify these intuitive conclusions and to discuss quantitatively the conditions under which fog can or cannot form.

DISTRIBUTION OF RADIATIVE TEMPERATURE CHANGE

The rate of temperature change at a point due to radiation may be developed from Schwarzchild's equation. Bruinenberg (1946) has expressed this rate of temperature change as the sum of integrals representing the upward and downward radiation. Following Brooks (1950), Bruinenberg's equation may be written for water vapor alone in the form

[1] Contribution No. 10, Department of Meteorology and Climatology, University of Washington.

$$\frac{\partial T}{\partial t} = \frac{q}{c_p}\left(\frac{p}{1000mb}\right)^{\frac{1}{2}}\left[\int_0^{w_1}\frac{\partial}{\partial w}(\sigma T^4)\frac{\partial \varepsilon}{\partial w}\,dw + \frac{\partial S_E}{\partial w} - \int_0^{\infty}\frac{\partial}{\partial w}(\sigma T^4)\frac{\partial \varepsilon}{\partial w}\,dw\right] \quad (1)$$

if it is assumed that $\partial\varepsilon/\partial w$ is independent of temperature and that both surface and atmosphere are horizontally homogeneous. The symbols have the following meanings: T, absolute temperature; t, time; q, specific humidity; c_p, specific heat at constant pressure; p, pressure; ρ, air density; σ, Stefan's constant; ε, emissivity of water vapor; w, optical path length of water vapor between the reference height, h, and the variable height, z $({}_h\int^z \rho q dz)$; w_1, w evaluated between the reference height and the top of the water vapor atmosphere; S_E, radiation flux due to water vapor at top of the water vapor atmosphere.

The effect of radiation absorbed and emitted by carbon dioxide is not considered explicitly in what follows; this appears to be justified because the error due to neglecting carbon dioxide probably is less than that due to the approximations introduced for simplicity.

Since w is a function of the single independent variable, z,

$$\frac{\partial T}{\partial w}\,dw = \frac{\partial T}{\partial z}\,dz\,.$$

Furthermore, if calculations are made only near sea level, (1) may be written

$$\frac{\partial T}{\partial t} = \frac{4\sigma q}{c_p}\left[\int_h^{\infty} T^3\frac{\partial \varepsilon}{\partial w}\frac{\partial T}{\partial z}\,dz + \frac{\partial S_E}{\partial w} + \int_h^{0} T^3\frac{\partial \varepsilon}{\partial w}\frac{\partial T}{\partial z}\,dz\right]. \quad (2)$$

The change of sign preceding the second integral is due to the fact that below the reference height $dw = -\rho q dz$.

The problem discussed here concerns temperature lapse rates of the order of degrees per meter very near the reference height. For this case, T^3 properly may be considered constant and $\partial S_E/\partial w$ may be neglected. Thus, (2) may be written

$$\frac{\partial T}{\partial t} = \frac{4\sigma q T^3}{c_p}\left[\int_h^{\infty}\frac{\partial \varepsilon}{\partial w}\frac{\partial T}{\partial z}\,dz - \int_0^{h}\frac{\partial \varepsilon}{\partial w}\frac{\partial T}{\partial z}\,dz\right]. \quad (3)$$

The rate of temperature change may be expressed as a function of height if $\partial\varepsilon/\partial w$ and $\partial T/\partial z$ are expressed as functions of height. By combining the theoretical result of the work by Ladenburg and Reiche (1913) for very short optical paths with the summarized

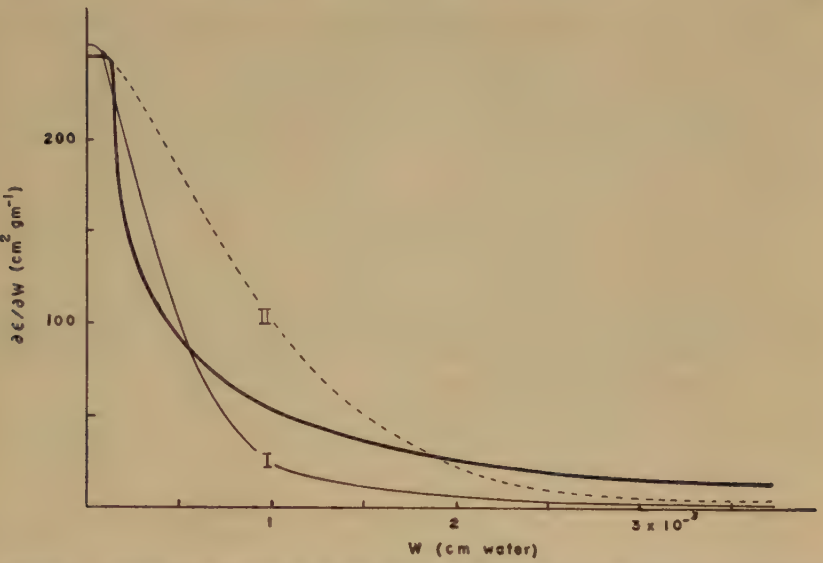

Figure 1. Slopes of the water vapor emissivity curve ($\partial\epsilon/\partial w$) as a function of optical path length (w) determined from Ladenburg and Reiche (1913) and Brooks (1950) [heavy line] and computed from equation (4), using $a = 250$ cm² gm^{-1}, $b = 3950$ cm² gm^{-1} [curve I] and $a = 250$ cm² gm^{-1}, $b = 2000$ cm² gm^{-1} [curve II].

experimental data given by Brooks (1950), it is possible to represent the dependence of $\partial\epsilon/\partial w$ on w as shown in Fig. 1 by the heavy line. This line may be approximated by the relation

$$\frac{\partial \epsilon}{\partial w} = a\,(1 + bw)\,e^{-bw}\,, \tag{4}$$

where a and b are constants to be determined from the curve.[2] It is particularly important to fit the curve accurately in the region of very short path lengths. Contrasting curves computed from two values of b are shown in Fig. 1. The slope of the emissivity curve may be expressed as a function of height if the plausible assumptions of uniform density and specific humidity are made. Then (4) becomes for the region above the reference height

$$\left(\frac{\partial \epsilon}{\partial w}\right)_{z>h} = a\,[1 + b\rho q(z - h)]\,e^{-b\rho q(z-h)} \tag{5}$$

and for the region below the reference height

$$\left(\frac{\partial \epsilon}{\partial w}\right)_{z<h} = a\,[1 - b\rho q(z - h)]\,e^{-b\rho q(z-h)}\,. \tag{6}$$

[2] The form of equation (4) was suggested by Maurice Rattray.

The temperature in the neighborhood of a ground or water surface may be expressed with fair generality by

$$T = T_0 + (T_a - T_0)(1 - e^{-\gamma z}), \tag{7}$$

where T_0 represents temperature at the surface and γ represents a constant. It follows that

$$\frac{\partial T}{\partial z} = (T_a - T_0)\,\gamma\, e^{-\gamma z}. \tag{8}$$

Undoubtedly, large differences occur in temperature lapse rates immediately before fog formation. For this reason, two different values of γ are used in the numerical examples which follow.

Upon substituting (5), (6), and (8) in (3) there results

$$\frac{\partial T}{\partial t} = \frac{4\sigma a q \gamma T^3 (T_a - T_0)}{c_p} \left\{ e^{ph} \int_h^\infty \left[(1 - ph)\, e^{-z(p+\gamma)} + pze^{-z(p+\gamma)} \right] dz - e^{-ph} \int_0^h \left[(1 + ph)\, e^{z(p-\gamma)} - pze^{z(p-\gamma)} \right] dz \right\}, \tag{9}$$

where $b\rho q \equiv p$. Integration gives

$$\frac{\partial T}{\partial t} = A \left\{ e^{-h\gamma} \left[\frac{2p + \gamma}{(\gamma + p)^2} - \frac{2p - \gamma}{(p - \gamma)^2} \right] + e^{-ph} \left[\frac{ph}{p - \gamma} + \frac{2p - \gamma}{(p - \gamma)^2} \right] \right\}, \tag{10}$$

where the coefficient of the large bracket in (9) is represented by A.

The properties of equation (10) may be most easily understood by considering numerical examples. Fig. 2 shows the vertical distribution of $\partial T/\partial t$ computed from (10) by using the following values: a, 250 cm^2gm^{-1}; b, 3950 cm^2gm^{-1}; ρ, 1.25×10^{-3} gm cm^{-2}; q, 8 gm kg^{-1}; γ, 9.0×10^{-3} cm^{-1} (A), 1.6×10^{-3} cm^{-1} (B); T, 280 K; $T_a - T_0$, $10C$; It is clear that the air immediately above the surface is warmed by radiation, whereas the air above 70 cm or so is cooled by radiation. The rate of radiative temperature change increases with increase in curvature of the temperature profile (increase in γ), but the approximate height of the boundary between the regions of cooling and warming is not affected much by change in γ. It should be understood that the rate of temperature change computed from (10) prevails only so long as the temperature profile remains essentially unchanged.

The rates of radiative cooling computed from curve II in Fig. 1 are greater than and the rates of warming are less than the rates computed from curve I, but the qualitative results are unchanged. Thus, the depth of the layer of cooling air does not appear to depend critically on the accuracy of the extrapolated emissivity curve or on the shape of the temperature profile.

If the air temperature, T_a, is less than T_0, the curves on the left side of Fig. 2 are reversed; and there is radiative cooling immediately above the surface with radiative warming higher up.

Upon setting $\partial T/\partial t$ in (10) equal to zero, the height which separates radiative warming from cooling may be determined by solving the remaining equation for h.

Differentiation of (10) with respect to h permits determination of the height of the maximum rate of temperature change, h_m, from the equation

$$\gamma e^{ph_m}\left[2p - \gamma - \frac{(2p+\gamma)\ (p-\gamma)^2}{(p+\gamma)^2}\right] + pe^{\gamma h_m}\left[2p - \gamma + (p-\gamma)\ (1 - ph_m)\right] = 0\,. \quad (11)$$

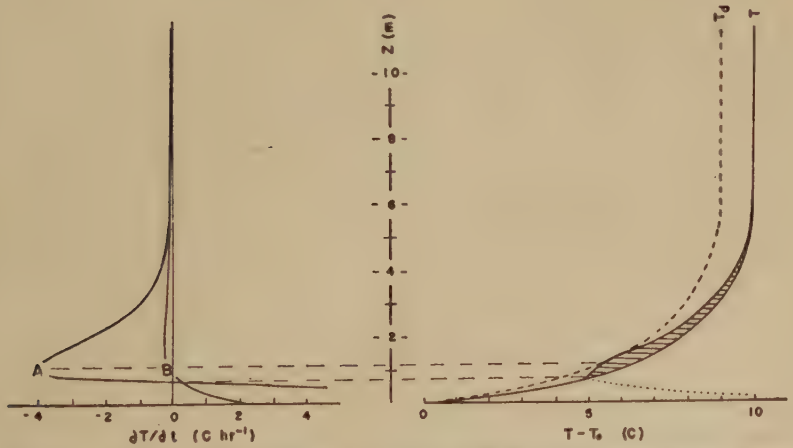

Figure. 2. *Left.* Vertical distribution of rate of radiative temperature change computed from equation (10), using $p = 3.95 \times 10^{-2}$ cm^{-1} and $\gamma = 9.0 \times 10^{-3}$ cm^{-1} (A), $\gamma = 1.6 \times 10^{-3}$ cm^{-1} (B). *Right.* Vertical temperature distribution computed from equation (7), using $\gamma = 9.0 \times 10^{-3}$ cm^{-1} (curve T), corresponding vertical distribution of dew point (curve T_d), and 15-minute radiational temperature change computed from equation (10). Dotted curve below 70 cm represents the fictitious temperature computed for this region.

THE FORMATION OF FOG

The preceding analysis of the rate of radiative temperature change near black-body surfaces indicates that fog can form only within a layer bounded on one side by the height of zero radiative temperature change. The processes which lead to fog formation above a cold moist surface are illustrated in Fig. 2. Turbulent eddies conduct heat and moisture from the air to the surface, with the result that the dew point temperature and air temperature approach one another near the surface. Immediately above the surface, radiative warming assures that the temperature does not fall to the dew point; but within the region of radiative cooling, the air temperature eventually reaches the dew point, as shown on the right side of Fig. 2. The radiation absorbed just above the surface results in only slight increase in temperature because this energy is conducted promptly to the cold surface.

Above a warm moist surface the processes which lead to fog formation are similar although the results are different. Turbulent eddies carry heat and moisture upward, with the result that the air temperature and dew point distributions are represented by a mirror image of the corresponding curves in Fig. 2 with labels reversed. Radiative cooling then occurs immediately above the surface, and radiative warming occurs above a height of the order of one meter. Thus, fog may form promptly at the surface and somewhat more slowly higher up, but fog is not likely to form above the height of zero radiative temperature change. As Emmons and Montgomery (1947) have pointed out, fog can be produced in other ways under rather special conditions; these include adiabatic expansion, condensation on highly hygroscopic particles at less than 100% relative humidity, the more rapid molecular diffusion of moisture over diffusion of heat above a warm water surface, and the mixing of saturated parcels at different temperatures. These effects appear to be less important than radiation except in special cases, e. g., rapid orographic lifting, condensation in the neighborhood of a smoke source, warm rain falling through cold air, and the emission of warm moist air from a building.

The preceding discussion leads to the conclusion that fog classification based on the physical processes responsible for producing saturation should include only two major types. Logically these may be called *cold surface fog* and *warm surface fog*. It is clear that the terms advection fog, radiation fog, steam fog, frontal fog, etc., may describe certain features of the weather situation; but they do not help very much in understanding the physical processes which bring about the fog.

After fog has formed, the physical processes are altered greatly. The fog acts essentially as a black-body radiating surface, and the

latent heat released by condensation introduces a new factor into the problem. The subsequent temperature distribution and its effect on turbulent diffusion have been discussed by Fleagle, Parrott, and Barad (1952).

OBSERVATIONS

It is extremely difficult to make accurate observations which may be used to test the validity of the preceding theory. Horizontal homogeneity seldom can be assumed in accessible locations, and turbulent motions produce large fluctuations in the temperature distributions. However, several observations which are consistent with the theory have been made.

Observations made with thermocouples mounted on a four meter mast above a fresh water lake on San Juan Island early on the morning of August 19, 1952 indicate that the air was 10.4 C colder than the water and γ was about .02. The height of zero radiative temperature change computed from these data is about 25 cm, and the rate of radiative cooling at the water surface is about .15 C min^{-1}. Visual observation indicated that the fog formed only within a layer less than a meter in thickness and formed most rapidly at the water surface, which is in substantial agreement with the computations. Air currents then carried the fog upward so that eventually the fog occupied a layer ten meters or so in thickness.

Fog formation was observed over relatively cold San Juan Channel and Friday Harbor on the evening of August 26, 1952. By directing a flashlight beam vertically, it was possible to estimate the boundaries of the fog layer. It appeared that fog formed between about one meter and ten meters above the water surface. The vertical temperature distribution measured by thermocouples at the end of a cantilever pier indicated that γ was of the order of 10^{-2} cm^{-1}; accurate determination of $T_a - T_0$ and γ was not possible because the water surface temperature varied considerably. The corresponding height of zero radiative temperature change computed from (10) is about 40 cm and the height of maximum radiative cooling computed from (11) is 50 cm.

On other occasions fog layers have been observed above the relatively cold waters of San Juan Channel and Haro Strait, but formation was not observed. In these cases the height of the lower surface of the fog varied from place to place, but generally it was a meter or so above the water surface. On one occasion the lower surface of fog in a particular region was observed to slope down to the water surface, which suggests that the water in this region was warmer than the air.

REFERENCES

Brooks, D. L.
1950. A tabular method for the computation of temperature change by infrared radiation in the free atmosphere. J. Meteor., *7* (5): 313–321.

Bruinenberg, A.
1946. Een numerieke methode voor de bepaling van temperatuurs-veranderingen door straling in de vrije atmosfeer., K. ned. meteor. Inst. Meded. Verh., B. *1* (1): 52 pp.

Emmons, G. and R. B. Montgomery
1947. Note on the physics of fog formation. J. Meteor., *4* (6): 206.

Fleagle, R. G., W. H. Parrott, and M. L. Barad
1952. Theory and effects of vertical temperature distribution in turbid air. J. Meteor., *9* (1): 53–60.

Ladenburg, A. and F. Reiche
1913. Uber selektive Absorption. Ann. Physik, (4) *42* (11): 181–209.

A RECORDING BATHYPITOTMETER[1]

By

WILLEM V. R. MALKUS

Woods Hole Oceanographic Institution[2]
Woods Hole, Massachusetts

ABSTRACT

The stability of a cable towed through the sea has suggested the use of its weighted end as a platform for velocity measurement. This report describes an instrument, lowered on standard hydrographic wire, which uses mechanical sensors to record speed, temperature, and pressure on a waxed paper roll. Initial measurements are presented which indicate that the vertical profile of an ocean current can be determined in approximately one hour.

INTRODUCTION

The direct determination of change of an ocean current with depth has become an urgent need in modern oceanography. The vertical structure of a velocity field is probably the most sensitive indicator of the physical processes which dominate its evolution. Most theories on the development of currents due to wind stress, and theories on the mixing processes that modulate this development, can be tested critically by their ability to predict this variation with depth. Also, it is essential to supplement with other data the information concerning fluid transport obtained by the geostrophic relation from density measurements; for while these density measurements are indicative of the average fluid motions, the forces responsible for the time-dependent meanders raise the most recent questions.

Such direct velocity measurements have not been made extensively because of the difficulty of creating a stable reference platform in a tossing sea. Another problem is the time element in making observations to great depth; if the velocity field is fluctuating continuously, establishing the mean velocity might require a longer period than the persistence of the investigated structure at the place of measurement.

This report describes a technique of measurement with an instrument that permits the determination of the vertical structure of a current in one hour.

[1] This work was performed under the auspices of the Office of Naval Research, Contract N6onr–27701.

[2] Contribution No. 634 from the Woods Hole Oceanographic Institution.

THE CATENARY PLATFORM

The catenary-like curve of a long wire weighted at its end and towed by a ship acts as a filter for the short period roll and pitch of a ship. The horizontal and vertical stability of the weighted end has suggested its use as a platform for velocity measurements. The difference between such a measurement and the ship's mean velocity through the surface water is the change in velocity of the ocean current between the surface and the depth of the platform. The absolute surface velocity may be found by making a lowering into quiet waters below the current, or, if none exists, by lowering to a point just above the bottom. Three difficulties confront this suggestion. The first concerns the time necessary for the catenary to come to equilibrium at a specific depth. If this time is longer than a few minutes, then the time involved in the complete measurement might be excessive. The second difficulty is the necessity of maintaining a constant mean surface velocity during the measurement. The third is the problem of shallow and surface measurements where the catenary has lost its value as a stable platform.

These problems have been resolved by using the standard 3/32″ hydrographic wire with a 150-pound instrument in the ship's mean speed range of 3½–5½ knots. It is found that the catenary attains its new equilibrium two to three minutes after changing the instrument depth 100 m. Surface velocity can be determined and maintained by a carefully checked ship's pit log, or other secondary measurement and by cautious correction of the helm.

AN INSTRUMENT

A simple rugged device whose calibration could be checked on board was sought for the velocity measurement. The pitot seemed like such a device, but it indicates speed only, not direction. The instrument developed is tentative in character due to the assumption that ocean currents have little or no change in direction with depth and that their speed alone is worth investigating. It is necessary, therefore, to determine or estimate the direction of the surface current with the Geomagnetic Electrokinetograph (von Arx, 1950), by drift measurements, by Loran or Navigation, or from the thermal structure. The ship is then headed into the current and the simple speed versus depth measurements are interpreted as indicative of the velocity. A more refined tool must embody a direction indicator as well, but this is complicated by the normal long-period fluctuations in ship direction undamped by the catenary. The pitot measurement is relatively insensitive to either small angular changes in course or to a small constant deviation of ship motion from due upstream.

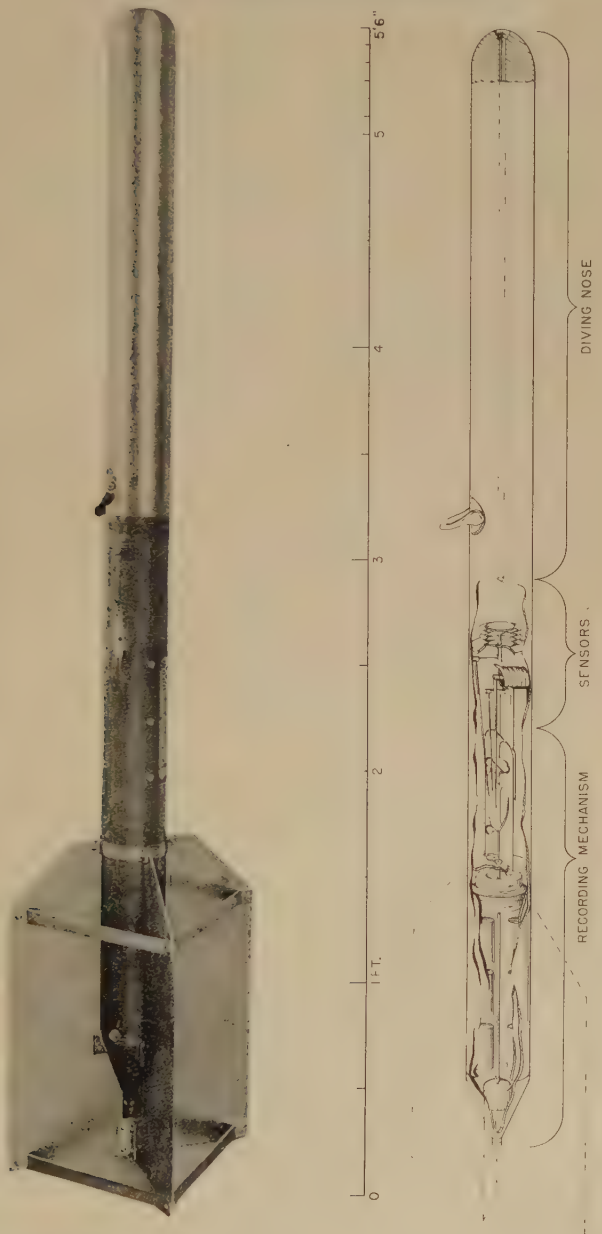

Figure 1. A schematic drawing and photograph of the complete bathypitotmeter.

The decision to record the measurements on commercially available rolls of waxed paper has influenced to a large extent the character of the sensors and auxiliary equipment used in the particular instrument which was constructed. Briefly, a sylphon bellows, activated by the pitot pressure, drives a stylus across the waxed paper. A pressure case contains batteries and a small electric motor. The motor is magnetically coupled through the pressure case to the paper, which is open to the sea. A second stylus is driven by a bourdon pressure element to measure depth. A third stylus is driven by a flushed bimetal strip to record temperature, while a fourth stylus provides a reference line to remove errors due to lateral drift of the paper. Back lash is avoided by the use of flexural couplings between sensor and stylus; these couplings also remove the problems of corrosion created by pivoted linkages. A schematic diagram and a photograph of the instrument appear in Fig. 1. The component details will be discussed in separate paragraphs.

THE SENSORS

Fig. 2 shows the three sensors and a detail of a flexural amplifier. The phosphor bronze flexure coupling is ¼″ wide, .008″ shim stock with full range deflection of ± 10° in this application. The amplification factor of the flexure is controlled by the distance between the shims and the length of the pen and can be made very large if stiffer sensors are desired. The high natural frequency of a stiff sensor reduces the problem of stylus vibration which attends the use of any sensitive indicator.

The pitot sylphon, with sturdy positive and negative stops to avoid excessive strain when the instrument is diving, has a full range of 5½ knots. Its full scale response time is less than a second.

The temperature element is a $6 \times 1.0 \times 0.1''$ bimetal; while it is thermally insulated from the water in the instrument case by the formica block in which it is mounted, it is continuously flushed by small louvres that are open to the surrounding sea. Its response time to 1/e of its final value is approximately one second. However, the attainment of final equilibrium of all sensors is limited by the frictional drag of a stylus on the paper. With the paper in motion and with the normal vibration of the whole instrument, this equilibrium is reached in less than ten seconds.

The depth-indicating bourdon is interchangeable to permit several depth scales.

Fig. 3 shows the "shallow" grid that is used to interpret a record for measurement down to 800 m.

Calibration of the pitot is accurate to ± 1/20 knot, though changes in velocity of .02 knot are easily detected between 3 and 5½ knots.

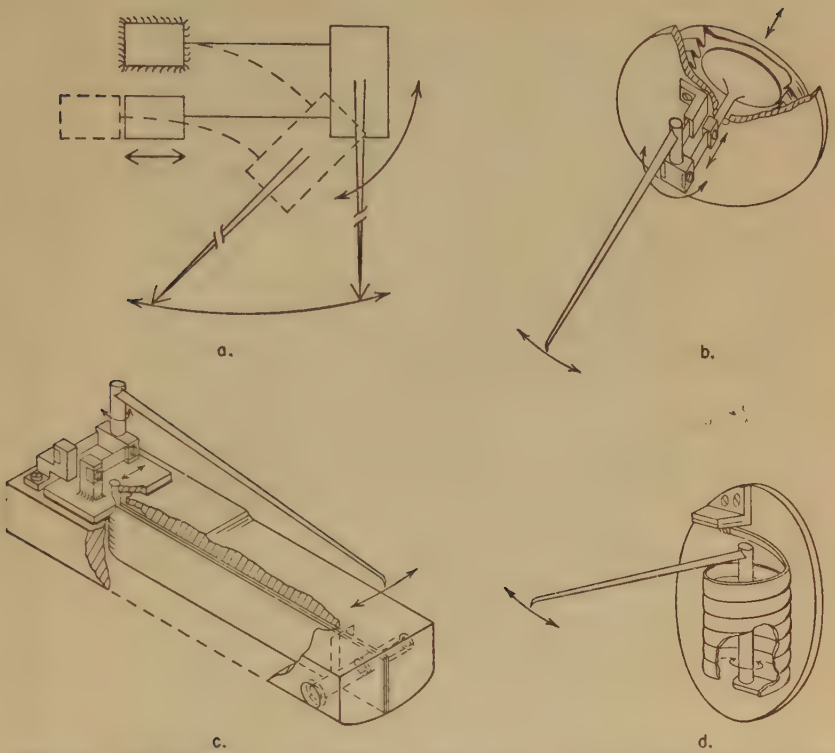

Figure 2—Detail of the sensors and their couplings: (a) a flexural amplifier; (b) the speed sensor; (c) the temperature sensor; (d) the pressure sensor.

Recalibration of the pitot aboard ship can be performed with a water manometer. Calibration of the bimetal is initially correct to $\pm$ 0.1° F, but the drift with time and use has not been ascertained.

THE RECORDING MECHANISM

An "O" ring sealed stainless steel pressure case with 1/8" walls and an inside diameter of 2½" contains batteries and the paper drive motor. A salt water switch on the tail actuates the motor when the instrument is in the sea. The batteries will last for at least 100 operating hours and can be quickly changed at sea. A permanent magnet pair, one in the pressure case and one in the sea, transmits the motion to the paper roll at 1" or 5/16" a minute, depending on the choice of an external gear. The spools which contain the paper are removed and inserted as in a camera. The waxed paper, which comes

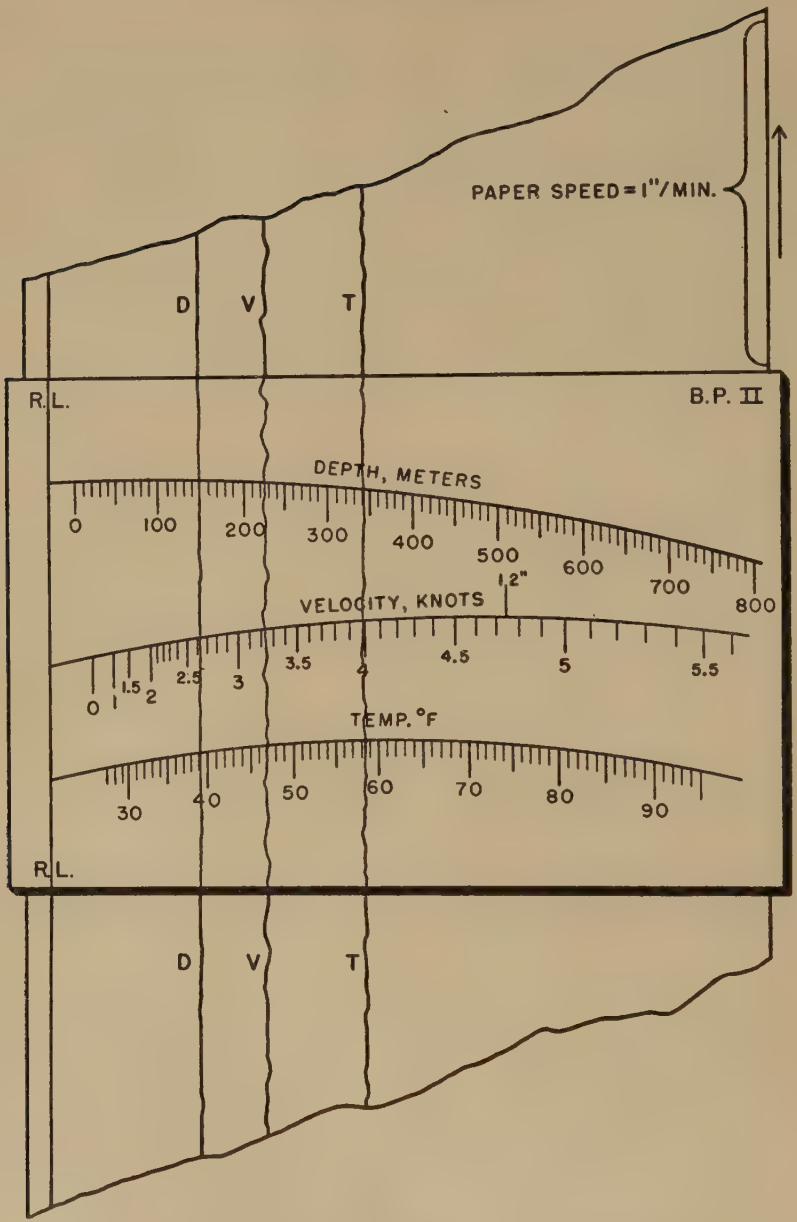

Figure 3—A calibrated grid superimposed on the waxed paper record.

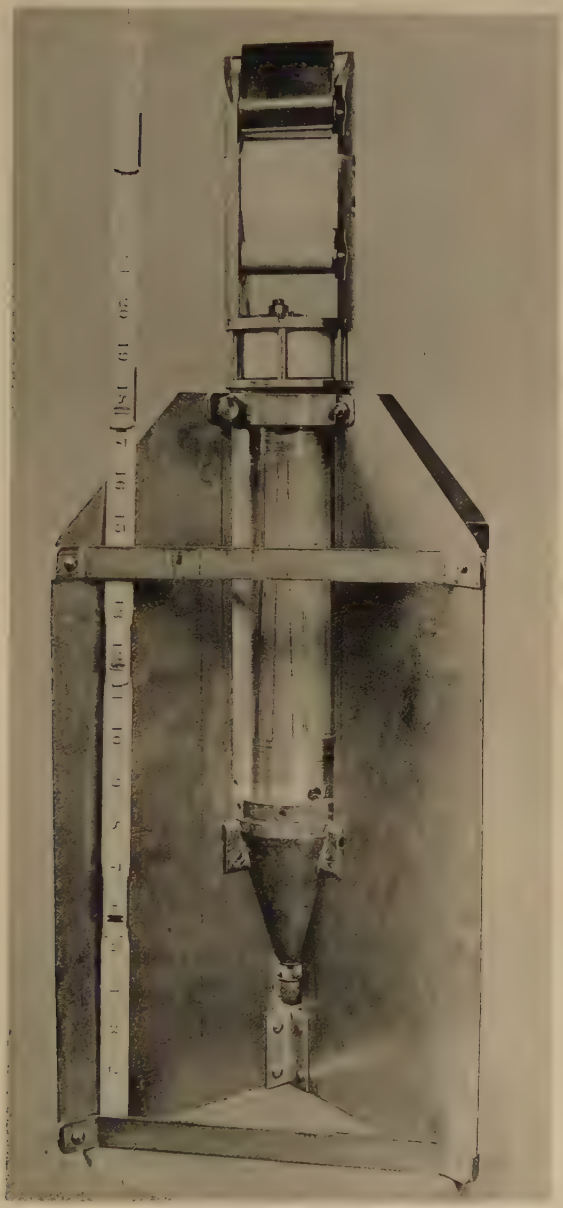

Figure 4. The recording mechanism.

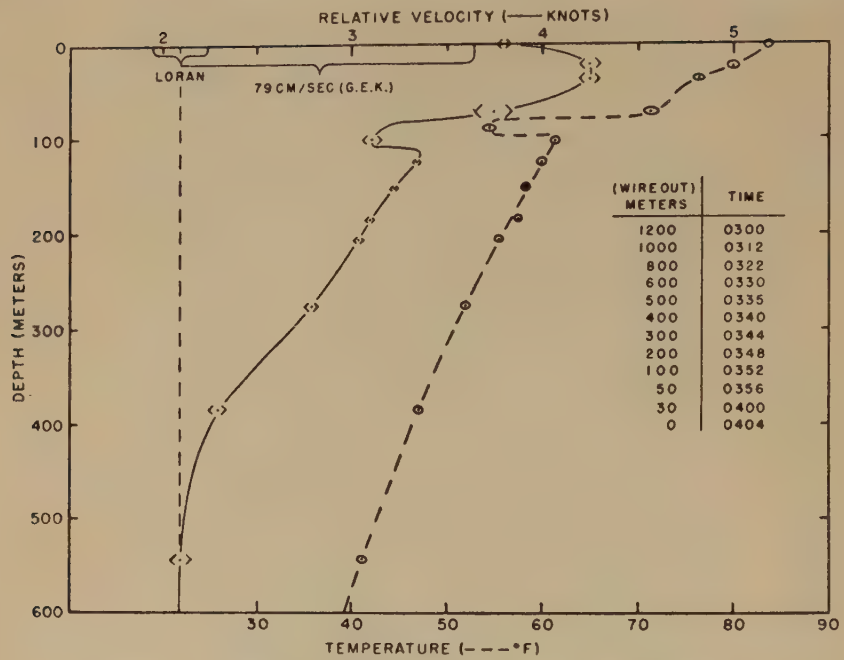

Figure 5—A sample record from the northern edge of the gulf stream.

to the surface with its back thoroughly soaked, is permitted to dry several minutes before a reading. Four knurled screws near the tail permit the withdrawal of the recording mechanisms (Fig. 4) from the body of the instrument for loading and recovery of the paper.

A SAMPLE RECORD

The following record, presented to clarify the operational use of the instrument, does not necessarily represent a typical section of a current.

In a northern edge of the Gulf Stream, off Cape Hatteras, the vessel was headed into the current at a surface speed of 3.8 knots. The direction of the surface current was established by a careful G. E. K. observation just before this operation. Triple Loran observations were made to ascertain the ship's way with respect to the earth.

After 1200 m of hydrographic wire had been reeled out, the bathypitotmeter was allowed 20 minutes to swing to its first equilibrium at 542 m depth. At this time it was assumed that the measurement commenced. The wire was then retrieved in 12 steps as indicated. The waxed paper was dried and read through a grid to produce the record given in Fig. 5. It is significant, perhaps, that fluctuations

around the mean at all depths were small and slow. They are indicated on the record by the double ended arrows at each velocity datum and by ellipses at each temperature datum.

The Loran observations, with a bracket estimating their probable error, support the indication of the lowest measurement that the water at 500 m had little or no velocity relative to the earth. The G. E. K. observations, drawn as a long bracket from the Loran "zero," is further evidence that the absolute velocity as well as the relative velocity of the stream at each depth was determined. The discrepancy between the indicated G. E. K. surface velocity and the actual surface velocity is a measure of the average total transport of fluid at this section (Malkus and Stern, 1952).

The record contains several uncommon features, such as the thermal inversion at 90 m and a maximum velocity at 30 m below the surface, but it gives evidence of how such phenomena may be observed and correlated.

The work of Mr. Angelo Cangiamila in preparing the instrument for use and in the observational program is gratefully aclnowledged. The trouble-free operation of the instrument is attributed to the ingenuity of Mr. Myron Howland, who is responsible for its construction.

REFERENCES

Malkus, W. V. R. and M. E. Stern

1952. Determination of ocean transports and velocities by electromagnetic effects. J. mar. Res., *11* (2): 97–105.

von Arx, W. S.

1950. An electromagnetic method for measuring the velocities of ocean currents from a ship underway. Pap. phys. Oceanogr. Meteor., *11* (3): 1–62.

ABUNDANCE AND GROWTH OF *VENUS MERCENARIA* AND *CALLOCARDIA MORRHUANA* IN RELATION TO THE CHARACTER OF BOTTOM SEDIMENTS[1]

By

DAVID M. PRATT

Narragansett Marine Laboratory
University of Rhode Island

ABSTRACT

The distribution patterns of *Venus mercenaria* and *Callocardia morrhuana* in Narragansett Bay are shown to be related to the character of the bottom. *Venus* is most abundant where the dominant sediments are fine, but its abundance in these sediments is strongly related to the presence of large particles such as shell and rocks as minor constituents of the substratum. The numbers of *Callocardia* are consistently correlated with the fineness of bottom sediments. A theory is advanced to explain these distribution patterns in terms of bottom current velocities, in so far as these velocities can be inferred from sediment particle sizes. It has been shown that the growth rate of *Venus* depends directly or indirectly on the nature of the substratum; populations living in sand grew 24% faster than did those living in an adjacent plot of sandy mud containing much organic matter.

INTRODUCTION

The quahog, *Venus mercenaria* L., is one of the most widely distributed and successfully adapted species of bivalves on the Atlantic Coast. In spite of a heavy fishery, it is abundant from the Gulf of St. Lawrence to the Gulf of Mexico, and it probably owes its continued success in part to a high tolerance for variations in such ecological factors as temperature, salinity and type of substratum. Its occurrence in a wide variety of substrata suggests that it is equally well adapted to several bottom types, and perhaps it is this apparent lack of preference which has led us to overlook the possible influences of sediment type on the biology of the species. There appear to be no published quantitative statements that relate the abundance or growth rate of *Venus* to the character of the bottom.

A dredging survey of Narragansett Bay has shown that the quahog is the most abundant animal of its size in or on the bottom in the estuarine waters of Rhode Island. In certain areas it is replaced by another bivalve, *Callocardia* (*Pitar*) *morrhuana* (Lindsley). The distribution patterns of these two species appear to be strongly related

[1] Contribution No. 5 from the Narragansett Marine Laboratory.

to the nature of the bottom sediments. Furthermore, the results of an experiment in which quahogs were grown in different bottom types indicate that the character of the substratum materially affects the growth rate of *Venus*.

ABUNDANCE OF *VENUS* AND *CALLOCARDIA* IN RELATION TO BOTTOM SEDIMENT TYPES

An approximately quantitative survey of the quahog populations in Narragansett Bay was conducted in 1949 and 1950. At 123 stations based on a grid of one-mile interval, samples were taken by the 37-foot dragger LIL-JOY and a commercial quahog dredge of the Fall River type. The dredge was provided with removable lead weights so that its total weight could be adjusted to approximately 200, 250 or 300 pounds, depending on the hardness of the bottom. Eight 7-inch teeth were so set that they cut a swath approximately 14 inches wide. The dredge was lowered and raised on the vessel's winch wire, but the actual towing was done on a one-inch manila line. The elasticity of the rope enhanced the efficiency of the drag. For this work, the chain-link bag which caught and sifted the material dredged by the teeth was lined with a twine bag of such a mesh that a quahog 36 by 31 mm could barely be forced through it. Drags were standardized to four minutes at a fixed setting of the vessel's throttle which gave a speed of approximately three knots. The skilled assistance of Captain R. E. Sutcliffe throughout this work is gratefully acknowledged.

There are three disadvantages to this dredge as a sampling device. (1) In this and similar dredges (as opposed to grabs) the spatial relationships between different materials sampled are destroyed by thorough mixing; that is, two or more strata of different sediments are so mixed that they lose their identities. (2) Where there are insufficient amounts of cohesive materials, such as clay or organic silt, fine particles are washed out and hence the sediment sample obtained is not representative. Fortunately, in most parts of Narragansett Bay the dominant sediment is a mud high in organic content. From such bottoms the dredge always recovered large sediment samples (usually more than a bushel) in which the minor constituents such as sand and shell fragments were retained. It is believed that relatively few of the samples collected in this survey suffered serious alteration through washing. (3) Its efficiency is reduced on rocky bottoms, where the dredge digs and bounces, as evidenced by the alternate straining and relaxation of the towline. Thus the amount of material dug and passed through the bag is relatively less than that taken in a normal drag on soft bottom. This last drawback is more serious than

the first two in that it concerns the reliability of sampling objects (such as adult quahogs) which are theoretically large enough to be captured quantitatively.

However, this type of dredge is advantageous in that it is possible to secure a large sample of the bottom and its populations in a single operation. Experience of quahog fishermen has shown that the distribution of individuals in a bed is spotty, the numbers often varying greatly from one square yard to the next; hence a large number of grab samples is required to make an adequate census. In the dredge sample this unevenness is averaged out. Thus, in spite of its failings, the dredge appears to be especially suited to rapid and approximately quantitative quahog sampling in an extensive area such as Narragansett Bay. Repeated sampling at various localities has produced consistent results; except where rocks were numerous, the dredge sample gave a reliable index (if not an absolute census) of the relative concentration of quahogs.

The character of the bottom was judged by gross inspection of the dredged material. Five types were distinguished by appearance and feel: clay, mud, sand, shell, and rocks, the last defined as stones bigger than a man's fist. A description of the bottom at each station consisted primarily of one of these, usually with one or more additional materials as minor constituents. Although no quantitative measurements were made of particle size distribution, it is felt that the classification of the five sediment types is based upon differences which are readily appreciable without refined means of measurement. The distinction between clay and mud may be questionable. The term "clay," rarely used, was applied only to decidedly plastic matter. A proper sedimentological study of the area would likely reveal considerably greater amounts of clay, particularly as a minor constituent.

Venus mercenaria

This survey showed that the main centers of quahog abundance are concentrated in the inner (northern) areas of the Bay. No doubt its distribution reflects the influence of salinity (and possibly temperature) as well as several other factors, one of which appears to be the character of the bottom.

The average number of quahogs captured per standard drag in each of the types of bottoms sampled is given in Table I. In several cases the dragging time exceeded four minutes, and many of the stations were sampled more than once. In Table I all samples are reduced to numbers per four minute drag, and all drags at each station are averaged to give a single figure for the station. All told, approximately 9,000 quahogs were taken in the course of the survey.

Of the five types of bottom materials, only three occurred as major constituents: mud, sand and rocks. In Table I the quahog abundance is correlated with these three in the order just named: bottoms chiefly of mud yielded an average of 39 quahogs per four-minute drag; sand, 36; rocks, only 8. Due to the relatively inefficient operation of the

TABLE I. MEAN ABUNDANCE OF *Venus mercenaria* AND *Callocardia morrhuana* IN RELATION TO BOTTOM TYPE

Bottom Materials		*Venus*		*Callocardia*	
Major constituent	*Minor constituents*	*Stations sampled*	*Mean number per drag*	*Stations sampled*	*Mean number per drag*
MUD	——	31	15	25	13
	sand	9	70	8	8
	rocks	5	15	4	3
	clay	6	2	6	45
	shell	9	50	7	7
	sand, rocks	6	16	6	16
	sand, clay	5	14	5	20
	sand, shell	3	157	1	12
	rocks, shell	4	81	1	25
	sand, rocks, clay	1	0	1	0
	sand, rocks, shell	3	191	3	2
	sand, clay, shell	1	37	1	2
		Total 83	Mean 39	Total 68	Mean 14
SAND	——	4	3	4	0
	mud	7	32	7	9
	rocks	5	9	4	3
	shell	3	31	2	0
	mud, rocks	3	34	3	4
	mud, shell	7	52	5	8
	rocks, shell	2	2	2	1
	mud, rocks, shell	3	129	3	2
		Total 34	Mean 36	Total 30	Mean 4
ROCKS	sand	2	0	2	0
	shell	1	2	1	2
	sand, shell	3	15	3	3
		Total 6	Mean 8	Total 6	Mean 2
Grand Totals and Averages		123	36	104	11

dredge in rocky bottoms, it is probable that all of the figures given for quahog numbers in such locations are low. This conclusion is supported by the opinion, universal among local fishermen, that rocky areas, while difficult to work, are frequently rich in quahogs.

The data may also be used for a comparison of the average population density in bottoms *containing* each of the different sediment types, i. e. by calculating the average numbers in all bottoms that include clay, the average in bottoms containing mud, and so forth. This comparison (see Fig. 1) shows that, on the average, bottoms containing clay support the sparsest populations, those containing shell the densest populations, with mud and sand intermediate. Here

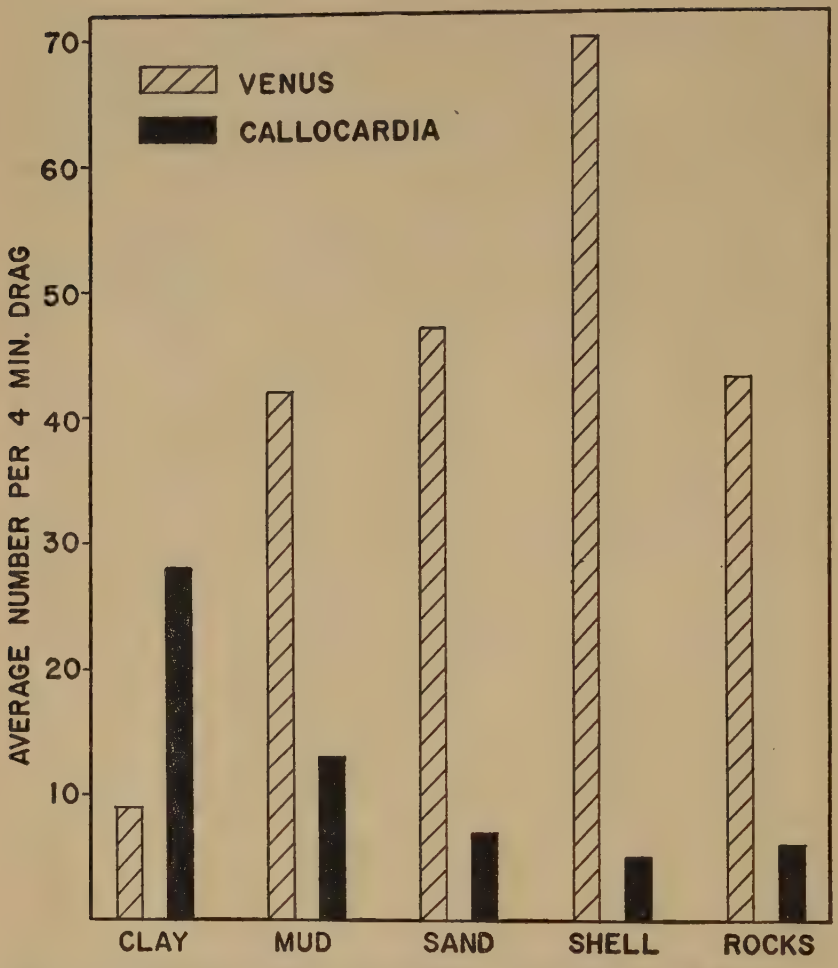

Figure 1. Abundance of *Venus* and *Callocardia* in bottoms which include different sedimentary materials.

again the average number given for bottoms that include rocks is probably low. "Shell" consists of fragments and whole shells of a number of mollusks including *Crepidula*, *Anomia* and *Venus*, as well as *Ensis*, *Callocardia*, *Mya*, *Ostrea*, and others. Although the quahog shells were outnumbered in most cases by those of other species, we have here a good example of an animal's presence altering the environment so as to render it more favorable to its progeny.

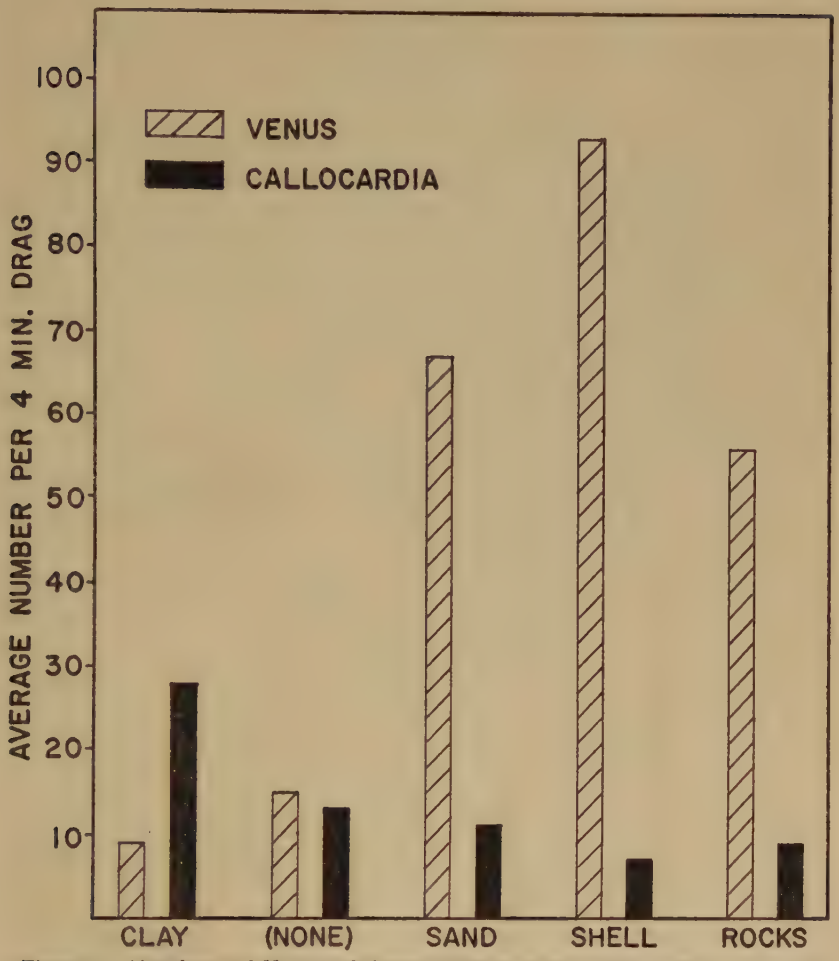

Figure 2. Abundance of *Venus* and *Callocardia* in predominantly muddy bottoms when such bottoms are classified by the presence of minor constituents.

In a third comparison (Fig. 2), numbers of quahogs are correlated with the presence of clay, sand, shell and rocks as minor constituents of bottoms consisting mainly of mud. This figure closely resembles the preceding one because mud is the dominant sediment of the Bay, and the great majority of quahogs were taken from such bottoms. As noted above, bottoms with mud as the major constituent maintain, on an average, the densest populations. From Fig. 2, however, it is clear that the virtue of mud bottoms depends largely on sand and shell as

minor constituents, since mud alone appears to be a poor environment, scarcely better than mud + clay. Rocks might also prove to be a beneficial minor constituent of mud if truly representative samples could be dredged from areas containing them.

The abundance of quahogs is correlated with particle size of the bottom sediments in a consistent if somewhat complex fashion. Population density is negatively correlated with the particle size of the major bottom constituent: greatest average concentration in predominantly muddy grounds, less in sandy bottoms, and least in rocky areas—see Table I. However, when bottoms are classified on the basis of the inclusion of each of the five materials, as in Fig. 1 (in which sediment types are arranged in series from fine to coarse particles), quahog abundance increases with increasing particle size (again with the exception of rocks). The same relationship holds between population density and particle size of the minor constituents when bottoms consisting chiefly of mud are compared *inter se* (Fig. 2). To sum up, quahogs are most abundant in predominantly fine sediments, but in such sediments their abundance is generally a function of the coarseness of the minor constituents.

Whether this relationship of quahog numbers to sediment particle size results from an active selection of substratum by the settling larvae or from factors quite beyond their control is a question that cannot be answered from available information. However, an explanation of the observed distribution in terms of entirely passive behavior seems plausible. In the absence of current measurements along the bottom of Narragansett Bay, it is reasonable to assume that in general fine bottom sediments indicate low current velocities, coarser sediments progressively greater velocities. At any given locality the abundance of quahogs of the sizes sampled by the dredge must have been determined by the numbers of viable larvae which set and survived, and the speed of the bottom currents probably affected both setting and survival. Presumably a low current velocity favors setting, but it probably also results in three conditions adverse to survival: (1) rapid deposition of fine silt which may bury or smother the young set, (2) low rate of supply of food and oxygen, and (3) slow removal of metabolic wastes. On the other hand, a high current velocity probably allows only limited setting of the larvae and may cause a grinding action of coarse particles severe enough to injure the spat, but undoubtedly it favors survival by high rates of food and oxygen supply and waste removal.

If quahog distribution with reference to sediment types is related to these current effects, then current velocities which produce the optimal combined effect on setting and survival are somewhere in the

range of those that occur over predominantly muddy grounds. By comparison, currents which are fast enough to reduce setting and survival, particularly of the spat, occur over sandy areas and dominantly rocky bottoms.

Pursuing these ideas further, let us consider the varying abundance of quahogs in bottoms constituted primarily of mud. Theoretically, bottoms of mud + clay (followed in close sequence by mud alone) would be associated with minimal currents which contribute to heavy setting but low survival. Mud + sand would be related to somewhat faster currents whose combined effects should result in much denser populations. The presence of shell and rocks would indicate currents of sufficient speed to prevent the burial of these larger constituents by finer sediments. However, in such situations, where rocks and shells break the bottom surface to form pockets and hollows, small depressions probably result in very local but sharp reduction of the current velocity, thus assisting the deposition of larvae and affording protection against molar action. Shell and rocks would thus make it possible for quahogs to profit from the favorable effects of high current velocities while escaping their unfavorable effects.

Theoretically, by comparison with bottoms of mud only, one should expect to find greater average concentrations in each of the following types of mud bottom: (1) mud (major constituent) + sand (minor constituent), (2) mud + rocks, (3) mud + shell, (4) mud + sand and rocks, (5) mud + sand and shell, (6) mud + rocks and shell, and (7) mud + sand, rocks and shell. The data in Table I bear out these expectations, possibly with the exception of (2) and (4), in which the population densities are not as high as anticipated. However, failure to support the theory in these cases may have been due to the inadequacy of the dredge in rocky grounds. If mud + clay signifies slower currents than mud alone, one should expect quahogs to be scarcer in mud + clay. This is indeed the case. The combination of clay with any other minor constituent in mud gives contradictory indications of current velocity and cannot be interpreted according to the theory. Indeed, it is possible that clay has some special effect on quahogs that is not related to current speed—an effect on behavior such that spat avoid clay when setting, or a detrimental effect on postlarval survival.

Areas containing sand as a major sediment and mud as a minor constituent can be interpreted as indicating slower currents than those in areas containing only sand. If, as already assumed above, the optimal current velocities for the development of adult populations is of the order that results in predominantly muddy deposits, then sandy bottoms containing mud should be more suitable than those lacking mud. As in muddy bottoms, the presence of shell or rocks in

sandy bottoms should render the substratum more favorable for quahogs. Thus the addition of mud, shell or rocks should increase the average quahog capacity of sandy habitats. Table I shows seven types of sandy bottoms so modified, and in all but one (sand + rocks and shell) the expectations are confirmed. The interference of rocks in the operation of the dredge may account for the exception.

The data for quahog numbers in primarily rocky bottoms are too scanty to warrant analysis or interpretation according to current speed.

The attempt to relate quahog abundance to current velocity rests on the plausible assumption that current velocity is statistically related to sediment particle size. If we then take into account the fact that the population figures for bottoms containing rocks are probably erroneously low, the dual relationship of quahog numbers to sediment types can be explained to a large extent and in consistent detail on the basis of the combined effects of current velocity upon set and survival.

It should be noted that the highest mean concentrations of quahogs occur only in the presence of shell, usually accompanied by rocks. Provided that quahog abundance is truly related to current velocity as postulated, this fact would indicate that shell and rocks are indeed effective in inducing set and probably in affording protection to the young spat.

Callocardia morrhuana

Early in this survey, *C. morrhuana*, which closely resembles small specimens of *Venus*, attracted attention because of its abundance and distribution, which appeared to complement that of *Venus*. One or the other species was taken at all but 15 stations, usually in reciprocal numbers, which were clearly related to the character of the bottom.

The abundance of *Callocardia* with reference to sediment types has been analyzed in the same fashion as that of *Venus*, and the results are presented in Table I and Figs. 1 and 2. The information for this species is less complete than that for *Venus*, since no record of *Callocardia* numbers was kept in the early phase of the survey. The distribution of *Callocardia* is similar to that of *Venus* in two respects: (1) both species occur in greater average numbers in predominantly muddy bottoms than in sandy or rocky areas, and (2) where sand is the major constituent, the presence of mud favors both species. Here the resemblance in distribution ends. If the sediment type is judged on the basis of inclusion of each of the five bottom materials (Fig. 1), then *Callocardia* population density decreases steadily with increasing sediment particle size. Likewise, where the major bottom constituent is mud, *Callocardia* is progressively less abundant with increasing particle size of the minor constituents (Fig. 2).

Thus the abundance of *Callocardia* is consistently correlated with fineness of bottom sediments. If this distribution pattern is also interpreted on the basis of presumed current velocities, the data suggest that minimal currents produce the optimal effect upon set and survival of *Callocardia*. Under this interpretation it might be assumed that minimal currents result in maximal setting, that survival under these conditions is not reduced as in the case of *Venus*, and that faster currents with their attendant molar action do not result in greater survival of *Callocardia*, even when shell and rocks are present. According to this view, the observed differences in distribution between *Callocardia* and *Venus* result, at least in part, from such factors as: (1) differences in resistance to silting and low rates of food and oxygen supply in slow currents, and (2) differences in ability to withstand molar forces in faster currents.

However, factors other than current speed may well have been influential in bringing about the contrasting patterns of distribution. There may be differences in behavior of the larvae of the two species at the time of setting, including the active selection or avoidance of certain substrata because of textural or other qualities. This possibility seems particularly strong where clay is involved as a minor constituent of the bottom. It seems unlikely that the presence or absence of clay in predominantly muddy bottoms indicates significant differences in current velocities. For this reason the considerable effect which clay has on the relative numbers of the two species strongly suggests active selection by *Callocardia* and avoidance by *Venus* of substrata containing clay. For an excellent discussion and review of literature on the active selection of substrata by the planktonic larvae of benthonic invertebrates, see Wilson (1952).

GROWTH OF *VENUS* IN RELATION TO BOTTOM TYPE

A problem that has been largely neglected is whether the nature of the substratum has any influence, direct or indirect, upon the growth rate of *Venus*. Apparently the only study of this problem is one conducted by Kerswill (1941) in the course of an extensive investigation of environmental factors that affect the growth of *Venus*. Two groups of 50 quahogs were grown in adjacent plots, one consisting of "sandy mud," the other of "clean sand." At the end of one growth season no significant difference in growth was observed.

To compare more amply the growth of quahogs in two different types of bottom materials under otherwise theoretically identical conditions, the following experiment was preformed. In mid-November of 1950, eight bottomless wooden frames, each four feet square and eight inches deep, were forced into the bottom of Wickford Harbor

until their tops were nearly flush with the bottom surface. They were so placed as to be exposed on only the extreme low tides. The sediment here was classified, on gross inspection, as sandy mud (see below for analysis), black with added organic matter, and smelling rather strongly of H_2S. For simplicity this material will be referred to as "mud." In four of the frames the indigenous mud was replaced with sand of a medium coarseness; the mud in the remaining frames was left unaltered except for the removal of native quahogs. Four hundred measured quahogs ranging from 20 to 50 mm long, with a sharp length-frequency mode at about 30 mm, were planted in each frame. The water temperature at the time averaged about 10° C, below which quahog growth is negligible (Belding, 1931; Kerswill, 1941). To determine the amount of growth during different parts of the growing season as well as in an entire year, the animals from one sand frame and one mud frame were removed, measured and replaced on June 18, 1951, those from a second pair of frames were observed on July 16, from a third pair on September 14, and all were removed and measured on November 27, 1951. This schedule left one sand frame and one mud frame undisturbed for an entire year so that any interruption in growth due to the temporary removal of the animals from the other frames during the growing season could be detected. In every digging more than 85% of the quahogs were recovered; in most cases more than 90%.

At the end of the year's observations, sediment samples from the frames were analyzed for particle size distribution by Mr. Ivory A. Canty, to whom I am indebted. By this time the surface layer in the sand frames (about one inch or so) had received from the water an admixture of finely divided black organic matter such as that which characterizes the local bottom. The samples, after purging of the organic matter with H_2O_2, were analyzed by a combination of sieve and hydrometer methods. The results (Table II), after removal of the organic content, showed that the "mud" was actually half sand and half silt-plus-clay, while 96% of the "sand," both at the surface and below, consisted of particles classed as sand or larger. The only conspicuous change that occurred during the year in these surface layers was not detected by this analysis, viz., the addition of organic matter.

Growth was determined by measuring the total shell length of each individual recovered in each frame, by plotting the length-frequency curve for comparison with the original curve, and by noting the shift of identifiable peaks. In most of the comparisons there were seven or more positive features common to the two curves, hence growth increments over the entire range of sizes could be read with ease.

Since these increments usually varied by less than 2 mm in any given comparison of curves and since they showed no consistent relation to the absolute length, they have been averaged to obtain a single mean increment for each frame in each growth period.

For the four populations living in sand, the means of annual growth varied from 15.3 to 16.3 mm, and the mean for the population left undisturbed throughout the year was 16.1 mm. For the populations in mud frames, the annual mean increments ranged from 11.7 to 13.7 mm, and the population left undisturbed grew 13.2 mm. Since the

TABLE II. Particle Size Distribution of Sediments in Experimental Frames

Particles	*Size range*	*"Mud"*	*Sand, top inch*	*Sand, subsurface*
Pebbles	>3.96 mm	1.2%	4.1%	6.9
Granules	3.96–1.98	0.1	3.2	8.3
Sand	1.98– .062	50.7	89.2	81.2
Silt	.062–.004	34.2	2.6	2.1
Clay	<.004	13.8	1.0	2.0

means of growth in the undisturbed frames were not the highest observed in either sand or mud, evidently the temporary removal of animals from other frames in midseason did not seriously interrupt their growth. In growth studies of *Venus*, therefore, we conclude that measurements of progress during various parts of the growing season can be made without fear of influencing the outcome of the investigation.

Growth Relative to Type of Sediment. To obtain a comparison of growth in the two kinds of bottom materials, all of the individual measurements of annual increment in sand and in mud were averaged. Twenty-three measurements of annual increment, obtained from the four populations in sand, yielded a grand average of 15.93 mm, with a standard deviation of 0.968. Populations in mud (28 measurements) showed a grand average annual growth of 12.89 mm, standard deviation 1.071. The standard error of the difference is 0.292. The observed difference between the means is more than ten times the standard error and thus can hardly have arisen from chance variation.

On an average, the quahogs in sand grew 24% faster than did those living in mud, and this difference is shown to be highly significant. No observations were made which might have explained the difference in growth. Since the frames were contiguous, the water cannot have varied from one frame to the next, except as it may have been locally influenced by the sediments in the frames. Therefore the difference

in growth rate must have arisen directly or indirectly from benthonic factors. What these might be we can only surmise. Loosanoff and Tommers (1948) have shown that suspended silt has a marked effect on the pumping rate and hence on the feeding of oysters; as little as 0.1g of silt per liter of water reduced the average pumping rate 57%, and the oysters expelled large amounts of silt as pseudo-feces. Quahogs probably react to suspended silt in a similar manner. The necessity of frequent clearing of the animal's filtering apparatus might seriously interfere with the process of feeding, thus reducing appreciably its total nutrition. In the mud frames the currents may have kept the water along the surface of the bottom roiled with silt, whereas in the sand frames this thin but important layer of water may have been relatively free of suspended silt. Such a difference in the microenvironment and in the relative feeding efficiency of the quahogs might account for the observed difference in annual growth. The amounts of dissolved oxygen in the water just above the bottom may also explain the difference: perhaps the mud bottom, rich in decomposing organic matter, reduces the oxygen content of the water much more than does the sand.

Growth by Season. As noted above, the populations in mud and in sand showed somewhat various annual increments. These variations must be taken into account in calculating the increments for the different parts of the growth season in order to arrive at figures representative of all four populations in each bottom type. Accordingly the partial increments have been adjusted to the grand averages for the year's growth in sand and in mud. Each increment (Table III) bears the same ratio to the mean annual growth in sand or in mud as the observed partial increment bears to the observed annual growth in the given population.

If we can assume that the period of constructive growth coincides approximately with that in which water temperatures are 10° C or higher, the growth season in 1951 lasted from mid-April to mid-November according to a semiweekly temperature record kindly supplied by Mr. Warren S. Landers of the U. S. Fish and Wildlife Service. During mid-April to mid-July the animals living in sand put on more than 50% of their year's growth, those in mud about 75%. Furthermore, plankton studies by Mr. Landers show that the great bulk of the year's quahog spawning at this locality occurred in June and early July. The period of most rapid growth came earlier in the season than it does in the waters of Cape Cod, where, according to Belding (1931), August and September show the fastest growth. In the Bideford River, Prince Edward Island, more than half of the

year's growth occurs between mid-July and mid-September (Kerswill, 1941). Annual differences may account in part for these discrepancies.

In an attempt to explain the distribution of growth in the growing season, the temperature record and a series of weekly plankton samples from mid-April to mid-November have been analyzed without satisfactory results. The temperature record yields a fairly symmetrical curve with a maximum 2-week average of 24.0° C in the latter half of July (absolute maximum of 25.7° August 13). Temperatures of 10°–22.5° were associated with the rapid growth between mid-April and mid-July, and with growth at a much lower rate (especially in mud) from September 1 to mid-November. The plankton samples, preserved in 1% neutralized formalin, were collected by pouring 50 gallons of water through a net in which the mesh apertures averaged approximately 45 μ in their greatest diameter; for these I am again indebted to Mr. Landers. Qualitative and quantitative studies of these samples have failed to yield an explanation for the more rapid growth in spring and early summer than in subsequent months. Indeed, several categories of objects, notably the plants and animals with greatest dimension less than 75 μ, were counted and were found to be relatively scarce until late August, after which they reached great maxima in September and October when quahog growth was slow. It is quite possible that particles too small to be retained quantitatively by the net, particularly nannoplankton forms which disintegrate even in dilute preservations, constitute an important part of the quahog diet.

TABLE III. Growth by Parts of the Year, Adjusted to the Mean Annual Growth in Sand and in Mud (See Text).

	Sand		*Mud*	
Period	*mm*	*% of total*	*mm*	*% of total*
Before 18 June	6.1	38	3.8	29
18 June–16 July	3.2	20	6.0	47
16 July–14 Sept.	4.3	27	2.9	22
After 14 Sept.	2.6	16	0.2	2

Mortality of quahogs during the experiment was light and appeared to be randomly distributed as regards size and seasons. Totals for the year were: sand, 59 (3.7%); mud, 77 (4.8%).

As in studies by other investigators, size and growth of quahogs in this experiment are expressed in terms of a linear dimension of the shell. Such measures can be made rapidly, easily, and exactly, and they bear a fairly constant relationship to total volume. However, other possible measures, such as weight or carbon content of meats, would probably give more meaningful indices of size and growth, particularly in inter- and intra-seasonal studies. Growth of soft

parts, i. e. excess of assimilation over catabolism, in a given interval of time is perhaps not reflected in increased shell dimensions until after a lag of unknown duration. If this is true, measurements of the shell cannot give an accurate record of growth of the soft parts by months or other subdivisions of the annual cycle.

SUMMARY

1. The distribution patterns of *Venus mercenaria* and of *Callocardia morrhuana* in Narragansett Bay are complementary in general and show decided correlations with the character of the bottom. *Venus* is most abundant in bottoms consisting principally of fine sediments, but its abundance in these sediments is strongly related to the presence of large particles such as shell and rocks as minor constituents of the substratum. Again, if bottoms are classified on the basis of the inclusion of each of the recognized sediment types, quahog numbers vary directly with particle size. The abundance of *Callocardia* shows a consistent inverse correlation with the particle size of bottom sediments.

2. It has been shown that the growth rate of *Venus* depends directly or indirectly on the nature of the substratum: populations living in sand grew 24% faster than did those living in an adjacent plot of sandy mud containing much organic matter.

REFERENCES

Belding, D. L.

1931. The quahog fishery of Massachusetts. The Commonwealth of Massachusetts. Marine Fisheries Series—No. 2.

Kerswill, C. J.

1941. Some environmental factors limiting growth and distribution of the quahog Venus mercenaria L. Ph.D. thesis, University of Toronto.

Loosanoff, V. L. and F. D. Tommers

1948. Effect of suspended silt and other substances on the rate of feeding of oysters. Science, *107:* 69–70.

Wilson, D. P.

1952. The influence of the nature of the substratum on the metamorphosis of the larvae of marine animals, especially the larvae of *Ophelia bicornis* Savigny. Ann. Inst. oceanogr. Monaco, *27:* 49–156.

THE CHAETOGNATHA OVER THE CONTINENTAL SHELF OF NORTH CAROLINA WITH ATTENTION TO THEIR RELATION TO THE HYDROGRAPHY OF THE AREA[1]

By

E. LOWE PIERCE

Department of Biology, University of Florida

ABSTRACT

A series of vertical plankton samples and hydrographic data were obtained over and somewhat beyond the continental shelf off North Carolina by the Albatross III during four cruises covering the period from 24 May to 14 June 1949. Continental shelf, continental slope, and Florida Current waters were found in the area sampled. Initial mixing between the water masses apparently occurs near the edge of the continental shelf. Eleven species of chaetognaths were found in characteristic combinations depending on the water mass sampled. The greatest number of species was collected in a zone near the edge of the continental shelf where the hydrographic data indicate that mixing took place among the three water masses. These results show that the distribution of chaetognaths was directly related to the water masses in the area studied.

At a number of hydrographic stations made by the Albatross III between 24 May and 14 June 1949 (cruises 18, 19, 21, and 22), vertical plankton samples were collected over and somewhat beyond the continental shelf off North Carolina. This was a cooperative undertaking between the U. S. Fish and Wildlife Service and the University of North Carolina Institute of Fisheries Research. Woods Hole Oceanographic Institution also participated by sending observers and by analyzing the temperature and salinity distribution of the area. Since the published information concerning chaetognaths south of Cape Hatteras (Conant, 1895; 1896) is meager and since extensive hydrographic data accompanied the samples, some of which were taken in the Florida Current, it seems worthwhile to enumerate the species and to consider their relationship to the hydrography of the region.

[1] I am grateful to Dr. Wm. H. Sutcliffe of the Bermuda Biological Station for use of the samples which he collected during the above cruises. At that time he was on the staff of the University of North Carolina Institute of Fisheries Research. Mr. Dean F. Bumpus of the Woods Hole Oceanographic Institution has supplied numerous data on temperature, salinity and density distribution collected during these cruises as well as additional unpublished information concerning the hydrography of the southeastern Atlantic Coast; he also aided greatly in interpreting these data. I wish to thank Miss Ester Coogle, staff artist, for the drawings in this paper.

Description of Area Sampled. The continental shelf off North Carolina between Cape Fear and Cape Hatteras runs in a northeasterly direction and tapers from a width of 57 miles at Cape Fear to 21 miles off Cape Hatteras. The depth over the larger portion of the shelf ranges between 30 and 50 m. In fact, as a rule it is only on its outer edge that depths exceeding 60 m are encountered. Beyond the edge of the shelf, southeast of Cape Fear, the continental slope is gradual and reaches a depth of 600 m in five miles. In the Cape Hatteras area, about three miles southeast of the shelf and beneath the axis of the current as observed in these cruises, the depth is some 3,000 m.

Collection of Samples. The samples were collected by means of vertical hauls with a 0.5 m net. Its upper portion was made of number zero mesh and its lower portion of number two mesh. In the shallower water over the shelf the net was lowered to within a few meters of the bottom and then pulled to the surface, but near the edge of the continental shelf, or just beyond, the net was usually lowered between 100 and 200 m before being pulled to the surface; beyond the shelf the net was usually hauled through more than 200 m. This procedure, of course, resulted in filtering variable quantities of water at different stations. Therefore the actual number of specimens in a given sample cannot be compared exactly with those of another sample, and this is especially so regarding inshore and offshore samples. Of the 47 plankton samples obtained, 39 contained sufficient numbers of chaetognaths to warrant counting. Because of the uncertainty in identifying specimens less than 5 mm long, such data have been omitted. The general area of sampling extended from Cape Fear southeastward for approximately 150 miles and northeastward principally over the continental shelf to some 50 miles north and east of Cape Hatteras (Fig. 1). Most of the samples were collected over the shelf, but 10 came from beyond the shelf, most of which were within the limits of the Florida Current.

Temperature. Between Cape Fear and Cape Hatteras the inshore surface temperatures approached 70° F from 24 May–3 June 1949, but in the Florida Current they increased to 80° F (Figs. 1 and 2). There was no marked surface temperature gradient north from Cape Fear to Hatteras. The isotherms in this region, though quite irregular, ran roughly parallel to the coast. North of Hatteras, where colder water (65° F) was encountered over the inner half of the continental shelf, some of the isotherms curved shoreward. Warmer water (75° F and above) was present on the outer portion of the shelf and isotherms of these temperatures continued uninterrupted around

Figure 1. Surface temperature and salinity distribution for cruises 18 and 19. Circles indicate stations from which plankton samples were obtained. Arrows indicate the inner edge of the Florida Current. (Redrawn from figures supplied by D. F. Bumpus.)

the Cape. These observations support the conclusion reached by Parr (1933) that there is no temperature barrier in the waters off Hatteras in the summer and therefore no barrier to the northward movement of warm water animals around this Cape at that season. North of Hatteras, planktonic animals may be carried farther and farther offshore by the Current and may remain in essentially the same temperature. Inshore of the 75° F isotherm there is an abrupt barrier of cold southerly moving water which turns northward at Hatteras and may be carried into the Florida Current. Parcels of water which escape south around the Cape become modified south of Hatteras.

Over the greater portion of the shelf where the water is less than 50 m deep the bottom and surface temperatures usually differed by only 2 or 3 degrees. A temperature gradient of 20° or more between the surface and bottom was common at the edge of the shelf and somewhat beyond. This was especially evident at the western edge of the stream. Warmer water extended to deeper levels farther offshore near the center of the Florida Current, where, for example, the gradient was reduced to about 10° between the surface and 200 m.

In samples taken over the center or inner edge of the shelf the chaetognaths did not usually come from water having a temperature lower than 70° F. Near the edge of the shelf, or just beyond, any specimens taken near the bottom by one of the deeper hauls came from water of 55° F or lower.

Salinity. Surface salinities ranged from 35 to 37.2 ‰ over the greater portion of the shelf (Figs. 1 and 2). Salinities lower than these were found in a few instances where samples were taken closer to shore. Beyond the shelf and at the surface of the Florida Current, salinities of 36.0 to 36.3 ‰ were recorded. Over most of the shelf the salinity gradient from surface to bottom was slight. Near the edge there was a small gradient of 0.2 or 0.3 ‰ between surface and bottom. Farther offshore and into the Florida Current there was a gradually increasing vertical gradient from about 36.1 to 36.7 ‰ at 200 m. With but one or two exceptions, all chaetognaths were collected in water having salinities between 35.0 and 36.5 ‰.

Water Movement. The western edge of the Florida Current meanders northeastward along the edge of the continental shelf off North Carolina. A vertical section (Fig. 3) extending from the ten-fathom line near Cape Fear southeastward across the Florida Current illustrates the distribution of temperature and salinity in this region. The swiftest portion of the Current is found where the isotherms slope upward most sharply (Iselin and Fuglister, 1948). The western

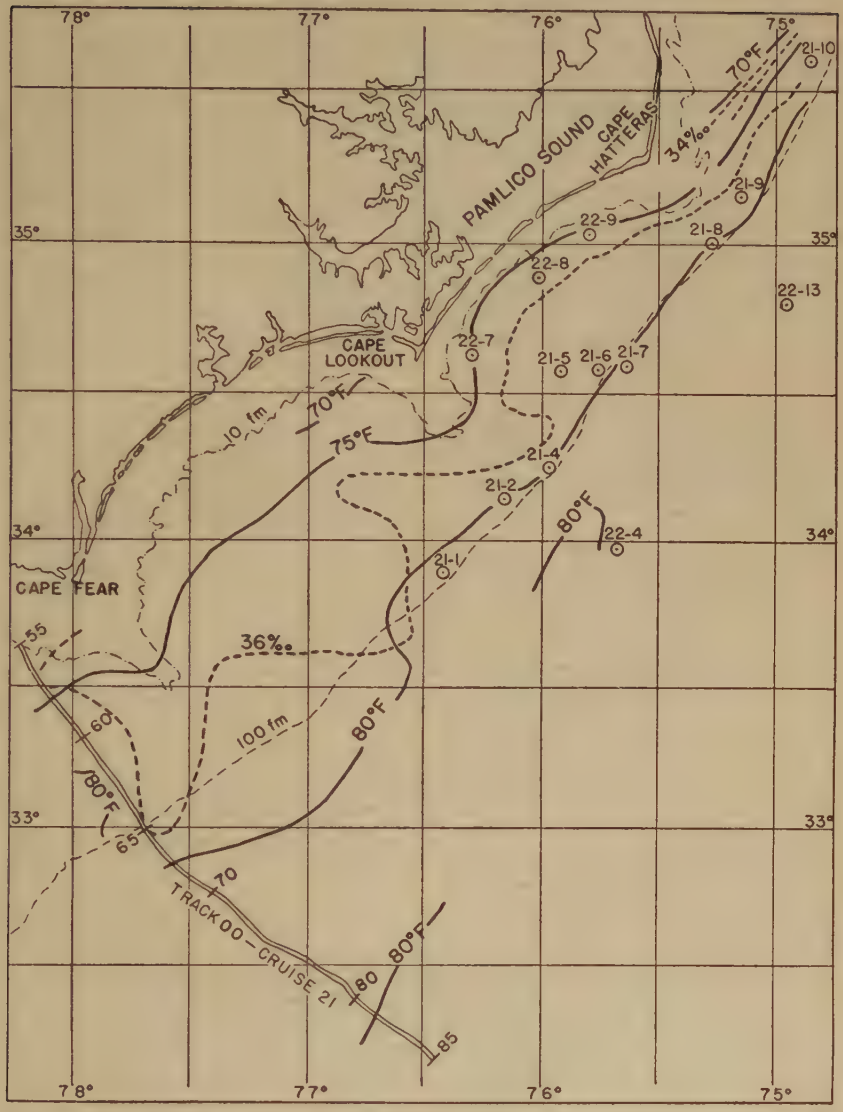

Figure 2. Surface water temperature and salinity distribution for cruises 21 and 22. Circles indicate stations from which plankton samples were obtained. (Redrawn from figures supplied by D. F. Bumpus.)

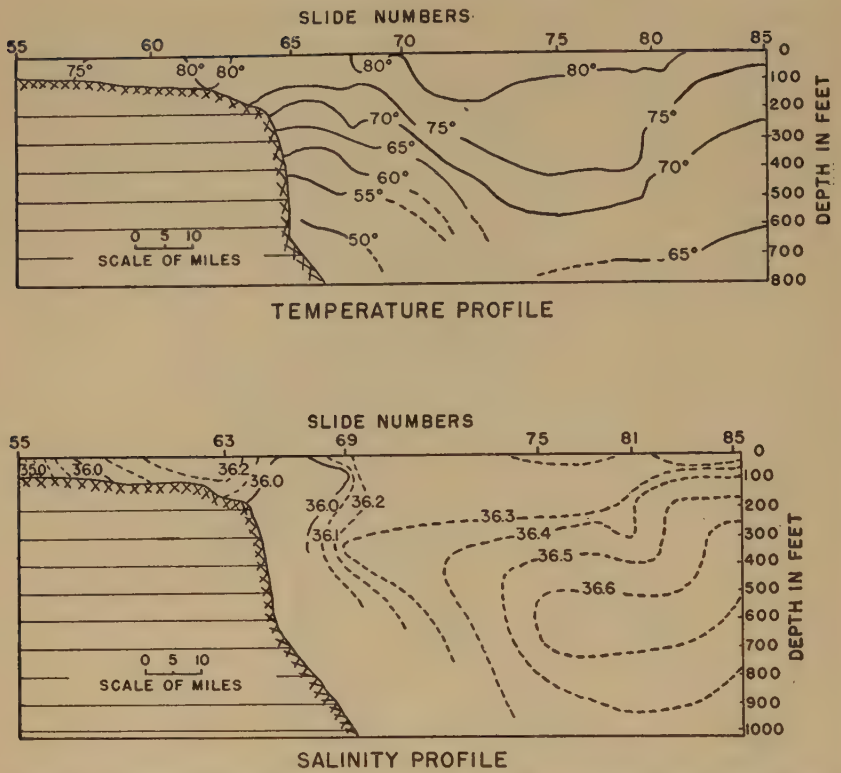

Figure 3. Vertical sections of temperature and salinity distribution taken during cruise 21 (see Fig. 2, Track 00-Cruise 21, for position of sections). Numbered lines across cruise track represent bathythermograph samples. These samples are also indicated in some instances by slide numbers across the top of sections in this figure. (Redrawn from figures supplied by D. F. Bumpus.)

edge of the Current is located just to the left of the upward sloping isotherms.

Water of 36.0 ‰ or above in this area appears to be derived from the Florida Current. Because the 36.0 ‰ isohaline swings in deeply over portions of the shelf (Figs. 1, 2, and 3), there is reason to believe that this represents water from the Florida Current which has swept over the shelf and is in the process of mixing with shelf water. Closer inshore and outside of the 36.0 ‰ isohaline, more typical and perhaps more constant shelf water is encountered. Over the inner half of the shelf, salinities between 36 and 35 ‰ are usually encountered until quite close to shore where the effects of greater dilution from land drainage are evident. The well mixed condition of the inner shelf water is illustrated in the vertical section shown in Fig. 3.

The source of all of the shelf water is not entirely apparent from these data. It is obvious that land drainage contributes something to this body of water, but the relative quantities contributed by the Florida Current and the bottom slope water through the processes of lateral mixing are not immediately evident. There appears to be no large movement of water south around Cape Hatteras.

On the outer edge of the shelf the Florida Current produces a net northeasterly movement of water, while on the inner border of the shelf, close to shore, the movement appears to be southwesterly. Bumpus and Wehe (1949) have pointed out that there may be several cyclonic eddies over the shelf between these two opposite movements of water or that one long sausage-shaped eddy may extend from Hatteras to northern Florida.

The Chaetognaths. The continental shelf beyond the 20 m line between Cape Fear and Cape Hatteras was sampled rather thoroughly. Moreover, numerous samples were taken beyond the shelf at the edge of and across the axis of the Florida Current. No plankton samples were taken close inshore.

The chaetognaths collected by the Albatross III between 24 May and 14 June 1949 over the continental shelf of North Carolina are: *Sagitta bipunctata* Quoy and Gaimard; *S. enflata* Grassi; *S. helenae* Ritter-Zahony; *S. hexaptera* d'Orbigny; *S. lyra* Krohn; *S. minima* Aida; *S. serratodentata* Krohn; *S. tenuis* Conant; *Krohnitta pacifica* Aida; *K. subtilis* Grassi; *Pterosagitta draco* (Krohn).

On inspection of Fig. 4 and Table I it becomes evident that most of the species were found near the edge of the shelf, with hauls in this strip of water frequently containing seven or eight species. By comparison, the inshore samples usually contained between two and five species.

Samples taken 15 or more miles beyond the shelf and well into the Florida Current contained an average of five species of chaetognaths and usually somewhat less than 100 specimens, this in spite of the fact that several of these hauls were the deepest made. It is noteworthy that the two deepest hauls (cruise 19, station 16, 660 m; and cruise 22, station 4, 560 m), in the Florida Current, contained respectively seven specimens representing four species and 25 specimens representing five species.

Distribution by Species. In the inshore area over the continental shelf, *Sagitta bipunctata* was usually absent, and when present it occurred in small numbers. Of the eight collections near the 10-fathom line, only two contained this species, one specimen being taken in one haul and two in another. Midway between the 10- and 100-fathom

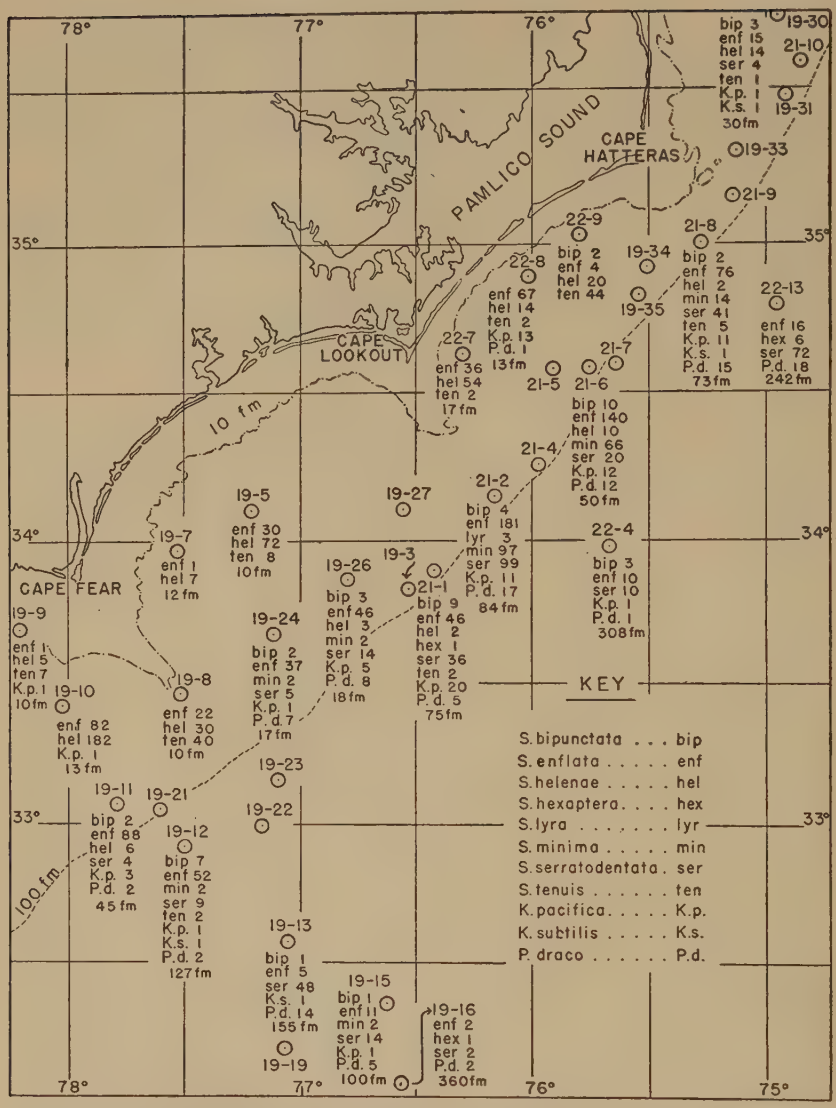

Figure 4. The distribution of chaetognaths by stations over and beyond the continental shelf. The figures after the species represent the number of specimens in each sample. The depth of the vertical tow is shown beneath each list.

lines, about half of the samples contained this species, usually 2 or 3 per haul. Beyond the 100-fathom line there was a perceptible increase in the numbers taken. Seven of the 10 samples contained specimens, but they were never very abundant, the largest number per haul being ten. The collections of *S. bipunctata* (Fig. 4, Table I) and the salinity distribution (Figs. 1 and 2) show that all specimens came from water having a minimum salinity of 36 ‰ or very close thereto. Ritter-Zahony (1911) has described this species as both neritic and oceanic, with a range between 40° N and 40° S Lat. in the epiplankton. Huntsman (1919) listed only seven specimens from about 200 miles southeast of Cape Sable, Nova Scotia, in what was probably the edge of the Gulf Stream. Neither Bigelow (1926) nor Redfield and Beale (1940) found this species at any time in the Gulf of Maine, and Bigelow and Sears (1939) reported none from the continental shelf between Cape Cod and Chesapeake Bay. Hence it is not as abundant or as widely distributed along our Atlantic Coast as is *S. enflata*, and apparently it is less tolerant of temperature and/or salinity fluctuations than is *S. enflata*. In view of its limited tolerance, its presence over the continental shelf suggests that it has been swept in by the Florida Current and that it will not persist in coastal waters when salinity and temperature are much below that of the Florida Current.

Sagitta enflata was the most abundant and most widely distributed chaetognath in the area sampled. It was abundant inshore (20 m) and offshore as well. Of the 39 samples containing chaetognaths, only two lacked this species; usually it constituted 40 to 60% of the total number of chaetognaths in a sample. In the salinity and temperature ranges encountered, no limiting effects could be observed. According to Huntsman (1919), *S. enflata* ranges along the Atlantic Coast as far north as 43° N Lat., and he believes that in these latitudes it is an indication of the incursion of Gulf Stream water. Bigelow (1915, 1926), Bigelow and Sears (1939), Redfield and Beale (1940), and Clarke, Pierce and Bumpus (1943) have recorded it from the northern portion of its range. In studies of its distribution off the west coast of Florida, Pierce (1951) found that it was abundant to within a few miles of shore. But closer inshore, where salinities of less than 30 ‰ were encountered, it disappeared. It is both oceanic and neritic, and in tropical and subtropical oceans its distribution is world-wide.

Generally the range of *Sagitta helenae* appears to be confined to waters over the continental shelf. Of the 28 samples taken over the shelf, 21 included this species, while only three of ten samples taken beyond the 100-fathom line included it (Fig. 4). There was a general decrease in relative abundance from the 10-fathom line to just beyond

TABLE I. Chaetognaths Collected during Cruises 19 and 21 Which Are Not Included in Fig. 4. Numbers Over the Listed Species Represent Cruise-station

19–3
S. enflata—32
S. serratodentata—18
P. draco—1
(90 fm)

19–19
S. bipunctata—3
S. enflata—31
S. hexaptera—1
S. lyra—1
S. serratodentata—3
P. draco—2
(70 fm)

19–21
S. bipunctata—1
S. enflata—25
S. helenae—2
S. minima—12
S. serratodentata—5
K. pacifica—6
P. draco—1
(80 fm)

19–22
S. bipunctata—4
S. enflata—76
S. helenae—2
S. minima—11
S. serratodentata—4
S. tenuis—3
K. pacifica—5
P. draco—1
(80 fm)

19–23
S. enflata—12
S. minima—1
S. serratodentata—12
P. draco—2
(80 fm)

19–27
S. bipunctata—2
S. enflata—68
S. helenae—4
S. serratodentata—15
S. tenuis—4
K. pacifica—3
P. draco—4
(18 fm)

19–30*
S. bipunctata—2
S. enflata—16
S. helenae—21
S. minima—3
S. serratodentata—35
S. tenuis—3
K. pacifica—2
(30 fm)

19–31*
S. enflata—52
S. helenae—6
S. serratodentata—44
(20 fm)

19–33*
S. bipunctata—1
S. enflata—10
S. tenuis—3
K. pacifica—1
(15 fm)

19–33*
S. bipunctata—10
S. enflata—75
S. helenae—2
S. serratodentata—35
S. tenuis—1
P. draco—4
(15 fm)

19–34
S. enflata—9
S. helenae—3
S. serratodentata—2
(25 fm)

19–35
S. bipunctata—2
S. enflata—56
S. helenae—12
S. minima—5
S. serratodentata—10
P. draco—1
(45 fm)

21–4
S. bipunctata—12
S. enflata—316
S. helenae—8
S. minima—188
S. serratodentata—88
K. pacifica—8
P. draco—16
(83 fm)

21–5
S. enflata—28
S. serratodentata—16
P. draco—6
(22 fm)

21–7
S. bipunctata—16
S. enflata—110
S. helenae—4
S. minima—186
S. serratodentata—52
K. pacifica—18
P. draco—2
(80 fm)

21–9
S. bipunctata—1
S. enflata—4
S. minima—3
S. serratodentata—7
K. pacifica—1
P. draco—1
(50 fm)

21–10
S. bipunctata—1
S. enflata—44
S. helenae—22
S. serratodentata—7
K. pacifica—8
(30 fm)

* Samples from stations 19–30, 19–31, 19–33 were obtained with a Clarke-Bumpus plankton sampler. Two samples from station 30 and 33 respectively contained enough chaetognaths to warrant inclusion. One sample from 19–30 is shown in Fig. 4; the others are listed above.

the 100-fathom line. The present records extend the range of this little known species considerably. Described originally by Ritter-Zahony (1910) from specimens collected near Dry Tortugas, Florida, it has been found along the west coast of Florida (Pierce, 1951) and is now recorded for the first time from points as far north as 35° 46′ N Lat. Bigelow and Sears (1939), in studies of plankton from Chesapeake Bay to Cape Cod, did not record its presence in any samples; hence it appears doubtful if its northern range extends much beyond Cape Hatteras.

Sagitta hexaptera was one of the least abundant chaetognaths. There were a few specimens in three of the 39 samples which contained chaetognaths. Two of these samples were beyond the shelf while the third was on the edge. Ritter-Zahony (1911) has described its range as between 40° N and 40° S. Usually it occurred in the surface layers down to the limits of visible light. Bigelow and Sears (1939) have indicated its presence at only one station near the edge of the continental shelf, somewhat southeast of Long Island. Huntsman (1919), who found *S. hexaptera* in small numbers at six stations just beyond the Nova Scotian shelf, has stated, "As it is a form characteristic of intermediate depths, from 100 to 200 meters, its distribution is an indication of the extent to which this intermediate water has pressed in to our shores from the open Atlantic."

Sagitta lyra was represented by only four specimens in the entire collection: one specimen from a sample taken in the Florida Current and three from a haul at the edge of the shelf. These hauls extended to 70 and 84 fathoms respectively. *S. lyra* is cosmopolitan in all oceans and is able to exist in both relatively cold water as well as warm Gulf Stream water. Bigelow (1915) found a few specimens just beyond the shelf of Long Island. Huntsman (1919) collected specimens at the edge of the continental shelf and beyond in the region east of Nova Scotia. Redfield and Beale (1940) found it occasionally in samples from 170 m and deeper in the Gulf of Maine. Most of the records indicate that it prefers deep water, but Thomson (1947) has reported that it occurred most abundantly in the upper 100 m off southeastern Australia.

Sagitta minima was most abundant along the edge of the continental shelf in the zone where mixing apparently occurred between continental shelf, continental slope and Florida Current waters. In several of the samples taken in this area, *S. minima* was among the more abundant chaetognaths. It was never collected over the inner half of the shelf, and of those samples taken 15 or more miles east of the shelf, only one contained two specimens. Its relatively greater abundance in what appears to be a region of mixing of different water masses is certainly

worth further investigation. Ritter-Zahony (1911) has indicated that its range is world-wide between 40° N and 40° S Lat. No published records indicate that this species has been identified before from the entire continental shelf of the eastern United States.

Sagitta serratodentata, one of the most abundant species in the collections, was found in 31 of the 39 samples. Of the samples taken near the 10-fathom line, only one specimen was obtained in one of the nine hauls, but beyond the 100-fathom line every sample contained this species. At the farthest offshore stations its abundance approached and occasionally exceeded that of *S. enflata*, but at the inshore stations *S. enflata* was the dominant form. Being one of the most widespread of chaetognaths, it is found in the temperate and tropical waters of the Atlantic, Pacific and Indian oceans. It extends northward along the Atlantic Coast into the Gulf of Maine, where Redfield and Beale (1940) observed it as an immigrant from the Atlantic surface waters which are swept into the Gulf of Maine. Huntsman (1919) collected it commonly in the deeper waters beyond the continental shelf off Nova Scotia. Bigelow and Sears (1939) found it over the shelf between Chesapeake Bay and Cape Cod. However, it was more abundant in the southern portion of its range and less so in samples taken east of New York. Bigelow and Sears (1939) concluded that it was able to reproduce in this area and that the population was not dependent on immigrants from Gulf Stream water. Clarke, Pierce and Bumpus (1943) recorded this species from the eastern and southern margins of Georges Bank. Cowles (1930), who reported a few specimens inside the mouth of Chesapeake Bay, also reported gradually decreasing numbers from the 100-fathom line toward the mouth of the Bay.

Sagitta tenuis was found in 16 of the 39 samples. Although it was somewhat more common in inshore waters, it was present in several samples out to or beyond the 100-fathom line; however, none of the samples collected 30 miles or more beyond the shelf contained this species. It was most abundant (44 specimens) in a sample taken near an entrance to Pamlico Sound. From samples taken on other occasions (Pierce, 1951) it is known to be common in Beaufort Harbor and in the inshore areas of Florida (St. Augustine and Salerno). This appears to be a neritic species which can tolerate salinity variations from 36 to less than 30 ‰, hence it is occasionally found in samples some distance beyond the continental shelf. Conant (1896) has described *S. tenuis* from specimens received from Jamaica. Bigelow and Sears (1939) did not find it in the plankton over the continental shelf between Chesapeake Bay and Cape Cod. Many more records are needed before its range can be ascertained. It has not been reported from the Pacific.

Krohnitta pacifica occurred in about half of the samples from the entire area, from close inshore to many miles beyond the 100-fathom contour. It was never abundant in any sample, the maximum number being 20 from a haul near the edge of the shelf. It appears to be rather tolerant to variations in salinity and temperature. Because *K. pacifica* has often been confused with the somewhat rarer *K. subtilis*, published records of its distribution are not accurate. Pierce (1951) collected *K. pacifica* occasionally along the west coast of Florida, and Thomson (1947) and Tokioka (1939) recorded it from the western Pacific. The latter author illustrates its distinctive characters: slightly heavier body, larger ovary, and narrow lateral fins.

Krohnitta subtilis, rather uncommon, was found in only five samples, and in only one sample was more than one individual detected. With but one exception, these specimens were taken on the edge of or beyond the continental shelf. Although more data are needed, there is little evidence that it is a neritic species. It has been reported occasionally along the Atlantic, from the edge of the continental shelf and beyond, but in some of these instances the species was probably confused with *K. pacifica.*

Pterosagitta draco was present in small numbers in every sample taken beyond the shelf. The largest catch was 18 in one sample. Inside the 100-fathom line it was less abundant, and only one of the stations near the 10-fathom line contained a specimen. This species, as indicated by many reports, is world-wide in tropical and subtropical waters. In the Atlantic it ranges northward to 43° N Lat., where Huntsman (1919) reported one from the Nova Scotian banks at the edge of the Gulf Stream. Bigelow and Sears (1939) also caught a few specimens near the edge of the Gulf Stream at scattered points between 35° and 41° N. As a result of studies of North Atlantic plankton, Strodtmann (1892) considers that *P. draco* and *S. enflata* characterize the true region of the Gulf Stream in that area.

Description of Zones. In this study of the distribution of chaetognaths it is apparent that they tend to occur in three somewhat characteristic groups of species representing three zones. It should be understood that these zones, as discussed here, have no well defined borders and that they may shift position by many miles from time to time depending on the factors which affect currents and lateral mixing. Iselin (1939) and others, in describing the region north of Cape Hatteras, have pointed out that eddies from the Gulf Stream occasionally move in over the continental shelf and that masses of shelf water move offshore, and it is possible that such movements occur south of Cape Hatteras. In such a case there would certainly be a

temporary disruption of any zonation of water which paralleled the coast. However, the data do indicate that three zones with distinctive hydrographic features did exist during these cruises.

The Inner Shelf. Zone I. The water of this region, covering the inner portion of the shelf, is characterized by salinities of less than 36 ‰ and by vertical mixing from surface to bottom. The salinity of these waters directly reflects the effect of dilution by water from rivers and sounds.

The Outer Shelf. Zone II. This zone extends from the eastward limits of the 36 ‰ isohaline to the edge of the Florida Current proper, which is usually in the neighborhood of the edge of the shelf. Zone II, characterized by less complete mixing of the shelf, slope and Current water, shows some vertical stratification of temperature and salinity. A significant amount of initial lateral mixing of these water masses takes place here. The salinity varies from a little above to a little below 36 ‰, depending on the presence of Florida Current or slope water.

The Florida Current. Zone III. In this region the salinity ranged from 36.1 to 36.7 ‰. Both temperature, which reached 80° F at the surface, and salinity, which was usually close to 36.2 ‰ at the surface, were highest in this region. Stratification of temperature and salinity was evident.

Occurrence of Chaetognaths. Table II shows the occurrence of chaetognaths in the three zones. Considering those that were commonly taken, it is apparent that the fewest species were present in Zone I, the next smallest number in Zone III, and the largest number in Zone II. The commonly occurring members of Zone II, with the exception of *S. tenuis*, constitute a combination of the species that were taken in Zones I and III. This further substantiates the mixed condition of the water in Zone II.

One species, *S. minima*, rare in Zones I and III, was common in Zone II. This indicates that this zone of incompletely mixed water, although disrupted from time to time, must prevail at least along this section of the coast and that it may have considerable ecological significance in reference to the plankton.

Also obvious is the fact that certain species are relatively abundant in all three zones. *S. enflata* is the best example of a common and widely distributed form in this area. Two other species, *K. pacifica* and *P. draco*, occurred in all three zones. *S. helenae* appeared to be limited to the water over the continental shelf and was seldom found much beyond the edge, although it was often present close to or a few miles over the edge.

Conclusions. It is clear that there is a direct relationship between the hydrography of this region and the distribution of the chaetognaths. There is no random distribution of species from the Florida Current over the continental shelf just as there is no rapid movement of quantities of water from the Florida Current over the inner border of the shelf. In the region at the edge of the shelf, where shelf, slope, and Current waters come in contact and where initial mixing occurs, there also is found the greatest number of species.

TABLE II. The Distribution of Chaetognaths Over and Somewhat Beyond the Continental Shelf of North Carolina

Common	*Occasional*	*Rare*
	The Inner Shelf-Zone I	
S. enflata	*K. pacifica*	*S. bipunctata*
S. helenae	*P. draco*	*S. minima*
S. tenuis		*S. serratodentata*
	The Outer Shelf-Zone II	
S. bipunctata	*S. tenuis*	*K. subtilis*
S. enflata		*S. hexaptera*
S. minima		*S. lyra*
S. serratodentata		
S. helenae		
K. pacifica		
P. draco		
	The Florida Current-Zone III	
S. bipunctata		*S. minima*
S. enflata		
S. serratodentata		
K. pacifica		
P. draco		

This second zone appears to be particularly rich in species. Vertical or short oblique hauls which yielded seven and eight species are certainly above average. One reason for this appears to be the accumulation of species as a result of the mixing of three water masses in the immediate area.

At present at least two species present interesting possibilities in that they may be used as indicators of water masses in this region. *S. helenae* appears to be an indicator of continental shelf water in the area under consideration. *S. bipunctata* appears to be an indicator of Florida Current water and its lateral extensions over the shelf. Farther north, *S. enflata* becomes restricted to Gulf Stream water and is recognized by Strodtmann (1892) along with *P. draco* as an indicator of Gulf Stream water in the North Atlantic.

The present techniques in securing hydrographic data give a much better picture of the distribution of temperature, salinity, and other variables in many areas. So that these data may be most effectively utilized in studying the distribution of planktonic organisms, it is desirable to develop and use more accurate methods of collecting plankton samples with large nets from specific depths; such samples should be obtained as near as possible to the time and place where hydrographic casts are made for temperature, salinity and other measurements. It will be from such knowledge that we can determine the real value of certain animals as indicators of the movement and mixing of water masses.

Summary. A series of vertical plankton hauls and hydrographic data were obtained over and somewhat beyond the continental shelf of North Carolina by the Albatross III during four cruises covering the period from 24 May to 14 June 1949.

Temperature and salinity distributions are figured and discussed for the area. Three water masses, continental shelf, continental slope and Florida Current, are in contact at the edge of the continental shelf where initial mixing occurs.

Eleven species of chaetognaths were collected in the area sampled. The largest number of species was collected near the edge of the shelf (Zone II) where considerable initial mixing between the three water masses takes place. These samples frequently contained seven and eight species. Closer inshore, in typical shelf water (Zone I), two to three species were common, and in the Florida Current (Zone III) five species per sample was the average.

Certain species occurred in all three zones. *S. enflata* was the most widespread and abundant. *K. pacifica* and *P. draco*, although less abundant, were present in all three zones. Certain species appear to be restricted very largely to one water mass or to a mixture containing such water. For example, *S. helenae* was collected almost exclusively from Zones I and II. *S. bipunctata* was found in the Florida Current and in the vertically mixed water of Zone II in the majority of the samples.

These data demonstrate that the distribution of chaetognaths was directly related to the water masses in the area studied.

REFERENCES

Bigelow, H, B,

1915. Exploration of the coast water between Nova Scotia and Chesapeake Bay, July and August, 1913, by the U. S. Fisheries Schooner Grampus. Oceanography and Plankton. Bull. Mus. comp. Zool. Harv., *59* (4): 151–359.

1926. Plankton of the offshore waters of the Gulf of Maine. Bull. U. S. Bur. Fish., *40* (2): 1–509.

Bigelow, H. B. and Mary Sears
1939. Studies of the waters of the continental shelf, Cape Cod to Chesapeake Bay. III. A volumetric study of the zooplankton. Mem. Harv. Mus. comp. Zool., *54* (4): 183–378.
Bumpus, D. F. and T. J. Wehe
1949. Coastal water circulation of the east coast of the United States between Cape Hatteras and Florida. WHOI Ref. No. 49–6 (mimeo).
Clarke, G. L., E. L. Pierce and D. F. Bumpus
1943. The distribution and reproduction of *Sagitta elegans* on Georges Bank in relation to the hydrographical conditions. Biol. Bull. Woods Hole, *85* (3): 201–226.
Conant, F. S.
1895. Description of two new chaetognaths (*Spadella schizoptera* and *Sagitta hispida*). Ann. Mag. nat. Hist., (6) *16:* 288–292.
1896. Notes on the chaetognaths. Ann. Mag. nat. Hist., (6) *18:* 201–214.
Cowles, R. P.
1930. A biological study of the offshore waters of Chesapeake Bay. Bull. U. S. Bur. Fish., *46:* 277–381.
Huntsman, A. G.
1919. Biology of Atlantic waters of Canada. Some quantitative and qualitative plankton studies of the eastern Canadian plankton. 3. A special study of Canadian chaetognaths, their distribution, etc., in the waters of the eastern coast. Canad. Fish. Exped., 1914–15, Dept. Naval Sci., 421–485.
Iselin, C. O'D.
1939. Some physical factors which may influence the productivity of New England's coastal waters. J. mar. Res., *2:* 74–85.
Iselin, C. O'D. and F. C. Fuglister
1948. Some recent developments in the study of the Gulf Straem. J. mar. Res., *7* (3): 317–329.
Parr, A. E.
1933. A geographic-ecological analysis of the seasonal changes in temperature conditions in shallow water along the Atlantic Coast of the United States. Bull. Bingham oceanogr. Coll., *4* (3): 1–90.
Pierce, E. L.
1951. The Chaetognaths of the west coast of Florida. Biol. Bull. Woods Hole, *100* (3): 206–228.
Redfield, A. C. and A. Beale
1940. Factors determining the distribution of populations of chaetognaths in the Gulf of Maine. Biol. Bull. Woods Hole, *79:* 459–487.
Ritter-Zahony, R. von
1910. Westindische Chaetognathen. Zool. Jb., Suppl. 11, *2:* 133–143.
1911. Chaetognathi. Das Tierreich, *29:* 1–35.
Strodtmann, S.
1892. Die Systematik der Chaetognathen. Arch. Naturgesch., *58:* 338–377.
Thomson, J. M.
1947. The Chaetognatha of south-eastern Australia. Coun. Sci. Ind. Res. (Div. Fish. Rept. No. 14) Bull. No. 222: 3–43.

Tokioka, T.

1939. Chaetognaths collected chiefly from the bays of Sagami and Suruga, with some notes on the shape and structure of the seminal vesicle. Rec. Oceanog. Works Japan, *10* (2): 123–150.

A NOTE ON THE VELOCITY DISTRIBUTION AND BOTTOM STRESS IN A WIND-DRIVEN WATER CURRENT SYSTEM[1]

By

J. R. D. FRANCIS

ABSTRACT

The shear stress of the wind on a water surface is sometimes found by measuring the slope of the surface in a lake or wind tunnel. The stress on the bottom of the lake due to the return water current is an error term which has been variously estimated. An experimental method of determining the error is described, and the results indicate that it is but some 1½% of the wind stress.

One way of finding the aerodynamic stress of wind on a water surface τ_s is to observe the slope α of the surface along the direction of the wind. The wind causes both the slope and also a drift current towards the lee side in the upper layers of water; consequently, along the bottom of an enclosed lake or sea a return current exists which brings the water back again to the windward side and exerts on the bottom a shear stress τ_b. These two stresses act on the water in the same direction and are balanced by the hydrostatic force due to the rise in water level downwind. Thus, $\tau_s + \tau_b = g\rho\alpha h$, where h is the mean depth of water. It will be seen, therefore, that a measurement of α cannot alone be used to find τ_s, an important oceanographic quantity.

If it can be assumed that the flow throughout the water is laminar, the ratio τ_b/τ_s can be found by analytical methods. These are fully worked by Hellstrom (1941) and Keulegan (1951), where it is found that $\tau_b = 0.50\ \tau_s$. However, the water-flows in a lake or sea or even in a laboratory wind-wave tunnel are turbulent in all practical cases, and τ_b/τ_s may therefore be different from the laminar flow value. Hellstrom uses values of 0.15 to 0.80 depending on the depth of the water, and they are based on Boussinesq's theory for turbulent flow. Keulegan uses a purely arbitrary constant value of 0.25 for his wind tunnel experiments. Francis (1951), in some wind tunnel experiments of a similar nature, took measurements of the mean velocity of the return water current, and by applying the usual drag formula $\tau_b = c\rho u^2$ (u = water speed, c = drag coefficient), he found that τ_b never exceeded 3% of τ_s. In this last case, a conservatively high value of c

[1] Contribution No. 639 from the Woods Hole Oceanographic Institution.

was used in order to allow empirically for the oscillatory motion imposed by the wind-generated surface waves on the much slower mean velocity. It was thought that the turbulence added by the oscillations might increase the drag.

An attempt was made to measure τ_b directly in the small wind-wave tunnel mentioned above while the water currents were being wholly generated by wind. A flat smooth plate was arranged just to float

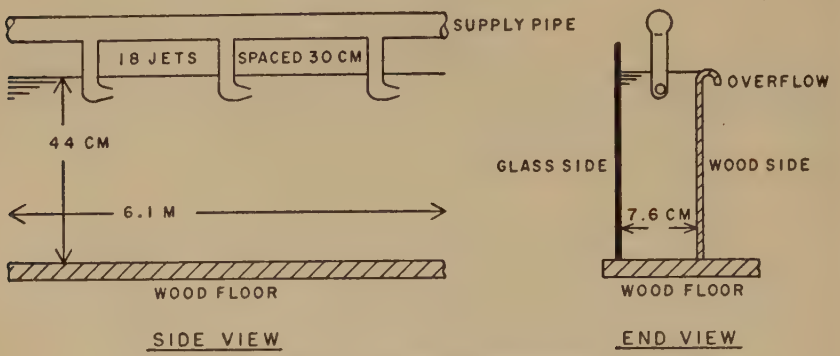

Figure 1. Tank used in experiments.

in the surface of a pool of heavy fluid at the bottom of the tunnel. The plate was constrained by a spring system so that the shear stress on the plate could be measured by its deflection. The experiment was a failure because the wave motions caused the plate to oscillate badly; not even a mean position could be determined. Better success has now been achieved with another experimental technique which uses horizontal jets of water to apply to the water surface the momentum that was applied before by the wind. This artifice ensures a surface without waves and water-flows in the tank that are noticeably steadier. The total amount of water in the tank is kept constant by a uniform overflow all along the top of one side of the tank; thus the jets add momentum but not mass to the water already there. Below the upper few centimetres there is no motion caused by the water overflow. A slight correction is made because of the finite size of the jets, since the momentum is really applied to a thin layer at the surface, making the effective surface for shear somewhat below the actual surface.

Fig. 1 shows the tank, which is 6.1 m long, 12.7 cm wide, and 44 cm deep from bottom to overflow. Eighteen jets, spaced 30 cm apart, were supplied with sea water through a 5 cm pipe parallel to the tank length and above the water level. The jet outlets, just in the surface of the water, were of an oval, flattened shape, the total cross-sectional

area of all the jets being 10.7 cm². The shear stress measuring-device is shown in Fig. 2. Its design is based upon the equipment used by Sheppard (1946) for measuring stress in the atmosphere. The circular moving plate is brass, 7.6 cm in diameter, and is of an inverted dish shape. It floats on carbon tetrachloride (density 1.70 gm cm^{-3}) in a shallow dish with only 5 mm clearance all round. A piece of small

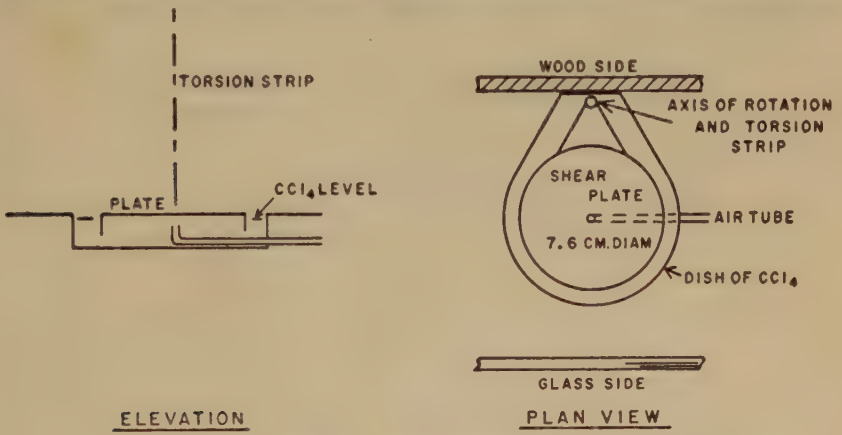

Figure 2. Detail of shear plate.

bore tube allows air to be blown into the underside of the plate so that its buoyancy may be adjusted with some precision to place the top of the plate, the surface of the CCl_4, and the top of the circumscribing dish all in one plane. A false floor 1.2 cm thick is laid in the tank so that the apparatus does not project into the flow. The plate is pivoted on a vertical axis at the side of the tank; and the spring restraint is a vertical torsion strip 2.1 mm by 0.3 mm by 17 cm long. It is clamped at its upper end clear of the water, with an adjustment for the no-load position of the plate. The position of the plate is observed by a travelling telescope (cathetometer) which views a mark on the periphery through the glass side of the tank. The torsion constant of the apparatus was measured by putting weights in a paper pan on a fine cotton thread attached to the plate; the resulting calibration was linear, with negligible scatter for load increasing and decreasing.

The jet discharge Q through the total orifice area a was calibrated against the pressure in the supply pipe by collecting the water in a large tank. The momentum supplied by the jets per second (the available thrust force) is therefore $\rho Q^2/a$. Not all of this is available for driving the water currents; some of it is counterbalanced by the backward thrust of the further end of the tank where the high velocity

stream strikes; some of it is counterbalanced by the thrust of the water on the backs of the jet pipes which must project into the fast surface stream; and some is counterbalanced by the shear stress of the fast upper stream on the sides of the tank. The last correction is necessary only because of the limited width of the tank in the shallow zone where there are fast velocities solely due to the dispersing jets. Below a depth of about 12 cm the velocities are low and the stresses on the

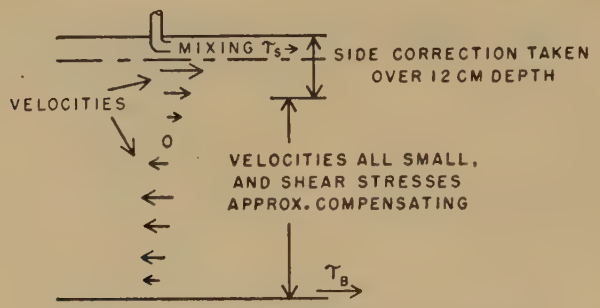

Figure 3. Position of hanging side correction plate.

sides caused by the forward velocity must nearly balance the stress in the opposite direction caused by the backward return current below (see Fig. 3). The correction terms were all measured directly, the first by placing a false flat end plate on a pendulum and measuring the deflection; the second by mounting a jet pipe on a pendulum and immersing to the appropriate depth; and the third by suspending similarly a smooth flat plate 90 cm long and 12 cm deep parallel to, and 0.4 cm away from, the glass side of the tank.

The observations for two different water-flows are summarized below.

Table of Forces on Water in Tank of Plan Area 7720 cm²

Q Water flow ($cm^3 . sec^{-1}$)	$\rho Q^2/a$ Input by jets (dynes × 10^3)	Corrections (dynes × 10^3) End	Side	Jets	Net input force (dynes × 10^3)	Net τ_s (dynes. cm^{-2})	Measured τ_b (dynes. cm^{-2})	τ_b/τ_s (%)
2230	480	98	72	54	256	33.1	0.46	1.4
2900	800	173	98	82	447	57.9	0.77	1.3

τ_b is the average of measurements at two places on the floor of the tank.

There was still a little oscillation of the shear plate, due presumably to large scale turbulence in the tank, but the mean deflection of the plate could be easily estimated. Lower jet speeds, however, gave such small deflections of the plate that the results are not significant. It will be seen that the bottom stress is small compared with the top

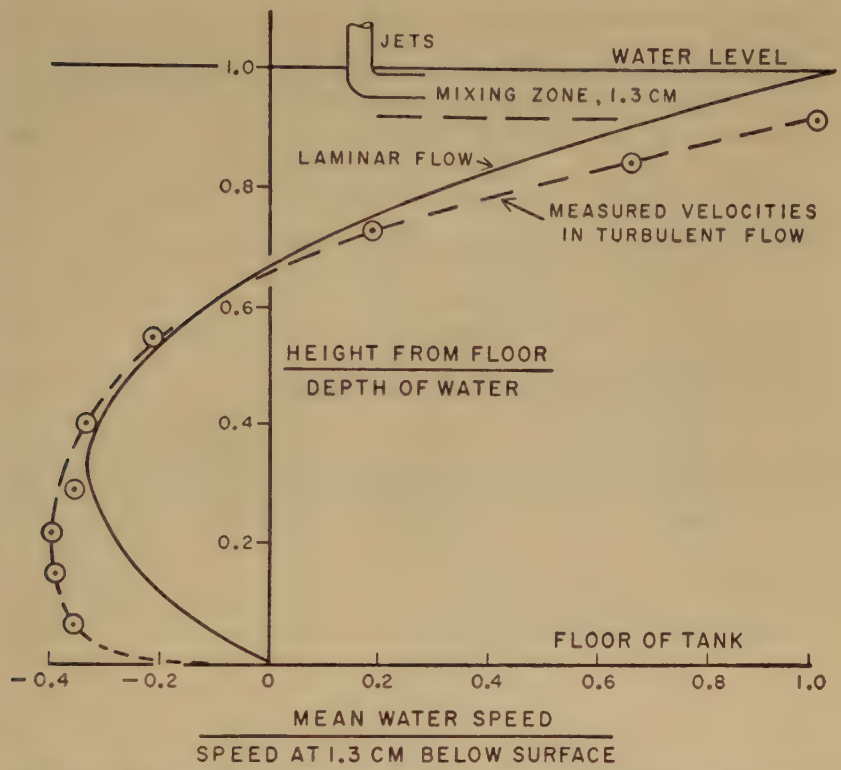

Figure 4. Comparison between theoretical and measured velocity profiles (measured velocity at 1.3 cm below surface = 26.3 cm sec^{-1}).

stress and can be neglected in most cases, for in practice the measurement of slope α is fraught with errors that are greater than this correction.

Velocity profile. The distribution of mean velocity was determined at one jet speed by a total head tube traversed on the centreline of the tank. The static pressure was taken at a tapping in the side of the tank in the plane of the traverse. The pressures were measured by a micrometer point in a glass stilling well.

The profile is shown in Fig. 4 together with the parabolic one for laminar flow. Both profiles are defined by nondimensional parameters, the reference velocity being that at 1.3 cm below the water surface. A reference velocity at or nearer the surface would be atypical of the drift system as a whole, for the occasional high speed jet gives a very nonuniform flow there. It will be seen that the two

profiles have a strong family likeness, the height of zero velocity being nearly the same. In the lower (return) current, however, the measured profile is a flatter one which gives larger gradients near the bottom.

The experimental work described above was done while I was holding a fellowship at, and granted by, the Woods Hole Oceanographic Institution.

REFERENCES

Francis, J. R. D.
1951. The aerodynamic drag of a free water surface. Proc. roy. Soc. London, (A) *206:* 387–406.

Hellstrom, B.
1941. Wind effects on lakes and rivers. Ingen. Vetensk. Akad. Handl., No. 158.

Keulegan, G. H.
1951. Wind tides in small closed channels. J. Res. Nat. Bur. Stand., Wash., *46:* 358–381.

Sheppard, P. A.
1946. The aerodynamic drag of the earth's surface and the value of von Karman's constant in the lower atmosphere. Proc. roy. Soc. London, (A) *188:* 208–222.

CIRCULATION IN THE UPPER MIXED LAYER OF THE EQUATORIAL NORTH PACIFIC[1]

By

KOZO YOSHIDA, HAN-LEE MAO AND PAUL L. HORRER

Scripps Institution of Oceanography
University of California
La Jolla, California

ABSTRACT

The circulation in the upper mixed layer in the equatorial region of the North Pacific is treated by solving the steady-state equations containing terms of Corioli's force, pressure gradient, and horizontal as well as vertical mixing. Assumptions made include: (1) The coefficient of vertical eddy viscosity is constant in the top homogeneous layer and vanishes at the bottom of the layer; (2) the horizontal velocity field may be approximated by a sinusoidal function, and thus horizontal mixing terms may be chosen in simple form; and (3) the mean wind-stress distribution and mean density distribution suggested by Reid are generally applicable. Mathematical development of the vertical motion is carried out in detail and numerical results are obtained. Agreement of the results obtained herein with available observed data and theoretical considerations by other investigators is discussed.

INTRODUCTION

During recent years, considerable progress has been made in the theoretical development of mass transport associated with the general oceanic circulation by Stockmann (1946b), Sverdrup (1947), Reid (1948a), Stommel (1948), Munk (1950), Hidaka (1951), and others. In these papers, however, the character of the vertical distribution of density is not specified and hence no vertical profile of current was obtained. Stockmann (1946a) and Hidaka and Takano (1952) dealt with the current profile but made the assumption of homogeneous water which is not very well justified in the actual case. Until the recent work of Weenink and Groen (1952), which appeared when our present investigation was nearly completed, the treatment by Defant (1936) for the Atlantic was still considered the classic of circulation in the upper mixed layer of the equatorial ocean. Defant's assumptions of no motion in the underlying water mass and of no net meridional transport of water ($M_y = 0$) in the upper mixed layer, and his approach of preassuming the value of surface current velocities, are questionable, especially in the light of recent knowledge. Some of Weenink

[1] Contributions from the Scripps Institution of Oceanography, New Series, No. 620.

and Groen's assumptions differ from those made in the following discussion, but their computational results were not made available. Thus, the ensuing treatment reconsiders the problem of circulation in the upper mixed layer of the equatorial Pacific, with emphasis on detailed discussion of the vertical motion, an aspect not included in previous works.

BASIC THEORY

Let the x-axis be positive eastward along the equator, the y-axis northward, and the z-axis vertically downward from the undisturbed level surface. The terms of horizontal mixing may be chosen as $-ku$ and $-kv$ as a close first approximation when u and v, the eastward and northward components of the current velocity respectively, vary sinusoidally with latitude, which, as we shall see later, is the case in the area considered. The coefficient of the vertical eddy viscosity is assumed constant in the upper mixed layer. If the nonlinear terms and the term including the vertical motion (i. e., $2\omega \cos \varphi w$) are considered negligible, the equations of steady horizontal motion are

$$\begin{aligned} -\lambda v &= -\frac{1}{\rho}\frac{\partial p}{\partial x} + \frac{1}{\rho}\frac{\partial}{\partial z}\left(A\frac{\partial u}{\partial z}\right) - ku \\ \lambda u &= -\frac{1}{\rho}\frac{\partial p}{\partial y} + \frac{1}{\rho}\frac{\partial}{\partial z}\left(A\frac{\partial v}{\partial z}\right) - kv, \end{aligned} \tag{1}$$

where p is pressure, ρ is density, A is the coefficient of vertical mixing, λ is Corioli's parameter given by $\lambda = 2\omega \sin \varphi$, ω is the angular velocity of the earth's rotation, and φ is latitude.

The parameter k (which may be called the "mixing number") is defined by

$$k = \frac{4\pi^2}{L^2} B, \tag{2}$$

where B is the coefficient of horizontal mixing and L is the wave length of the sinusoidal horizontal velocity profile. Generally the parameter k may be assumed as a function of the y-coordinate in the form of $-k(y)u$ and $-k(y)v$. (Recall that λ also varies with the y-coordinate.)

Let u and v be separated into two parts as follows:

$$\begin{aligned} u &= u_1(x, y) + u_2(x, y, z) \\ v &= v_1(x, y) + v_2(x, y, z), \end{aligned} \tag{3}$$

where u_1, v_1 and u_2, v_2 compose the "gradient current" and "drift current" respectively.

The pressure at any depth can be determined from the hydrostatic equation by using Reid's (1948b) model for the distribution of density

$$\begin{aligned} \rho &= \rho_0 \qquad\qquad \text{for } z \leqslant h\,(x, y) \\ \rho\,(x, y, z) &= \rho_d - \Delta\rho e^{1-z/h} \quad \text{for } z \geqslant h\,(x, y)\,, \end{aligned} \tag{4}$$

where $\Delta\rho = \rho_d - \rho_0$ and h is the lower boundary of the homogeneous layer.

Thus, the equations for u_1 and v_1 are

$$\left.\begin{aligned} -\lambda v_1 &= -\frac{1}{\rho_0}\frac{\partial p}{\partial x} - k u_1 \\ \lambda u_1 &= -\frac{1}{\rho_0}\frac{\partial p}{\partial y} - k v_1 \end{aligned}\right\} \text{for } z \leqslant h\,. \tag{5}$$

For simplicity, the subscript $_0$ in the density ρ_0 shall be dropped henceforth, since only the upper mixed water layer is of concern in this study. No attempt shall be made to discuss the motion in the underlying layer.

Then the solution of equation (5) can be given by

$$\begin{aligned} u_1 &= \frac{1}{\lambda^2 + k^2}\left(\frac{k}{\rho}\frac{\partial p}{\partial x} + \frac{\lambda}{\rho}\frac{\partial p}{\partial y}\right) \\ v_1 &= \frac{1}{\lambda^2 + k^2}\left(\frac{\lambda}{\rho}\frac{\partial p}{\partial x} - \frac{k}{\rho}\frac{\partial p}{\partial y}\right). \end{aligned} \tag{6}$$

For u_2 and v_2 we have

$$\begin{aligned} -\lambda v_2 &= \frac{A}{\rho}\frac{\partial^2 u_2}{\partial z^2} - k u_2 \\ \lambda u_2 &= \frac{A}{\rho}\frac{\partial^2 v_2}{\partial z^2} - k v_2\,. \end{aligned} \tag{7}$$

As boundary conditions we assume

$$\begin{aligned} \left.\frac{\partial u_2}{\partial z}\right|_{z=0} &= -\frac{\tau_x(y)}{A} \\ \left.\frac{\partial v_2}{\partial z}\right|_{z=0} &= -\frac{\tau_y(y)}{A} \\ \left.\frac{\partial u_2}{\partial z}\right|_{z=h} &= \left.\frac{\partial v_2}{\partial z}\right|_{z=h} = 0\,. \end{aligned} \tag{8}$$

The last equation indicates that A is discontinuous at $z = h$, being zero at this depth and constant above it. This equation is postulated with the understanding that the stress be continuous at the boundary.

The assumption that A is discontinuous at $z = h$, as a first approximation, is in fair agreement with the result of Munk and Anderson (1948) and is in accord with our present knowledge.

Under these assumptions,[2] we have

$$u_2 = \frac{U}{A\,(m^2 + n^2)(\cosh 2\theta - \cos 2\theta_1)}$$
$$v_2 = \frac{V}{A\,(m^2 + n^2)(\cosh 2\theta - \cos 2\theta_1)}, \tag{9}$$

where

$$\begin{aligned}
U &= (m\tau_x + n\tau_y)\,F_1 + (m\tau_y - n\tau_x)\,F_2\,,\\
V &= (m\tau_y - n\tau_x)\,F_1 - (m\tau_x + n\tau_y)\,F_2\,,\\
F_1 &= \sinh mz \cos(2\theta_1 - nz) + \sinh(2\theta - mz)\cos nz\,,\\
F_2 &= \cosh mz \sin(2\theta_1 - nz) + \cosh(2\theta - mz)\sin nz\,,\\
m &= \sqrt{\rho\,(k_1 + k)/2A}\,,\\
n &= \sqrt{\rho\,(k_1 - k)/2A}\,,\\
k_1 &= \sqrt{k^2 + \lambda^2}\,,\\
\theta &= mh, \quad \theta_1 = nh\,, \text{ and}\\
&\tau_x \text{ and } \tau_y \text{ are components of wind stress.}
\end{aligned}$$

For $\varphi = 0$, we have

$$u_1 = -\frac{1}{k\rho}\frac{\partial p}{\partial x} \qquad v_1 = -\frac{1}{k\rho}\frac{\partial p}{\partial y}$$
$$u_2 = \frac{\tau_x\{\sinh mz + \sinh(2\theta - mz)\}}{Am\,(\cosh 2\theta - 1)}$$
$$v_2 = \frac{\tau_y\{\sinh mz + \sinh(2\theta - mz)\}}{Am\,(\cosh 2\theta - 1)}. \tag{10}$$

[2] It is easily seen from our basic differential equation (1) that no lateral boundary condition is explicitly required to obtain our solutions. However, since $\partial p/\partial x$, $\partial p/\partial y$ and h are derived from mass-transport theory, which is based on the integrated forms of equation (1), in which a lateral boundary condition ($M_x = 0$ at eastern boundary) is used, our solutions satisfy this same lateral boundary condition.

As to the equation of continuity, the three-dimensional form will be taken into consideration in our later section on vertical motion. In this section on the discussions of horizontal motion, which is based on the approximate equation (1), only the integrated equation of continuity is used to derive the values of $\partial p/\partial x$, $\partial p/\partial y$ and h.

It can be shown that, except for the region of low latitudes, Reid's values of $\partial p/\partial x$, $\partial p/\partial y$ and h (see Discussion) are very close to ours. We shall see later that, for our numerical computations, Reid's values of these quantities have been actually used for $\phi > 7°$ N.

COMPUTATIONS

Using equations (6), (9) and (10) in the previous section, numerical computations of u and v can be performed. $\partial p/\partial x$ and $\partial p/\partial y$ in equation (6) may be derived with sufficient accuracy from the model of density distribution given by Reid (1948b). Hence, we have

$$\begin{aligned} \frac{\partial p}{\partial x} &= g\rho \frac{\partial \zeta}{\partial x} = 2\, g \Delta\rho \frac{\partial h}{\partial x} = \frac{2}{5h} \frac{\partial P}{\partial x} \\ \frac{\partial p}{\partial y} &= g\rho \frac{\partial \zeta}{\partial y} = 2\, g \Delta\rho \frac{\partial h}{\partial y} = \frac{2}{5h} \frac{\partial P}{\partial y}, \end{aligned} \tag{11}$$

where P is the vertically integrated pressure from the surface to the level of no motion, g is the acceleration of gravity, and $\zeta = \zeta\,(x, y)$ is the elevation of the surface.

Thus, for numerical computation, equation (6) may be transformed into

$$\begin{aligned} u_1 &= -\frac{2}{5\,(\lambda^2 + k^2)\,\rho h}\,(kf_1 + \lambda f_2) \\ v_1 &= \frac{2}{5\,(\lambda^2 + k^2)\,\rho h}\,(\lambda f_1 - k f_2), \end{aligned} \tag{12}$$

where $f_1 = \Delta P/\Delta x$ and $f_2 = \partial P/\partial y$, after Reid (1948a).

In the computations, use has also been made of Reid's model value of h except for $\varphi \leqslant 7°$ N, where it differs considerably (cf. Reid, 1948b: figs. 2, 3) from the actual distribution shown by the Carnegie data (Sverdrup, et al., 1944); therefore the Carnegie data have been used for this region. As to the parameter k, values of 5×10^{-6}, 2.5×10^{-6} and 1×10^{-6} are used respectively for $\varphi = 0°$, 1°, and 2° or greater. Further discussion about these are given in the last section. The coefficient of vertical eddy viscosity, A, which appears in equation (9), is assumed to be 10^2 cgs units, which seems reasonable according to Sverdrup, et al. (1946: 484) and Hidaka, et al. (1951). The numerical results u and v for each latitude,[3] obtained by summing the "gradient current" and "drift current," are tabulated in Tables IA and IB. Values of u and v at surface and at $z = h$ are illustrated in Figs. 1a and 1b. Characteristic profiles of velocity components in the South Equatorial Current, Equatorial Counter Current and North Equatorial Current are shown in Figs. 2a to 2c.

[3] Since the pressure field and velocity field are determined from the wind stress field, to which only mean values for all longitudes considered are given, any variation in longitudinal direction is not of concern in our study.

TABLE I-A—Distribution of East-West Component (u) of Current Velocity in the Equatorial North Pacific (in cm/sec)

Depth (m)	LATITUDE (°)																			
	0	1	2	3	4	5	6	7	8	9	10	11	12	13	14	15	16	17	18	19	20
0	−20.8	−10.5	−1.8	2.9	7.7	12.1	17.5	23.4	33.6	38.1	14.4	−0.8	−15.0	−23.5	−27.2	−26.5	−36.1	−26.5	−24.3	−20.3	−20.4
5	−20.0	−8.9	−0.5	3.9	8.3	12.6	17.9	23.7	34.1	38.7	15.3	0.2	−13.8	−22.4	−25.9	−24.9	−33.8	−24.3	−22.1	−17.8	−18.1
10	−19.2	−7.5	0.7	4.6	8.8	12.9	18.0	23.7	34.3	39.3	15.7	0.8	−13.4	−21.0	−24.4	−23.3	−31.7	−22.2	−20.0	−16.1	−14.8
15	−18.5	−6.3	1.6	5.2	8.9	13.0	18.0	23.6	34.4	39.6	16.1	1.1	—	−21.1	−23.7	−22.1	−29.7	−20.2	−18.1	−14.1	−12.5
20	−17.7	−5.2	2.4	5.5	9.0	12.9	17.8	23.4	34.5	39.9	16.6	—	—	—	−23.3	−21.3	−28.1	−18.6	−16.5	−12.9	−10.3
25	−17.1	−4.2	3.0	5.7	8.9	12.7	17.5	23.0	34.5	40.1	17.0	—	—	—	—	−21.0	−26.9	−17.3	−15.1	−11.8	−8.9
30	−16.5	−3.4	3.6	5.8	8.8	12.4	17.2	22.8	34.5	40.3	—	—	—	—	—	—	−26.2	−16.2	−14.2	−11.0	−7.7
35	−15.9	−2.7	4.0	5.8	8.5	12.0	16.8	22.4	34.4	40.3	—	—	—	—	—	—	−26.0	−15.5	−13.4	−10.4	−7.0
40	−15.4	−2.0	4.4	5.8	8.1	11.6	16.4	22.1	34.3	—	—	—	—	—	—	—	—	−15.1	−12.9	−10.0	−6.5
45	−14.9	−1.4	4.6	5.5	7.7	11.2	16.0	21.8	34.2	—	—	—	—	—	—	—	—	−14.9	−12.6	−9.7	−6.3
50	−14.5	−1.0	4.9	5.5	7.3	10.8	15.6	21.5	34.2	—	—	—	—	—	—	—	—	—	−12.4	−9.7	−6.2
55	−14.1	−0.5	5.0	5.2	6.9	10.3	15.3	21.3	34.1	—	—	—	—	—	—	—	—	—	−12.4	−9.6	−6.3
60	−13.7	−0.2	5.1	5.0	6.5	9.9	15.0	20.9	34.1	—	—	—	—	—	—	—	—	—	—	−9.6	−6.4
65	−13.4	0.0	5.2	4.8	6.2	9.6	14.7	20.7	—	—	—	—	—	—	—	—	—	—	—	−9.6	−6.5
70	−13.1	0.3	5.3	4.6	5.8	9.2	14.4	20.5	—	—	—	—	—	—	—	—	—	—	—	—	−6.5
75	−12.9	0.4	5.3	4.4	5.5	8.9	14.2	20.4	—	—	—	—	—	—	—	—	—	—	—	—	−6.6
80	−12.6	0.5	5.3	4.2	5.2	8.6	14.0	20.3	—	—	—	—	—	—	—	—	—	—	—	—	−6.6
85	—	0.5	5.3	4.1	5.0	8.3	13.8	20.2	—	—	—	—	—	—	—	—	—	—	—	—	—
90	—	—	5.4	4.0	4.8	8.1	13.6	20.1	—	—	—	—	—	—	—	—	—	—	—	—	—
95	—	—	5.4	3.9	4.7	7.9	13.5	20.0	—	—	—	—	—	—	—	—	—	—	—	—	—
100	—	—	—	3.9	4.6	7.8	13.4	20.0	—	—	—	—	—	—	—	—	—	—	—	—	—
105	—	—	—	—	4.6	7.7	13.4	—	—	—	—	—	—	—	—	—	—	—	—	—	—
110	—	—	—	—	—	7.6	13.4	—	—	—	—	—	—	—	—	—	—	—	—	—	—
115	—	—	—	—	—	7.5	13.3	—	—	—	—	—	—	—	—	—	—	—	—	—	—
120	—	—	—	—	—	7.5	—	—	—	—	—	—	—	—	—	—	—	—	—	—	—
125	—	—	—	—	—	7.5	—	—	—	—	—	—	—	—	—	—	—	—	—	—	—

TABLE I-B--Distribution of North-South Component (v) of Current Velocity in the Equatorial North Pacific (in cm/sec)

Depth (m)	LATITUDE (°)																				
	0	1	2	3	4	5	6	7	8	9	10	11	12	13	14	15	16	17	18	19	20
0	5.8	17.3	13.4	13.1	11.9	10.4	8.4	6.9	5.5	4.0	3.7	6.8	12.4	7.6	2.5	−0.7	−2.7	−3.1	−3.1	−2.6	−2.9
5	5.6	16.3	12.0	11.3	10.0	8.6	6.9	5.6	5.0	4.2	4.6	8.4	13.8	8.3	4.7	1.7	0.0	−0.7	−0.7	−0.3	0.3
10	5.4	15.4	10.0	9.4	8.2	7.0	5.4	4.5	4.5	4.2	5.4	9.4	14.5	9.5	6.2	3.3	1.6	0.8	0.7	0.9	2.0
15	5.2	14.5	9.3	7.8	6.6	5.5	4.3	3.6	3.9	4.2	5.9	9.9	—	9.8	6.7	4.2	2.8	1.7	1.4	1.4	2.2
20	5.0	13.7	7.9	6.2	5.1	4.3	3.3	2.8	3.5	4.2	6.1	—	—	—	7.2	4.9	3.3	2.0	1.7	1.6	2.9
25	4.8	12.9	6.7	4.9	3.8	3.1	2.4	2.1	3.1	4.2	6.1	—	—	—	—	5.1	3.7	2.1	1.4	1.4	2.8
30	4.7	12.3	5.4	3.6	2.7	2.1	1.7	1.6	2.9	4.2	—	—	—	—	—	—	3.9	1.9	1.2	1.0	2.2
35	4.5	11.8	4.3	2.4	1.6	1.3	1.1	1.2	2.5	4.1	—	—	—	—	—	—	3.9	1.8	0.7	0.6	1.3
40	4.4	11.1	3.5	1.4	0.8	0.7	0.6	0.9	2.3	—	—	—	—	—	—	—	—	1.7	0.3	0.1	1.0
45	4.2	10.5	2.6	0.4	0.1	0.1	0.3	0.7	2.2	—	—	—	—	—	—	—	—	1.6	0.0	−0.5	0.5
50	4.1	10.0	1.7	−0.4	−0.6	−0.3	0.1	0.6	2.1	—	—	—	—	—	—	—	—	—	−0.1	−0.6	0.0
55	4.0	9.6	1.0	−1.1	−1.2	−0.6	−0.1	0.4	2.0	—	—	—	—	—	—	—	—	—	−0.2	−0.8	−0.4
60	3.9	9.3	0.3	−1.8	−1.6	−0.8	−0.2	0.4	1.9	—	—	—	—	—	—	—	—	—	—	−0.9	−0.7
65	3.8	9.0	−0.1	−2.3	−1.9	−1.0	−0.3	0.4	—	—	—	—	—	—	—	—	—	—	—	−1.0	−0.8
70	3.7	8.8	−0.6	−2.7	−2.2	−1.1	−0.3	0.4	—	—	—	—	—	—	—	—	—	—	—	—	−1.0
75	3.7	8.7	−1.0	−3.1	−2.5	−1.2	−0.3	0.4	—	—	—	—	—	—	—	—	—	—	—	—	−1.1
80	3.6	8.6	−1.2	−3.4	−2.7	−1.2	−0.3	0.4	—	—	—	—	—	—	—	—	—	—	—	—	−1.1
85	—	8.5	−1.4	−3.7	−2.8	−1.2	−0.3	0.5	—	—	—	—	—	—	—	—	—	—	—	—	—
90	—	—	−1.4	−3.8	−2.9	−1.2	−0.2	0.5	—	—	—	—	—	—	—	—	—	—	—	—	—
95	—	—	−1.4	−3.9	−3.0	−1.1	−0.2	0.5	—	—	—	—	—	—	—	—	—	—	—	—	—
100	—	—	—	−4.0	−3.0	−1.1	−0.2	0.5	—	—	—	—	—	—	—	—	—	—	—	—	—
105	—	—	—	—	−3.0	−1.1	−0.1	—	—	—	—	—	—	—	—	—	—	—	—	—	—
110	—	—	—	—	—	−1.1	−0.1	—	—	—	—	—	—	—	—	—	—	—	—	—	—
115	—	—	—	—	—	−1.1	−0.1	—	—	—	—	—	—	—	—	—	—	—	—	—	—
120	—	—	—	—	—	−1.0	—	—	—	—	—	—	—	—	—	—	—	—	—	—	—
125	—	—	—	—	—	−1.0	—	—	—	—	—	—	—	—	—	—	—	—	—	—	—

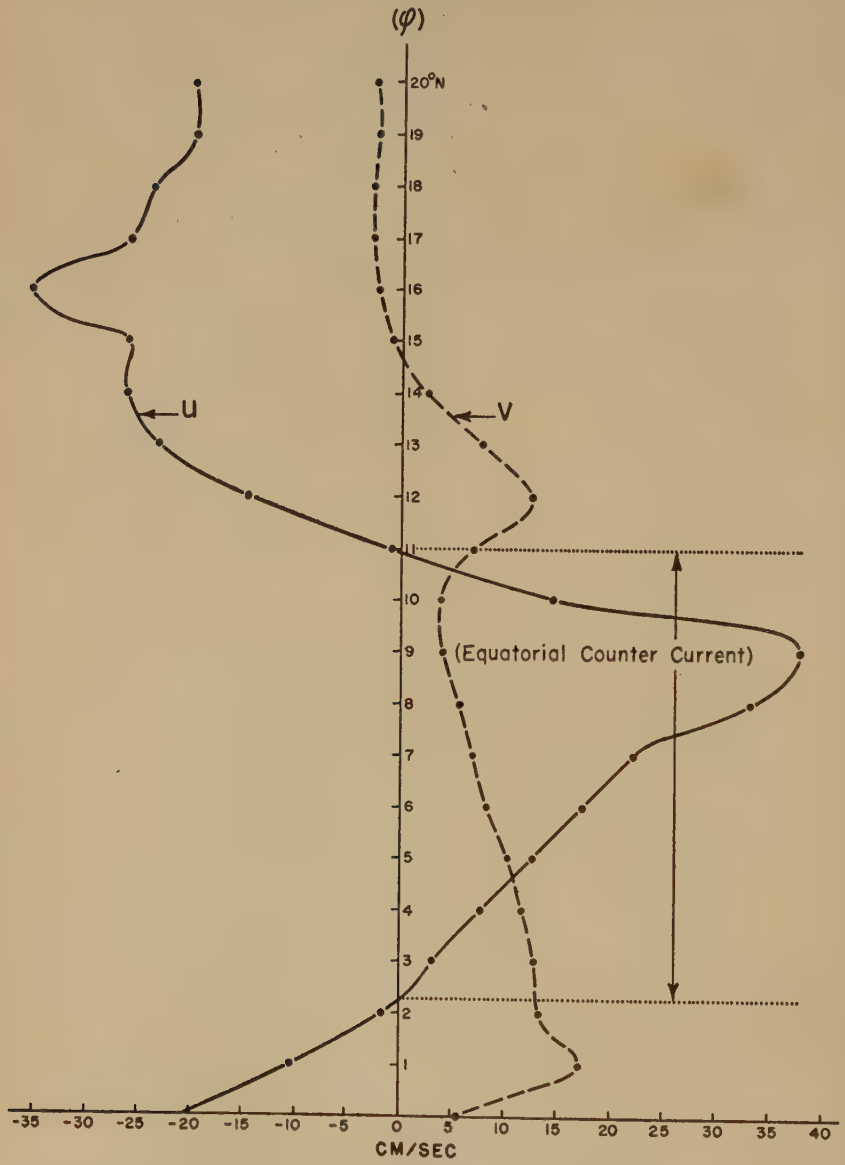

Figure 1a. Latitude dependence of the (horizontal) velocity components at surface.

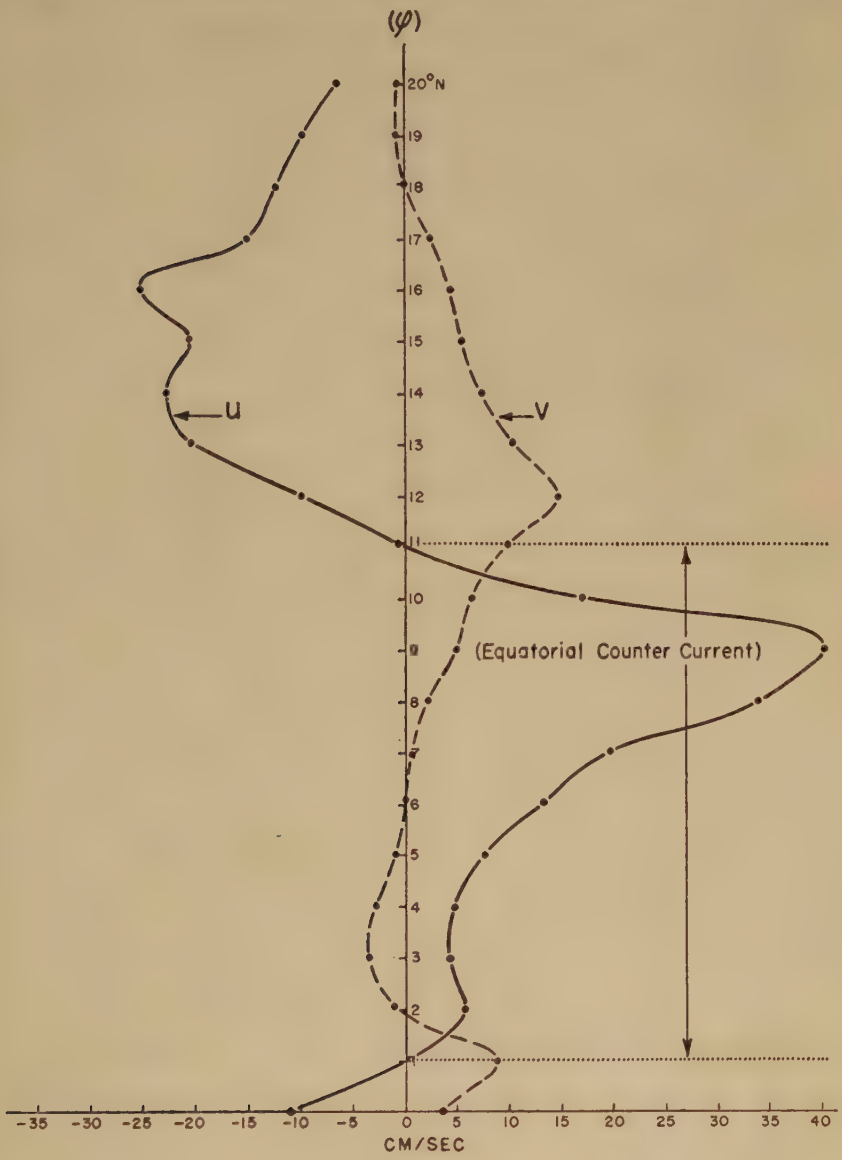

Figure 1b. Latitude dependence of the (horizontal) velocity components at boundary h.

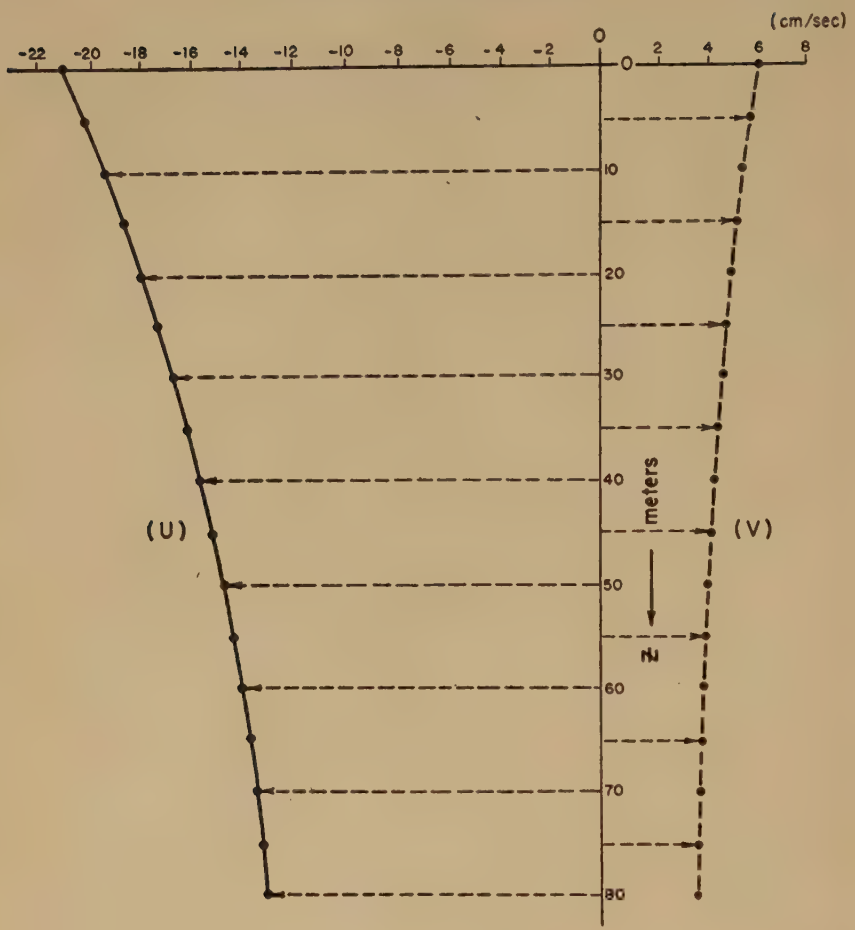

Figure 2a. Vertical profile of (horizontal) velocity components in the South Equatorial Current System (at equator).

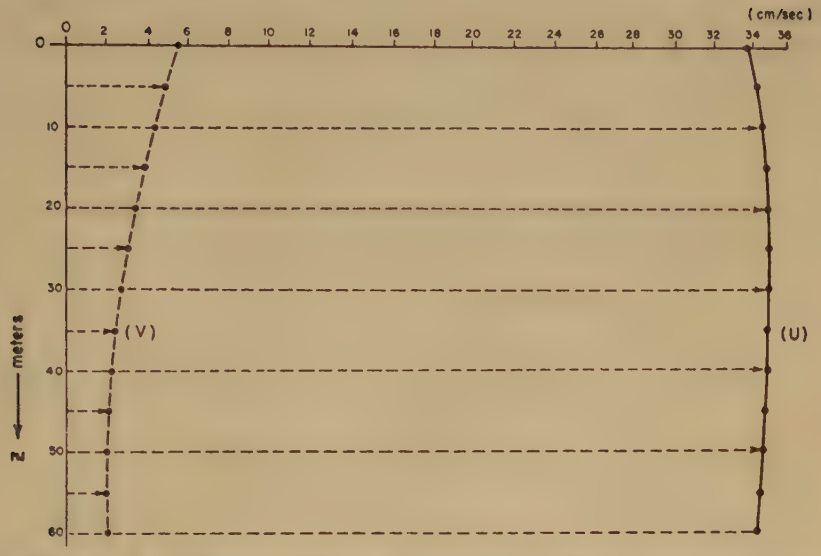

Figure 2b. Vertical profile of (horizontal) velocity components in the Equatorial Counter Current System (at 8° N).

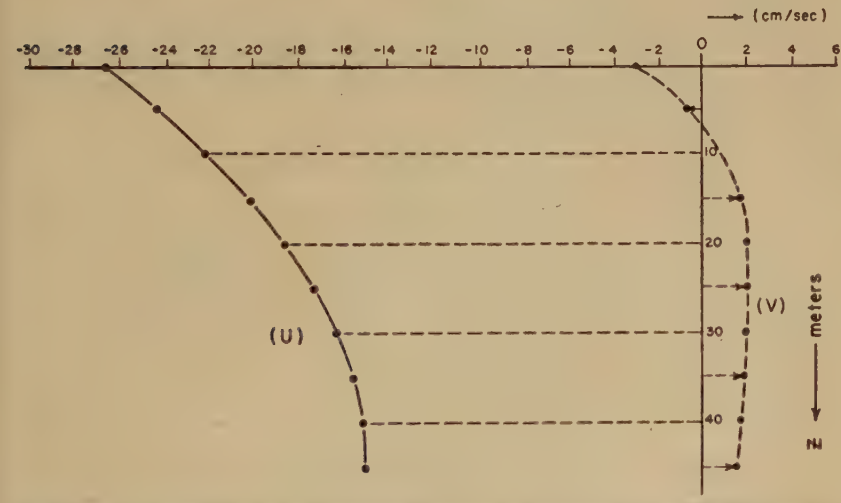

Figure 2c. Vertical profile of (horizontal) velocity components in the North Equatorial Current System (at 17° N).

THEORY AND COMPUTATIONS OF VERTICAL MOTION

The vertical velocity in the upper mixed layer, derived from the integrated equation of continuity, is

$$w(z) = -\int_{-\zeta}^{z}\left(\frac{\partial u}{\partial x}+\frac{\partial v}{\partial y}\right)dz\,, \tag{13}$$

provided that w is vanishingly small along the sea surface ($z = -\zeta$). For the vertical velocity at $z = h$, we have

$$\begin{aligned} w(h) &= -\int_{-\zeta}^{h}\left(\frac{\partial u}{\partial x}+\frac{\partial v}{\partial y}\right)dz \\ &= -\left\{\frac{\partial}{\partial x}\int_{-\zeta}^{h}u\,dz+\frac{\partial}{\partial y}\int_{-\zeta}^{h}v\,dz\right\} \\ &\quad + u_h\frac{\partial h}{\partial x}+v_h\frac{\partial h}{\partial y}\,, \end{aligned} \tag{14}$$

provided that

$$u_\zeta\frac{\partial\zeta}{\partial x}\ll u_h\frac{\partial h}{\partial x}\,, \qquad v_\zeta\frac{\partial\zeta}{\partial y}\ll v_h\frac{\partial h}{\partial y}\,,$$

which are easily fulfilled.

From this equation it is seen that the divergence of mass transport is explicitly involved in the derivation of the vertical velocity, and thus it is desirable at this time to proceed somewhat further in the development of mass transport theory for both the upper homogeneous layer and the underlying layer. To avoid confusion, the following notations shall be adopted:

$$\begin{aligned} &M_x = \int_{-\zeta}^{d}\rho u\,dz\,, \quad M_y = \int_{-\zeta}^{d}\rho v\,dz \text{ (for the whole layer)} \\ &M_x' = \int_{-\zeta}^{h}\rho u\,dz\,, \quad M_y' = \int_{-\zeta}^{h}\rho v\,dz \text{ (for the upper homogeneous layer)} \\ &M_x'' = \int_{h}^{d}\rho u\,dz\,, \quad M_y'' = \int_{h}^{d}\rho v\,dz \text{ (for the underlying layer),} \end{aligned} \tag{15}$$

where d is depth of no motion.

Integrating the basic equation of motion (1) from the surface to depth of no motion, we obtain

$$\begin{aligned} M_x &= \frac{1}{\lambda^2+k^2}\left[-(kf_1+\lambda f_2)+k\tau_x+\lambda\tau_y\right] \\ M_y &= \frac{1}{\lambda^2+k^2}\left[(\lambda f_1-kf_2)+k\tau_y-\lambda\tau_x\right]. \end{aligned} \tag{16}$$

In a similar manner, the mass transport for the upper homogeneous layer, M_x' and M_y', is

$$\begin{aligned} M_x' &= \frac{1}{\lambda^2 + k^2}\left[- (kf_1' + \lambda f_2') + k\tau_x + \lambda\tau_y \right] \\ M_y' &= \frac{1}{\lambda^2 + k^2}\left[(\lambda f_1' - kf_2') + k\tau_y - \lambda\tau_x \right], \end{aligned} \tag{17}$$

where $f_1' = \dfrac{\partial}{\partial x}\displaystyle\int_{-\xi}^{h} p\,dz$ and $f_2' = \dfrac{\partial}{\partial y}\displaystyle\int_{-\xi}^{h} p\,dz$.

By use of the relations

$$f_1' = \frac{2}{5} f_1 \text{ and } f_2' = \frac{2}{5} f_2, \tag{18}$$

which are easily found from Reid's model of density distribution, we obtain

$$\begin{aligned} M_x' &= \frac{2}{5} M_x + \frac{3}{5}\frac{1}{\lambda^2 + k^2}(k\tau_x + \lambda\tau_y) \\ M_y' &= \frac{2}{5} M_y + \frac{3}{5}\frac{1}{\lambda^2 + k^2}(k\tau_y - \lambda\tau_x) \end{aligned} \tag{19}$$

for the upper layer, and

$$\begin{aligned} M_x'' &= -\frac{3}{5}\frac{1}{\lambda^2 + k^2}(kf_1 + \lambda f_2) \\ M_y'' &= -\frac{3}{5}\frac{1}{\lambda^2 + k^2}(\lambda f_1 - kf_2) \end{aligned} \tag{20}$$

for the underlying layer.

From equation (19) and the integrated equation of continuity for the whole water column,

$$\frac{\partial M_x}{\partial x} + \frac{\partial M_y}{\partial y} = 0, \tag{21}$$

we obtain

$$\frac{\partial M_x'}{\partial x} + \frac{\partial M_y'}{\partial y} = \frac{3}{5}\frac{\partial}{\partial y}\left[\frac{1}{\lambda^2 + k^2}(k\tau_y - \lambda\tau_x)\right], \tag{22}$$

provided that τ_x and τ_y are functions of y only.

By substituting equation (22) in equation (14) [the other quantities in the right-hand side of equation (14) are known], w at $z = h$ can be determined.

An approximation of w for $-\zeta \leq z \leq h$ is

$$w^*(z) = -\int_{-\zeta}^{z} \frac{\partial v}{\partial y}\, dz\,. \tag{23}$$

Therefore

$$\begin{aligned} w(h) &= w^*(h) - \int_{-\zeta}^{h} \frac{\partial u}{\partial x}\, dz \\ &= w^*(h) - \frac{\partial M_x'}{\partial x} + u_h \frac{\partial h}{\partial x} \\ &= w^*(h) + \frac{2}{5}\frac{\partial M_y}{\partial y} + u_h \frac{\partial h}{\partial x} \end{aligned} \tag{24}$$

if the relationship

$$\frac{\partial M_x'}{\partial x} = \frac{2}{5}\frac{\partial M_x}{\partial x} = -\frac{2}{5}\frac{\partial M_y}{\partial y}$$

is used.

Our results suggest that

$$\int_{-\zeta}^{z} \frac{\partial u_2}{\partial x}\, dz \ll \int_{-\zeta}^{z} \frac{\partial u_1}{\partial x}\, dz$$

and

$$\left| u_h \frac{\partial h}{\partial x} \right| \ll \left| \frac{2}{5}\frac{\partial M_y}{\partial y} \right|$$

so that the following approximation

$$-\int_{-\zeta}^{z} \frac{\partial u}{\partial x}\, dz \approx -\frac{\partial u_1}{\partial x} z \approx \frac{2}{5}\left(\frac{z}{h}\right)\frac{\partial M_y}{\partial y} \tag{25}$$

can be derived. Combining equations (13), (23) and (25), the expression for w (z) is given as

$$w(z) = w^*(z) + \left(\frac{z}{h}\right)\left(\frac{2}{5}\frac{\partial M_y}{\partial y}\right). \tag{26}$$

TABLE II—Distribution of Vertical Component (w) of Current Velocity in the Equatorial North Pacific (in 10^{-3} cm/sec)

Depth (m)	LATITUDE (°) 0	1	2	3	4	5	6	7	8	9	10	11	12	13	14	15	16	17	18	19	20
0	−.43	.00	.01	.07	.09	.11	.08	.07	.04	−.01	−.16	−.23	.19	.15	.11	.08	.01	−.01	−.02	.01	
5	−.69	−.13	.04	.16	.18	.21	.15	.11	.02	−.07	−.35	−.39	.32	.19	.16	.15	.01	−.04	−.05	.01	
10	−.97	−.29	.08	.25	.26	.30	.21	.12	−.02	−.17	−.53	−.54	.44	.23	.19	.21	.03	−.06	−.07	−.02	
15	−1.20	−.37	.14	.34	.33	.38	.25	.11	−.09	−.28	−.71	—	—	.26	.21	.26	.06	−.08	−.08	−.04	
20	−1.40	−.46	.19	.43	.39	.44	.27	.09	−.18	−.40	−.80	—	—	—	.23	.32	.09	−.08	−.09	−.08	
25	−1.55	−.53	.24	.50	.44	.49	.30	.06	−.29	−.53	—	—	—	—	—	.37	.14	−.07	−.09	−.13	
30	−1.69	−.57	.30	.57	.49	.54	.32	.01	−.40	−.59	—	—	—	—	—	.40	.21	−.05	−.09	−.15	
35	−1.79	−.56	.36	.64	.52	.58	.33	−.03	−.53	—	—	—	—	—	—	—	.28	−.02	−.09	−.26	
40	−1.88	−.55	.44	.68	.55	.59	.31	−.08	−.66	—	—	—	—	—	—	—	.31	.03	−.08	−.29	
45	−1.95	−.49	.52	.72	.56	.59	.31	−.16	−.81	—	—	—	—	—	—	—	—	.10	−.06	−.20	
50	−2.01	−.47	.59	.76	.56	.58	.30	−.22	—	—	—	—	—	—	—	—	—	.11	−.02	−.18	
55	−2.05	−.41	.67	.78	.54	.57	.28	−.27	—	—	—	—	—	—	—	—	—	—	−.02	−.16	
60	−2.10	−.35	.75	.79	.53	.56	.26	−.34	—	—	—	—	—	—	—	—	—	—	—	−.15	
65	−2.16	−.27	.84	.79	.50	.54	.24	−.43	—	—	—	—	—	—	—	—	—	—	—	—	
70	−2.23	−.19	.90	.79	.46	.51	.22	—	—	—	—	—	—	—	—	—	—	—	—	—	
75	−2.26	−.12	.98	.78	.40	.48	.19	—	—	—	—	—	—	—	—	—	—	—	—	—	
80	−2.30	.01	1.05	.77	.35	.45	.16	—	—	—	—	—	—	—	—	—	—	—	—	—	
85	—	.15	1.14	.75	.30	.43	.14	—	—	—	—	—	—	—	—	—	—	—	—	—	
90	—	—	1.22	.73	.24	.41	.12	—	—	—	—	—	—	—	—	—	—	—	—	—	
95	—	—	1.32	.70	.17	.38	.09	—	—	—	—	—	—	—	—	—	—	—	—	—	
100	—	—	—	.68	.09	.35	.06	—	—	—	—	—	—	—	—	—	—	—	—	—	
105	—	—	—	—	.02	.32	.03	—	—	—	—	—	—	—	—	—	—	—	—	—	
110	—	—	—	—	−.04	.30	—	—	—	—	—	—	—	—	—	—	—	—	—	—	
115	—	—	—	—	—	.26	—	—	—	—	—	—	—	—	—	—	—	—	—	—	
120																					

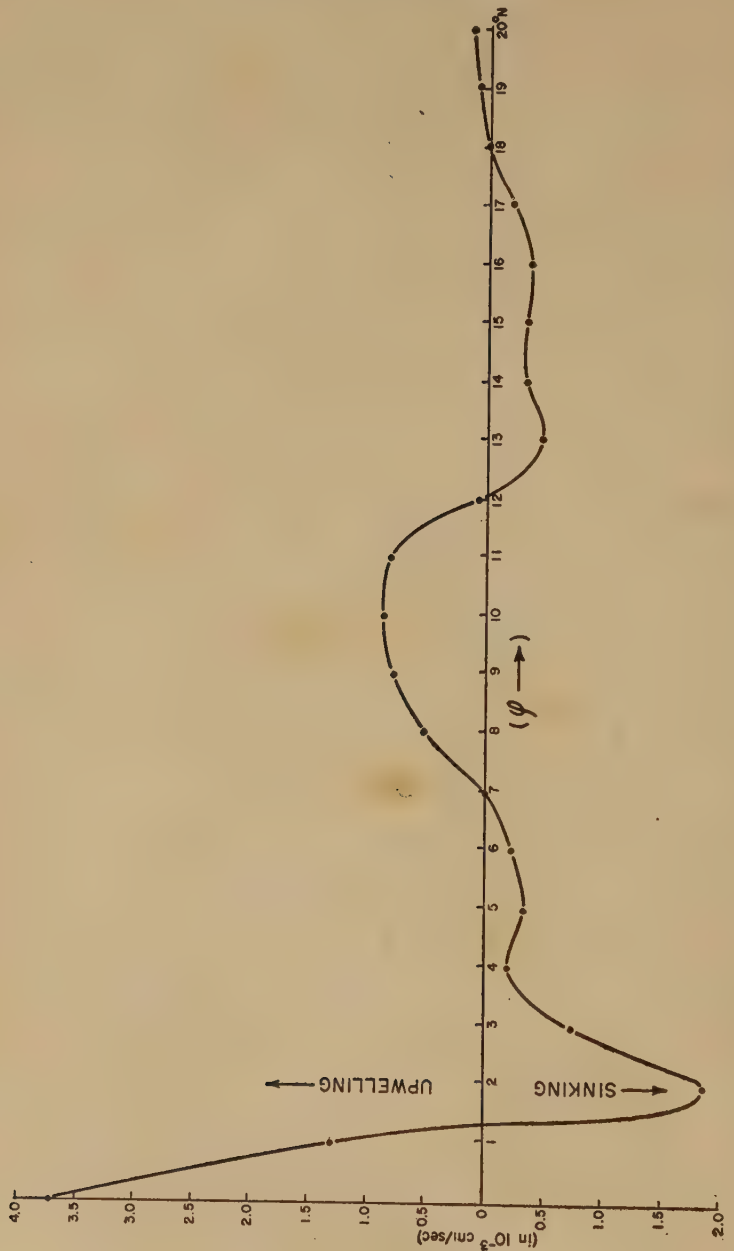

Figure 3. Latitude dependence of the vertical motion at the lower boundary of the shallow water layer h.

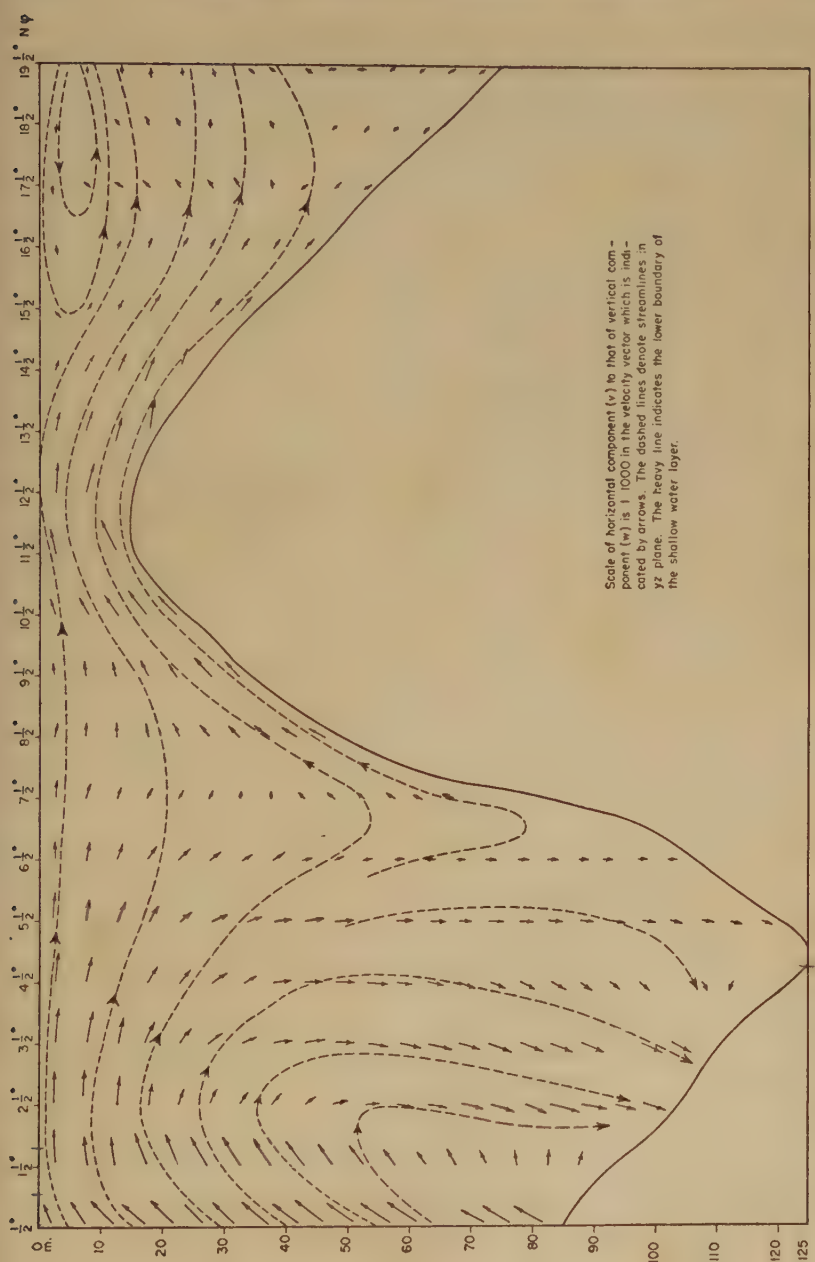

Figure 4. Representation of shallow water circulation in a vertical plane along the North-South direction.

The numerical results of w integrated vertically for increments of 5 meters are tabulated in Table II. The vertical velocity at depth $z = h$ for various latitudes is given in Fig. 3. Combining the corresponding values of v and w from Tables IB and II, we obtain a picture of the velocity field in a vertical plane as shown in Fig. 4.

CONCLUSIONS

Based on the results of previous sections, the general features of the velocity field in the equatorial area of the North Pacific may be described. The boundaries of the Equatorial Counter Current are located at about 2½° N and 11° N at the surface of the upper mixed layer and at approximately 1° N and 11° N at the bottom of the upper mixed layer. The locations of the surface boundaries agree satisfactorily with most observational data available. Our results suggest that the southern boundary is inclined to the south with increasing depth, thus conforming to the widening of the Counter Current with depth as indicated by the CARNEGIE profile (Sverdrup, et al., 1946: 710, fig. 198). Preliminary results of the recent SHELLBACK Expedition (Wooster, 1952) in the eastern equatorial North Pacific suggest that portions of the Counter Current underlie the Equatorial Current.

The maximum horizontal velocity in the Equatorial Counter Current system, calculated from equations derived in the present study, is somewhat over 40 cm/sec at the surface. This agrees well in magnitude with the computed results of the CARNEGIE data, with current meter observations by Japanese investigations (Japanese Hydrographic Department, 1933) and with recent geomagnetic electrokinetograph (GEK) observations made on SHELLBACK. Values of the drag coefficient of the wind stress used herein, adopted from Sverdrup (1947), Munk (1947), and Reid (1948a), are in disagreement with the values obtained by Neumann (1948) and Weenink and Groen (1952). Except at the boundary zones between the different current systems, the zonal component (u) of the surface flow is always much larger than its meridional component (v), and it is especially so at some distance within each of the major current systems (Figs. 1a and 1b). Recently, the U. S. Fish and Wildlife Service (1952) reported that the surface flow of the Equatorial Counter Current was almost entirely from west to east and that there was no appreciable north-south component.

The typical vertical profiles of the horizontal velocity within each of the three major current systems in the equatorial area differ considerably (Figs. 2a to 2c). The Counter Current system is distinctive in that horizontal velocities are virtually constant with depth in the stirred layer. (SHELLBACK Expedition data confirm this result.)

This is due to the predominant role played by the "gradient current" (which is independent of depth in the homogeneous layer) in the Counter Current area where the wind stress is very small.

The numerical results of the distribution of the vertical velocity found in this study are reasonable; the main features are: (1) Very strong upwelling at and near the equator (equatorial divergence); (2) strong sinking at the southern boundary of the Counter Current (note the subsurface convergence in Fig. 4); and (3) fairly strong upwelling at the northern boundary of the Counter Current. The order of magnitude of vertical velocity is from 10^{-4} to 10^{-3} cm/sec. This corresponds closely to values found off the California Coast by McEwen (1919).

DISCUSSION

In this study extensive use has been made of Reid's value of h in the numerical computations. It is to be noted that, in Reid's model, lateral mixing is neglected, while in the present study it is included. Fortunately numerical computations show that, for a high value of the lateral mixing coefficient (that is, 10^8 cgs for B in our notation), the effect of lateral mixing is negligible except very near the equator. Therefore, at higher latitudes Reid's model values of h are sufficiently accurate for use in this study. However, in the very low latitudes, where lateral mixing may be important, values of h have been taken from actual observed data (Sverdrup, et al., 1944).

Substitution of $-ku$ and $-kv$ for the lateral mixing terms permitted mathematical simplification. This should be a close first approximation when the velocity distribution is essentially sinusoidal along the y-coordinate, which is very close to the actual case within the area considered. The horizontal distribution of v (Figs. 1a and 1b) which was obtained from our results departs somewhat from a sinusoidal pattern which we assumed in introducing the lateral-mixing effect. However, it can be seen from equation (1) that deviation from a perfect sinusoidal curve would not materially alter our results.

Assignment of values for the parameter k is based mainly on reasonable values of the wave length (L) of the sinusoidal velocity distribution as well as that of the coefficient of lateral mixing (B) (Montgomery, et al., 1940; Sverdrup, et al., 1946: 485). Since it is generally thought that the curvature of the horizontal current profile (cf. Fig. 1a) is comparatively large very near the equator, which means that the wave length of the sinusoidal velocity distribution is smaller, larger values of the parameter k should be employed in the vicinity of the equator.

Our approach differs considerably from that by Defant (1936). First, in Defant's work, surface values of v are preassigned, while in ours they are determined from consideration of the mean distribution of wind stress. Second, in Defant's work, the N-S component of surface flow is always in reverse directions to that of subsurface flow as a result of his assumption of $M_y = 0$ in a vertical plane; this is considered rather arbitrary and is avoided in our work. Third, Defant's result shows that the current always follows the lower boundary surface of the homogeneous layer (at $z = h$); however, our results demonstrate that it is not necessarily true. It has been shown in equation (14) that the flow does not follow the inclined surface of the lower boundary if the divergence of mass transport in the upper mixed layer does not vanish, and this proves to be the case in low latitudes (below 7° N). Fourth, obvious divergence or convergence at the boundaries of the three major current systems, as shown in Defant's result, does not appear in our picture except for the subsurface divergence at the southern boundary of the Counter Current. Direct measurements of the current at the surface and subsurface levels (especially at the boundaries of the major current systems) will test these two models.

Papers by Weenink and Groen (1952) and Kajiura (1952), which share common interest with our study, have been published recently. One of the essential differences between their works and ours is that they assume the coefficient of vertical eddy viscosity to be constant for the whole water column while we have adopted a discontinuous function at $z = h$. The merits of this assumption are twofold. First, it takes into consideration the fact that the momentum transfer due to turbulent motion is largely reduced where vertical stability is high. This is the case at $z = h$, as is shown in Reid's model of the density distribution. Second, the circulation in the upper stirred layer can be treated semi-independently of the underlying circulation, thus facilitating a simpler mathematical solution. The circulation in the upper layer depends upon the distribution of h, which may be affected in turn by motion in the underlying mass.

Although Weenink and Groen's work is concerned only with the surface current while Kajiura's work included discussions of subsurface current, their approximate solutions are identical. Such solution is based on the assumption that $1 \ll h\sqrt{\frac{\lambda\rho}{2A}}$. It can be shown numerically that, if A is assumed to be 10^2, as used by Kajiura, the approximate solution deviates about 10 to 25 % from the exact one in the area between 9° N and 15° N, where $h\sqrt{\frac{\lambda\rho}{2A}}$ is not large. At

the equator itself and its vicinity, both Weenink and Groen's solution and ours are finite by different approaches; the fitness of the two requires further investigation. In Kajiura's work, the proximity of the equator was excluded.

It is interesting to note that there are certain discrepancies between our result and the direct measurements on SHELLBACK in the latitudinal variation of the horizontal velocity; GEK measurements did not detect the North Equatorial Current but gave current velocities commonly as high as about 1 knot (50 cm/sec) on the northern boundary of the South Equatorial Current (Wooster, 1952). In Fig. IA it is immediately seen that at the northern limit of the Counter Current the velocity shear is large and the width of the horizontal boundary zone narrow while at its southern limit the opposite is the case. These discrepancies probably can be explained largely as a result of the near coastal location of SHELLBACK observations and of other variations in the velocity field that might be expected at a greater distance from land (Robinson, 1952). The large velocity shear at the northern boundary of the Counter Current might possibly lead to the meandering of the Current which might eventually cause the formation of the "large-scale" eddies which have been noted by the SHELLBACK Expedition and which have been borne out by the CROSSROADS data (Barnes, et al., 1948). Such velocity shear and eddies will be considered further in our next work.

REFERENCES

BARNES, C. A., D. R. BUMPUS AND JOHN LYMAN
1948. Ocean circulation in the Marshall Islands area. Trans. Amer. geophys. Un. *29:* 871–876.

DEFANT, ALBERT
1936. Schichtung und Zirkulation der Atlantischen Ozeans. Die Troposphäre. Wiss. Ergebn. dtsch. Atlant. Exped., *6* (3): 316–326.

HIDAKA, KOJI
1951. Drift currents in an enclosed ocean. Part III. Geophys. Notes, Geophys. Inst., Tokyo Univ., *4* (3): 1–19.

HIDAKA, KOJI AND KENZO TAKANO
1952. Wind-driven current and lateral mixing in a zonal ocean. Geophys. Mag., Tokyo, *23* (4): 487–495.

HIDAKA, KOJI, AND TEIICHIRO KUSUNOKI
1951. On the mixing coefficient and the meridional component of velocity in the Equatorial Counter Current. J. Oceanogr. Soc. Japan, *6:* 168–173.

JAPANESE HYDROGRAPHIC DEPARTMENT
1933. Bulletin of the Hydrographic Department of the Imperial Japanese Navy, *6:* 187–211.

KAJIURA, KINJIRO
1952. The velocity distribution of wind currents in the eastern part of the equatorial Pacific. J. Oceanogr. Soc. Japan, *8:* 15–22.

McEwen, G. F.
1919. Ocean temperatures, their relation to solar radiation and oceanic circulation. Semicentennial Publ. Univ. Calif., 1868–1918: 335–421.
Montgomery, R. B., and E. Palmen
1940. Contribution to the question of the Equatorial Counter Current. J. Mar. Res., *3:* 112–133.
Munk, W. H.
1947. A critical wind speed for air-sea boundary processes. J. Mar. Res., *6:* 203–218.
1950. On the wind-driven oceanic circulation. J. Meteorol., *7:* 79–93.
Munk, W. H., and E. R. Anderson
1948. Notes on a theory of the thermocline. J. Mar. Res., *7:* 276–295.
Neumann, Gerhard
1948. Uber den Tangentialdruck des Windes und die Rauhigkeit der Meeresoberflache. Z. Meteorol., *2:* 193–203.
Reid, R. O.
1948a. The equatorial currents of the eastern Pacific as maintained by the stress of the wind. J. Mar. Res., *7:* 74–99.
1948b. A model of the vertical structure of mass in equatorial wind-driven currents of a baroclinic ocean. J. Mar. Res., *7:* 304–312.
Robinson, M. K.
1952. Sea temperature in the Marshall Islands area, 20° N–5° S., 155° E–175° W. SIO Reference, 52–45 (unpublished).
Stockmann, W. B.
1946a. A theory of equatorial currents in the ocean. C. R. Acad. Sci. URSS., *52:* 309–312.
1946b. Equation for a field of total flow induced by wind in a non-homogeneous sea. C. R. Acad. Sci. URSS., *54:* 403–406.
Stommel, Henry
1948. The westward intensification of wind-driven ocean currents. Trans. Amer. geophys. Un., *29:* 202–206.
Sverdrup, H. U.
1947. Wind-driven currents in a baroclinic ocean; with application to the equatorial currents of the eastern Pacific. Proc. nat. Acad. Sci., *33:* 318–326.
Sverdrup, H. U. and J. A. Fleming.
1944. Scientific results of cruise VII of the CARNEGIE, 1928–29. Oceanography I–A. Observations and results in physical oceanography II. Results in physical oceanography. Publ. Carnegie Inst., 545: 83–148.
Sverdrup, H. U., M. W. Johnson and R. H. Fleming.
1946. The oceans. Prentice-Hall Inc., New York. 2nd ed., 1087 pp. (pp. 484 and 710).
U. S. Fish and Wildlife Service
1952. Pacific Oceanic Fishery Investigation, Cruise Report, Cruise 16.
Weenink, M. P. H. and Pier Groen.
1952. On the computation of oceanic surface current velocities in the equatorial region from wind data. Koninkl. Nederl. Akad. Weten., Proc., (B) 55: 239.
Wooster, W. S.
1952. Preliminary report, Shellback Expedition, 17 May to 28 August 1952. SIO Reference 52–47 (unpublished).

INTERFERENCE PHENOMENA IN THE TIDES OF THE WOODS HOLE REGION[1]

By

ALFRED C. REDFIELD

Woods Hole Oceanographic Institution

ABSTRACT

The relations of mean range of tide, time of high water, and time of slack water along Vineyard and Nantucket Sounds may be attributed to the interference of tidal waves entering the sounds from their opposite ends. Interference of the semidiurnal constituents is maximal in the neighborhood of Woods Hole where the great reduction of these constituents, relative to the diurnal constituents, results in a pronounced diurnal inequality in the range of successive tides at appropriate phases of the moon. The tide gauge record at Woods Hole is distorted in form as a result of the development of shallow water harmonics combined with the reduction of the fundamental semidiurnal constituent by interference. The inequality in the duration of flood and ebb currents in Woods Hole Passage may be attributed to the effect of these harmonics on the tide levels in Great Harbor.

In discussing the complicated system of tides in Nantucket and Vineyard Sounds in 1855, Bache stated that "observations already made pointed to the interference of the several tide-waves having access to this space as the source of the seeming irregularities." In the present paper it will be shown that a number of characteristics of the tides in this region can be explained by interference between two systems of waves which enter Vineyard Sound, one directly from the ocean, the other from the Gulf of Maine via Nantucket Sound. The characteristics in question are: (1) The relation of time of high water and slack water and the mean range of tide along Vineyard and Nantucket Sounds; (2) The relative values of the diurnal and semidiurnal tidal constants at Woods Hole; (3) The specific form of the tide gauge curve at Woods Hole; and (4) The relative duration of flow eastward and westward in Woods Hole passage.

COTIDAL LINES

The simultaneous positions of the crest of high water, as the tidal wave approaches the New England Coast, were first drawn by Bache (1855) and were later amplified by Harris (1904). The cotidal lines for the region, modified to take account of the more complete information presently available (U. S. Coast and Geodetic Survey, 1951), are shown in Fig. 1.

[1] Contribution No. 636 from the Woods Hole Oceanographic Institution.

Figure 1. Cotidal and corange lines for the Gulf of Maine. Mean times of high water shown by continuous and broken lines in lunar hours relative to moon transit at Greenwich. Mean range of tide shown by dashed lines in feet.

High water occurs almost simultaneously at outlying points along the coast between Long Island, New York, and Nova Scotia. From offshore the crest of high water moves progressively along Vineyard Sound and enters Nantucket Sound from the west after a lapse of four hours. A similar movement into Nantucket Sound occurs through Muskeget Channel.

On entering the Gulf of Maine, the tidal wave is deflected to the left with the result that the delay in high water is greatest along the Massachusetts Coast. There the crest of high water moves southward and reaches the entrance to Nantucket Sound at Monomoy Point and Great Point about four hours after its occurrence on the outer coast.

Within Nantucket Sound high water is latest in an area bounded by Hyannisport, Dennisport, and Nantucket Harbor, where it occurs almost 4½ hours after high water at No Mans Land. In this region the wave that enters through Vineyard Sound and that from the Gulf of Maine meet from opposite directions.

THE TIME OF HIGH WATER, SLACK WATER, AND MEAN RANGE OF TIDE IN VINEYARD AND NANTUCKET SOUNDS

Cotidal and corange lines for Vineyard and Nantucket Sounds are shown in Figs. 2 and 3. Not only is the time of high water delayed as the tidal wave progresses along Vineyard Sound but the mean range of tide decreases from a value of 3.0 feet at Gay Head and No Mans Land to a minimum of 1.3 feet at Falmouth. Eastward of Falmouth the mean range increases to 3.7 feet at Monomoy Point. The interval by which slack water (current turns west) follows high water is about three hours in Vineyard Sound. Along the Falmouth shore, this interval decreases rapidly, and east of Succonessett slack water precedes high water by an interval which increases to about two hours at Monomoy Point.

Theory. These relations are superficially similar to those that would be expected by the interference of two progressive waves moving in opposite directions along the channel. They may be examined quantitatively by methods recently employed in the analysis of tidal phenomena in narrow embayments in which it is assumed that the reflection of the primary tidal wave by the barrier at the head of the embayment produces the mathematical equivalent to a second wave moving through the barrier in the opposite direction (Redfield, 1950). The assumptions necessary to the treatment are:

1. That irregularities in the cross section of the channel alter the velocity of the respective waves, thus distorting the geographical distribution of phase differences along the channel, but that they do not alter the fundamental relations of elevation, motion, and phase difference within the wave;
2. That damping is proportional to the phase change within the wave rather than to the distance traveled;
3. That the damping coefficient is constant along the length of the channel.

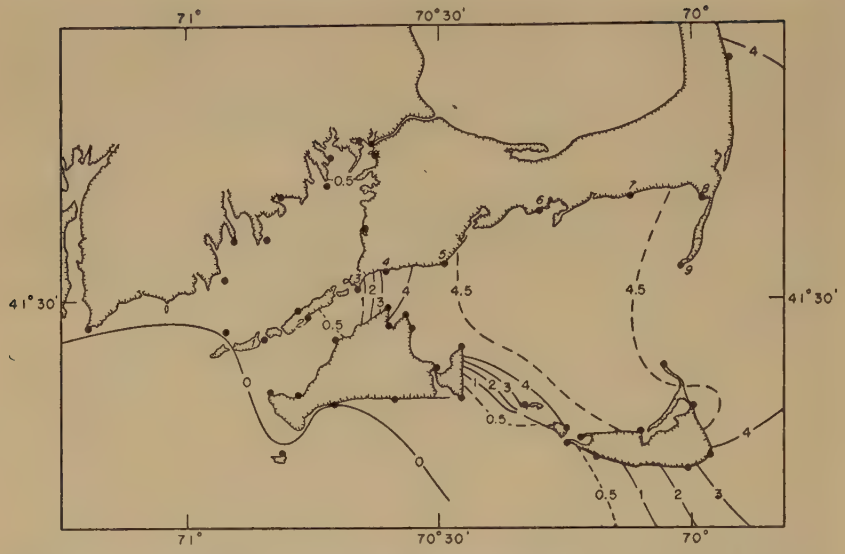

Figure 2. Cotidal lines for Vineyard and Nantucket Sounds. Mean times of high water shown in lunar hours relative to moon's transit at Greenwich.

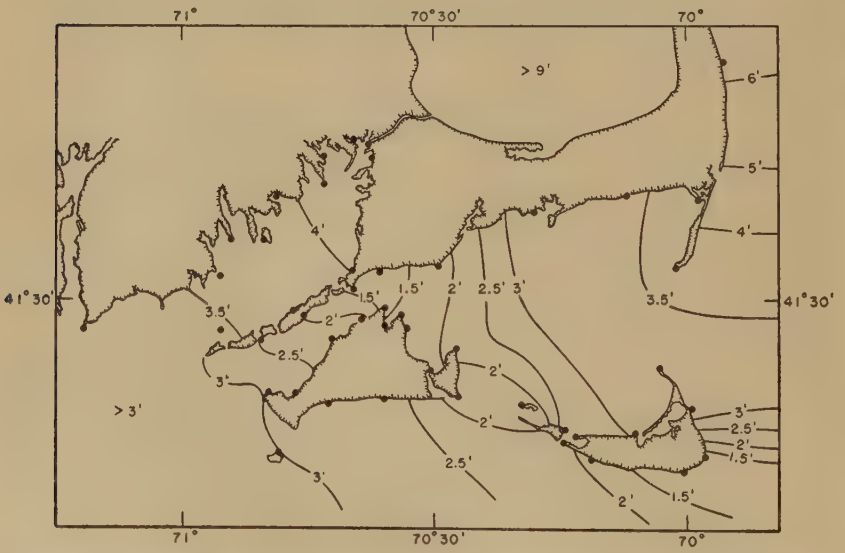

Figure 3. Corange lines for Vineyard and Nantucket Sounds, showing mean range of tide in feet.

In a strait separating an island from the mainland it may be expected that tidal waves will enter, meet, and pass in opposite directions. The following treatment should apply, provided the strait is sufficiently narrow to prevent the development of marked effects of the Coriolis force or the production of rotatory currents. It is evident that some point must exist where waves of like period are always in phase. The time of high water at this point of phase equality is taken as the origin of time. Letting σ be the change in phase per unit time, the time angle σt gives the phase at any point relative to the phase at the position of phase equality.

The position of phase equality is also taken as the origin from which phase differences due to position are measured. In a regular channel, phase differences may be expressed by kx, where k is the change of phase per unit of distance and x is the distance measured from the origin. Since phase changes in an irregular channel are not necessarily proportional to distance, x cannot be taken to represent distance in a geographic sense. However, k may be defined as a phase difference of 360° and x as that part of a cycle which a wave will complete in passing between any designated points. Consequently, kx denotes the phase difference due to position between any point and the position of phase equality.

Damping is assumed to be proportional to the phase change along the channel. The attenuation of each wave in its direction of progression is given by $e^{-\mu x}$, where the damping coefficient μ represents the attenuation per cycle and x is the fraction or multiple of the cycle completed.

To find the time of high water at any point. The elevation of the surface η at any time and place along the channel is given by the sum of the elevations of the respective waves, η_1 and η_2. If A and $(1 + f)$ A are the amplitudes of the respective waves at the position of phase equality,

$$\eta_1 = A \cos(\sigma t - kx)\, e^{-\mu x} \text{ and } \eta_2 = (1 + f)\, A \cos(\sigma t + kx)\, e^{\mu x},$$

η_2 being the elevation of the wave taken to be moving in the negative direction with respect to x.

Since $\eta = \eta_1 + \eta_2$,

$$\eta = A\left[\cos(\sigma t - kx)\, e^{-\mu x} + (1 + f) \cos(\sigma t + kx)\, e^{\mu x}\right]. \qquad (1)$$

High water occurs when $\delta\eta/\delta t = 0$ or when $\sin(\sigma t - kx)\, e^{-\mu x} + (1 + f) \sin(\sigma t + kx)\, e^{\mu x} = 0$, from which it follows that the local time angle of high water, σt_H, is given by

$$\tan^{-1}\left[-\tan kx \frac{(1 + f)\, e^{\mu x} - e^{-\mu x}}{(1 + f)\, e^{\mu x} + e^{-\mu x}}\right].$$

Letting F represent the term $\dfrac{(1+f)\,e^{\mu x} - e^{-\mu x}}{(1+f)\,e^{\mu x} + e^{-\mu x}}$,

this becomes

$$\sigma t_H = \tan^{-1}[-\tan kx \cdot F]\,. \tag{2}$$

To find the elevation at any point at high water. From (1) the elevation at any time and place may be written

$$\eta = A\,(\cos\sigma t\cos kx + \sin\sigma t\sin kx)\,e^{-\mu x} + (1+f)\,(\cos\sigma t\cos kx - \sin\sigma t\sin kx)\,e^{\mu x}\,.$$

At high water it follows from (2) that

$$\cos\sigma t_H = \frac{1}{\sqrt{1+F^2\tan^2 kx}} \text{ and}$$

$$\sin\sigma t_H = \frac{-F\tan kx}{\sqrt{1+F^2\tan^2 kx}}\,.$$

Consequently the elevation at high water η_H may be written

$$\eta_H = \tag{3}$$
$$A\,\frac{(\cos kx - F\tan kx\sin kx)\,e^{-\mu x} + (1+f)\,(\cos kx + F\tan kx\sin kx)\,e^{\mu x}}{\sqrt{1+F^2\tan^2 kx}}\,.$$

To find the time of slack water at any point. The velocity of the current due to the respective waves at any time and place is given by

$$u_1 = A\,\frac{b}{h}\left(\frac{1}{\sqrt{\mu^2+k^2}}\right)e^{-\mu x}\cos(\sigma t - kx) \text{ and}$$

$$u_2 = -(1+f)\,A\,\frac{b}{h}\left(\frac{1}{\sqrt{\mu^2+k^2}}\right)e^{\mu x}\cos(\sigma t + kx)\,,$$

where h is the depth and b the cross section of the channel.

At any point along the channel slack water occurs when $u_1 + u_2 = 0$, or when

$$e^{-\mu x}\cos(\sigma t - kx) - (1+f)\,e^{\mu x}\cos(\sigma t + kx) = 0, \text{ or}$$
$$\cos\sigma t\cos kx\,[e^{-\mu x} - (1+f)\,e^{\mu x}] + \sin\sigma t\sin kx\,[e^{-\mu x} + (1+f)\,e^{\mu x}] = 0\,.$$

Letting σt_s denote the local time angle of slack water, it follows that

$$\sigma t_s = \tan^{-1}\cdot\frac{F}{\tan kx}\,. \tag{4}$$

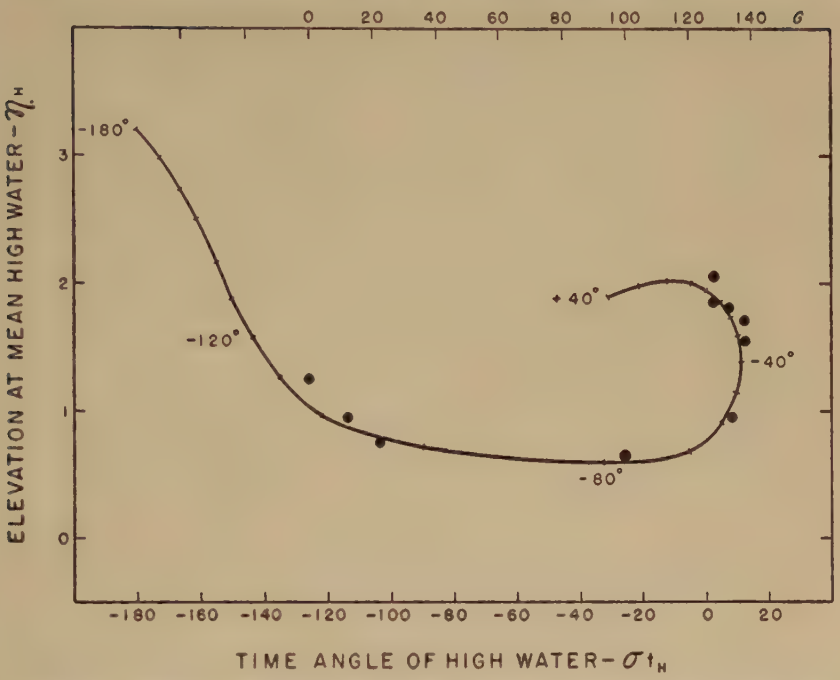

Figure 4. Relation between elevation at high water (ηH) and time angle at high water (σtH) along Vineyard and Nantucket Sounds. Curve estimated from equations (2) and (3) taking $\mu = 3$, $f = 2$, and $A = 0.65$ feet. Points represent stations recorded in Table I.

Applications. In this treatment, effects of the earth's rotation and the deformation of the tidal wave by shallow water and damping are neglected. In its application to Vineyard and Nantucket Sounds, the influence of tidal flow through the Muskeget Channel is not taken into account. For this reason, attention is limited to stations along the northern side of the Channel where there is a relatively unbroken boundary.

To test the application of equations (2), (3), and (4) to tidal relations in Vineyard and Nantucket Sounds, data from the tide and current tables of the U. S. Coast and Geodetic Survey relative to nine stations along the northern coast of the sounds have been selected. In Table I, times of high water and slack water at these stations are expressed by the Greenwich epoch G which is related to σt by $G = \sigma t + K$, where K is the Greenwich epoch of high water at the point of phase equality. The elevation at high water, η_H, is given as equal to one-half the mean range of tide.

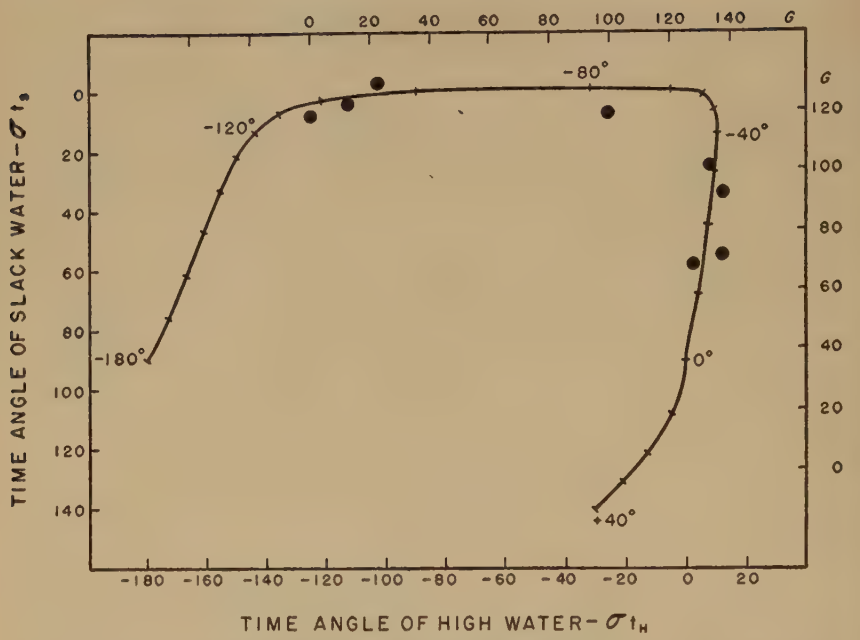

Figure 5. Relation between time angle at high water (σt_H) and time angle at slack water (σt_s) along Vineyard and Nantucket Sounds. Curve estimated from equations (3) and (4), taking $\mu = 3.0$, $f = 2$, and $A = 0.65$ feet. Points represent stations recorded in Table I. Note: Time angles of slack water should have negative signs.

By assuming arbitrarily chosen values for the constants μ, A, and f, and solving equations (2) and (3) for the values of σt_H and η_H corresponding to a series of values for kx, a curve may be drawn which shows the unique relations of the time of high water and the elevation at high water determined by the constants chosen, as in Fig. 4.

Along the curve a scale of values of kx corresponding to each combination is marked. The relations σt_H and σt_S or η_H and σt_S may be treated similarly, the former combination being shown in Fig. 5.

Appropriate pairs of observed parameters may be plotted on such diagrams and tested for correspondence with the theoretical curves. If η_H is plotted as its logarithm, the "shape" of the curves is determined solely by μ and f, and the values of A and K are found by the vertical and horizontal displacements of the observed points required to secure the best fit. A final test of fit is obtained by comparing the values of kx which may be assigned to the positions of observation by the analysis of different pairs of parameters.

The curves shown in Figs. 4 and 5 are drawn with $\mu = 3$, $f = 2$, $A = 0.65$ feet, and $K = 126°$. The observed points are distributed

TABLE I. Tidal Data for North Shore of Vineyard and Nantucket Sounds

No.	Station*	Mean Range (feet)	High Water interval (hours)	Slack Water interval† (hours)	η_H (feet)	G_H (degrees)	G_S (degrees)	kx (degrees)
1	Quicks Hole	2.5	7.66	11.62	1.25	1	118	−105
2	Tarpaulin Cove	1.9	8.02	11.76	0.95	13	122	−98
3	Nobska Point	1.5	8.53	12.00	0.75	23	129	−94
4	Falmouth Heights	1.3	11.00	11.66	0.65	100	119	−78
5	Succonnessett Point	1.9	12.16	11.38	0.95	134	111	−58
6	Hyannisport	3.1	12.33	10.76	1.55	138	92	−30
7	Dennisport	3.4	12.35	10.02	1.70	138	71	−20
8	Stage Harbor	3.6	12.20	—	1.80	133	—	−16
9	Monomoy Point	3.7	12.00	9.94	1.85	128	68	−10

* Positions of stations are identified by number in Fig. 2.
† Slack before current turns west.

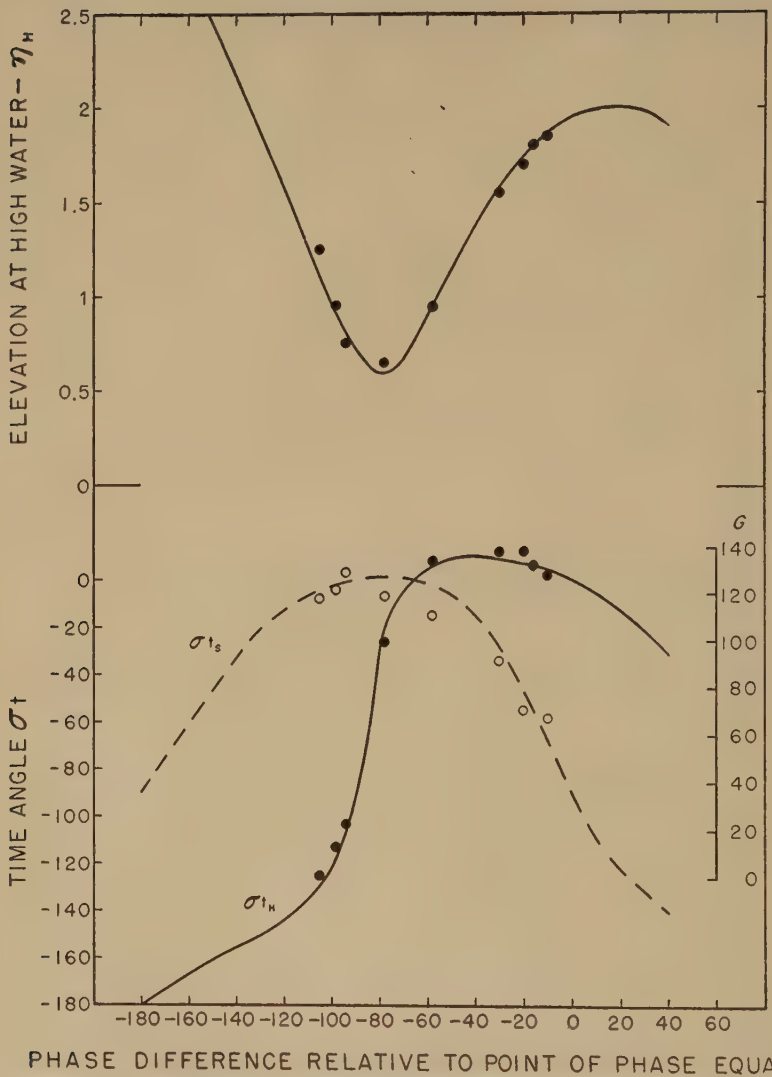

Figure 6. Curves showing the theoretically estimated relations of elevation at high water (ηH), time angle of high water (σt_H), and time angle of slack water (σt_s) to the phase difference along the channel. The plotted points represent observations at stations recorded in Table I.

closely along these curves. From the scales marked along the curves, approximate values of kx may be obtained for each position of observation and may be adjusted so as to reconcile the differences given by the two curves. The adjusted values, entered in Table I, represent

the phase difference of the waves at each station relative to the position of phase equality. In Fig. 6 the estimated values of η_H, σt_H, and σt_S are plotted as curves against the corresponding values of kx. The positions of observation are spaced along the abscissa in accordance with the values of kx assigned to each, and the measured values of the several properties of the tide at each position are plotted for comparison with the theoretical curves. Fig. 6 shows that the observed values for mean range of tide, time of high water, and time of slack water are consistent with the values estimated from the several equations.

The values of the constants chosen to represent the properties of the tide in Vineyard and Nantucket Sounds have been found by trial to give a reasonably good description of the observations. They are not necessarily those which give the best fit in any statistical sense. The value of the damping coefficient μ is somewhat greater than that deduced from Long Island Sound and the Bay of Fundy, where μ was between 1 and 1.5 (Redfield, 1950). This is reasonable in view of the limited depth of Nantucket and Vineyard Sounds. The value of f is concordant with the facts that the general range of tide is much greater in the Gulf of Maine than it is along the outer coast south of New England. The position of phase equality appears to lie to the east of Monomoy Point. At this position it may be expected that the value of G for mean high water is 126°, that the elevation at high water due to the wave moving eastward through Vineyard and Nantucket Sounds is 0.65 feet, and that the elevation at high water due to the wave moving westward from the Gulf of Maine is 1.95 feet above mean sea level.

Along the southern shore of Vineyard and Nantucket Sounds the general trend of tidal phenomena is similar to that on the opposite coast. In general the ranges of tide are somewhat greater along the shore of Marthas Vineyard than are those at corresponding points on the mainland; this may be attributed to effects of the earth's rotation. Along the shore of Nantucket, Tuckernuck, and Muskeget Islands, the relations are presumably determined primarily by interference between the wave originating in the Gulf of Maine and that entering Muskeget Channel, which should produce similar but not necessarily the same relations as those found along the northern coasts of the sounds.

In view of the correspondence of theory and observation along the northern coast and the qualitative agreement along the southern shore, it is concluded that the relations between the time of high water, slack water, and mean range of tide along Vineyard and Nantucket Sounds are satisfactorily accounted for by the interference of tidal waves of unequal amplitude which traverse the sounds in opposite directions.

THE AMPLITUDE OF THE DIURNAL AND SEMIDIURNAL TIDAL CONSTITUENTS AT WOODS HOLE

The foregoing analysis is based on the mean values for range of tide, high water interval, and slack water interval. Since the tidal phenomena in the North Atlantic are dominated by the M_2 constituent, it may be assumed that the analysis applies to a single wave having a speed number of 29° per hour (Proudman and Doodson, 1924). Thus, the interference phenomena described are those which affect the semidiurnal constituents of the tide. Nobska Point, at the entrance to Great Harbor, Woods Hole, is situated about ¼ wave length from the point of phase equality, and consequently the amplitude of the semidiurnal constituents is maximally reduced by interference in its neighborhood.

The diurnal waves that enter the sounds from opposite ends may be expected to be in phase at about the same position as the semidiurnal waves, since they move with similar velocity. However, the phase difference of the diurnal waves along the channel will be only half as great since the wave length is double. Consequently, the phase difference between Nobska Point and the position of phase equality will be approximately ⅛ wave length, and the reduction of the amplitude by interference will be much less than that in the case of the semidiurnal constituents.

The correctness of this reasoning is indicated by a comparison of the amplitude H of the principle tidal constituents at Woods Hole and at Atlantic City, which is on the outer coast where the local geographic conditions may be expected to have a minimal effect upon the ocean tide. The values of the principle constituents at these stations, based on analyses of complete records during the year 1940, are shown in Table II. With the exception of the small Q_1 component, the amplitudes at Woods Hole are reduced relative to those at Atlantic City. The proportional reduction of the semidiurnal constituents is substantially greater than that of the diurnal constituents. Taking the ratio of the sums of the amplitudes of each species to give a weighted expression, the combined amplitudes of the diurnal constituents at Woods Hole is 76% of those at Atlantic City, while the ratio for the semidiurnal constituents is 44%. The reduction of the semidiurnal constituents is thus more than twice that of the diurnal constituents, and this may be attributed to the interference phenomena associated with the topography of Vineyard and Nantucket Sounds.

The consequence of the unequal reduction of the diurnal and semidiurnal constituents at Woods Hole is to increase the diurnal inequality of the tidal range. This gives rise to a condition approaching the

mixed tides characteristic of the Pacific Ocean, where great inequality exists between the elevation of successive high (and low) waters at the time of the moon's maximum semimonthly declination and where periods of equality follow when the moon is over the equator. This characteristic of the tide at Woods Hole has not impressed local observers because the range of tide there is small and is subject to relatively great variation from meteorological causes. However, it appears clearly from measurements of tidal records (see Fig. 7).

TABLE II. Amplitude (H) of the Principle Constituents of the Tide at Woods Hole and Atlantic City

	Constituent	Woods Hole	Atlantic City	Ratio
Diurnal	K_1	0.224	0.344	0.652
	O_1	0.203	0.236	0.854
	P_1	0.075	0.113	0.664
	Q_1	0.053	0.039	1.36
	Sum (C_1)	0.555	0.732	0.76
Semidiurnal	M_2	0.759	1.928	0.393
	S_2	0.200	0.393	0.509
	N_2	0.246	0.447	0.551
	K_2	0.043	0.096	0.448
	Sum (C_2)	1.248	2.864	0.44

The ratio of the sum of the diurnal constituents C_1 to the sum of the semidiurnal constituents C_2 serves as a ready index of the tendency for diurnal inequality of the tide at any place. The following tabulation compares this index for Woods Hole with that for positions on the outer coasts of the Atlantic (Atlantic City, N. J.) and Pacific (Claoquot, B. C.). There is added the index for Victoria, B. C., where the tide is almost completely diurnal owing to the suppression of the semidiurnal constituents by interference similar to that ascribed to the Woods Hole tide (Redfield, 1950).

		C_1	C_2	C_1/C_2
Atlantic City	1940	0.732	2.864	0.255
Woods Hole	1940	0.555	1.248	0.444
Claoquot	1939	2.63	5.11	0.516
Victoria	1939	4.15	1.88	2.22

The index for Woods Hole approaches closely that for the example chosen for the Pacific Ocean.

THE FORM OF THE TIDE GAUGE CURVE AT WOODS HOLE

Records of the elevation of the sea surface by the tide gauge at the Woods Hole Oceanographic Institution on Great Harbor show a striking departure from the usual sinusoidal curve. The rise of the

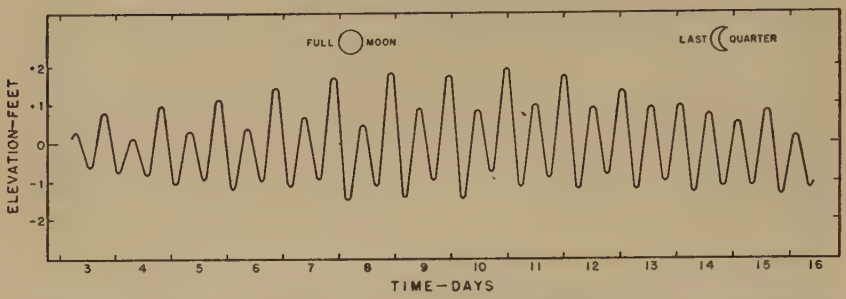

Figure 7. Diagram showing elevation of the tide at Woods Hole at successive high and low water during June 3–16, 1952. The form of the curve and the spacing of high and low waters are not represented exactly.

tide occupies about 5.4 hours, while 7.0 hours intervene between high water and the following low water. During the ebb, at about half tide, the fall is interrupted and the surface level remains constant or rises slightly for nearly an hour (see Fig. 8). The effect varies from day to day and appears to be most pronounced when the range of tide is relatively great.

The distortion of the record during the fall in tide level appears to be due to phenomena similar to those responsible for double high- and double low-waters which are discussed by Doodson and Warburg (1941) in relation to conditions near Southampton. A nearby case of double low-water is cited by Harris (1907) for Providence, Rhode Island. These phenomena in general are explained as follows. In shallow water tidal waves are distorted in such a way that they may

Figure 8. Record from tide gauge at Great Harbor, Woods Hole, September 30, 1952.

be described by the sum of a series of harmonics. At points where the fundamental constituent is suppressed by interference, certain of the harmonics are undisturbed or are reinforced, and thus they may stand out as recognizable distortions of the sinusoidal wave. The phase relations of these distortions depend on the topographic conditions which determine the interference patterns of the fundamental and its harmonics. Where the semidiurnal constituent M_2 is the principle constituent of the tide, the quarter diurnal constituent M_4 will be the harmonic largely responsible for the distortion of the

curve. If σt represents the phase of the M_2 wave, the phase of the M_4 wave is given by $2\sigma t + \theta$. If the angle θ is 180°, double high-waters may result; if it is 0°, double low-waters are possible. If θ is 90°, or thereabout, the effect is to steepen the rise of tide and to delay its fall when half tide level is reached. This is apparently the condition in the present case, and this is the phase relation which may be expected when harmonics are generated by progressive waves that undergo distortion in shallow water. These distortions are sufficient to reverse the slope of the record only when interference reduces substantially the amplitude of the fundamental wave relative to the harmonic.

An exact harmonic analysis of the tide at Woods Hole has been made by the U. S. Coast and Geodetic Survey for the years 1933 and 1940. The constants for the M_2 and S_2 components and their harmonics for 1933 are as follows:

	H	k
M_2	0.703	254.7
M_1	0.011	176.0
M_4	0.162	74.6
M_6	0.052	337.8
M_8	0.009	329.0
S_2	0.185	253.2
S_4	0.017	70.0

The principle harmonic present, M_4, has an amplitude of 23% of its fundamental M_2. The phase displacement of the M_2 and M_4 components may be estimated from the values of k so that $\theta = 75°$. The M_6 component also has sufficient amplitude to affect the shape of the tide gauge record appreciably. A curve calculated from the M_2, M_4, and M_6 components shows distortion which is similar to that of the record but which is less pronounced than that usually observed.

A curve which is a reasonable facsimile of the record is shown in Fig. 9, Curve B. The constants used in constructing this curve are given on page 138 and are such that $\theta = 90°$ in the case of both the M_4 and M_6 constituents. The nature of the distortion is shown by a comparison of Curve B with Curve A, which is that for the M_2 constituent alone.

The harmonics present in the tide at Woods Hole, and their exaggeration relative to the fundamental waves, may be explained by the distortion of tidal waves by the shoal water of Vineyard and Nantucket Sounds. Wherever the harmonics may be generated, the suppression of the semidiurnal wave, which is required to make their presence evident by the distortion of the tide record, is explained by the interference of the semidiurnal waves which traverse the sounds in opposite directions.

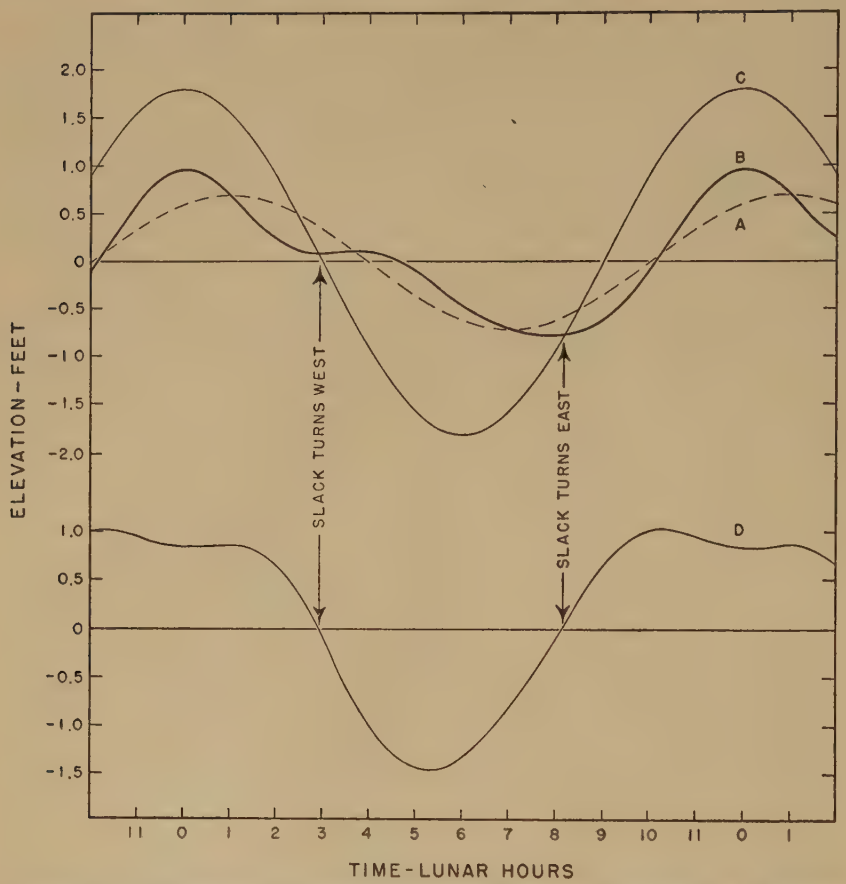

Figure 9. Tidal relations in Woods Hole Passage. Curve A: Elevation due to assumed M_2 constituent at Great Harbor. Curve B: Elevation of sea surface at Great Harbor resulting from sum of assumed M_2, M_4, and M_6 constituents. Curve C: Elevation at Uncatena Island represented by a single (M_2) constituent. Curve D: Hydrostatic head between Uncatena Island and Great Harbor. Time: Lunar hours relative to time of high water at Uncatena Island.

At Woods Hole, just ¼ wave length from the position of phase equality, the semidiurnal waves are maximally reduced by interference. If quarter-diurnal waves accompany these fundamentals at Woods Hole, they would be ½ their wave length from the position of phase equality and they would reinforce one another.

Harmonic analysis of the tide at a number of stations scattered about the area would be required to clarify the geographical origin of the phenomena. The existing information, however, is sufficient to

indicate that the form of the tide record at Woods Hole is due primarily to the M_4 and M_6 constituents. The suppression of the fundamental semidiurnal components, required to develop the observed distortion of the record, is explained adequately by the interference of the fundamental waves which traverse the sound in opposite directions.

THE TIDAL CURRENT IN WOODS HOLE PASSAGE

The movement of water through Woods Hole Passage is due to a hydraulic current resulting from inequalities of range and time of tide in Buzzards Bay and Vineyard Sound. These inequalities arise from the topography of these tidal basins.

Buzzards Bay is a relatively short closed embayment in which reflection of the advancing tidal wave produces a tide of the standing wave type. High water is delayed less than 45 minutes between its mouth and its head. The mean range of tide increases as the head of the bay is approached, being 3.4 feet at Penikese Island and 4.1 feet at Onset.

Vineyard Sound is a part of a long system of channels in which the tide advances as a progressive wave. The wave arising in the Gulf of Maine, and traversing the sounds in the opposite direction, produces interference effects. The length of the channel is such that off Woods Hole Passage the range of tide is greatly reduced. Because of the high degree of damping, the west-moving wave is so reduced in amplitude that interference is incomplete and the progressive character of the tidal wave which enters Vineyard Sound remains evident.

At the eastern end of Woods Hole Passage, in Great Harbor, the mean range of tide is 1.8 feet as compared to 3.6 feet at the western end, at Uncatena Island. The time of high water at Great Harbor is only 5 minutes later than at Uncatena Island, but low water is 1.7 hours later. Evidently the major condition responsible for the hydraulic head is the difference in level which amounts to about 1.0 foot at high water and nearly 1.5 feet at low water.

A striking characteristic of the currents in Woods Hole Passage is the unequal duration of flow in opposite directions. The duration of the eastward current exceeds that of the westward current by about two hours. This characteristic may be explained as the result of the peculiar form of the tide curve in Great Harbor which appears to arise from the presence of the harmonics in the tidal complex.

If the mean elevations on either side of the Passage were determined solely by the relative amplitudes and times of the semidiurnal tidal constituents in Great Harbor and Buzzards Bay, the differences in elevation and the resulting flow would follow a symmetrical sinusoidal curve, and the duration of the eastward and westward currents would

TABLE III. Comparison of Tidal Characteristics of Woods Hole Passage Estimated from Mathematical Model and Predicted by the Tide and Current Tables. *Lunar hours or feet.*

	Model	Tables	Difference
Uncatena Island HW	0	0	0
Great Harbor HW	0.1	0.1	0
Great Harbor LW	7.9	7.9	0
Current Turns West	2.9	2.6	+ 0.3
Current Turns East	8.2	7.6	+ 0.6
Current Flows West	5.3	5.0	+ 0.3
Current Flows East	6.7	7.0	− 0.3
Maximum Current West	5.6	5.7	− 0.1
Maximum Current East	11.0	10.8	+ 0.2
Mean Range:			
Uncatena	3.6	3.6	0
Great Harbor	1.73	1.8	0.07

	Maximum Head	Maximum Currents*
West	1.49 feet	3.6 knots
East	1.02 feet	2.7 knots
Ratio	1.46	1.33

* Current pole measurements (Haight, 1936)

be equal. The harmonics in Great Harbor produce an additional component of flow through the Passage. The time relations of this component of flow are such that it is eastward at both periods when slack water would result from the interaction of the semidiurnal components alone. In this way, the duration of the eastward current may be prolonged at the expense of that of the westward current.

Fig. 9 demonstrates this principle and approximates the observed conditions. The tidal elevations at Uncatena Island are represented by a single semidiurnal constituent, M_2, those at Great Harbor by the combination of a semidiurnal, M_2, a quarter diurnal, M_4, and a sixth diurnal constituent, M_6. The harmonic constants are as follows:

		H	k
Uncatena Island	M_2	1.8 feet	233°
Great Harbor	M_2	0.7 feet	263°
	M_4	0.3 feet	76°
	M_6	0.1 feet	339°

Note that the elevations due to the M_2 components, Curves A and C, are equal and that slack water would occur at hours 2.5 and 8.5 in the absence of the higher harmonics. At these times the elevations due to the combined harmonic constituents are negative, producing a hydrostatic head favoring flow eastward from Uncatena Island to

Great Harbor. Equal elevations occur 0.4 hours later during the falling tides and 0.3 hours earlier during the rising tides. This produces inequality in the duration of east and west flow.

The hydrostatic head between Uncatena Island and Great Harbor is shown in the lower part of Fig. 9. This curve resembles that which describes current measurements made by the U. S. Coast and Geodetic Survey off Devils Foot Island (Haight, 1936: fig. 32, Station 13035) in indicating that the westward current is not only shorter in duration but is also of greater maximum velocity. Table III shows how closely the characteristics of the tides in Woods Hole Passage, as represented by the mathematical model, agree with the predictions of the tide and current tables.

Acknowledgment is made to the U. S. Coast and Geodetic Survey which, through the kindness of Dr. Harry Marmer, has made available unpublished harmonic constants used in the preparation of this paper. Thanks are due Mr. Henry Stommel of the Woods Hole Oceanographic Institution for aid in the mathematical treatment of the interference of tidal waves.

SUMMARY

1. The relations of mean range of tide, time of high water, and time of slack water along Vineyard and Nantucket Sounds may be attributed to the interference of tidal waves entering the sounds from their opposite ends.

2. These waves are in phase at a position to the east of Monomoy Point. At this position the wave approaching from the Gulf of Maine has twice the amplitude of that which has traversed the sounds.

3. The damping coefficient of the tidal waves in the sounds is of the order of 3.0.

4. Interference of the semidiurnal constituents is maximal in the neighborhood of Woods Hole. The great reduction of the semidiurnal constituents relative to the diurnal constituents results in a pronounced diurnal inequality in the range of successive tides at appropriate phases of the moon.

5. The tide gauge record at Woods Hole is distorted in form as a result of the development of shallow water harmonics combined with the reduction of the fundamental semidiurnal constituent by interference.

6. The inequality in the duration of flood and ebb currents in Woods Hole Passage may be attributed to the effect of these harmonics on the tide levels in Great Harbor.

REFERENCES

Bache, A. D.
1855. Report of the Superintendent of the Coast Survey for the year 1854. Washington, D. C. 288 pp.

Doodson, A. T. and H. D. Warburg
1941. Admiralty Manual of Tides. London. 270 pp.

Haight, F. J.
1936. Currents in Narragansett Bay, Buzzards Bay, and Nantucket and Vineyard Sounds. Spec. Publ. U. S. Cst. geod. Surv., No. 208. Washington, D. C. 103 pp.

Harris, R. A.
1904. Manual of Tides. Part IVB. Cotidal lines for the world. Rep. U. S. Cst. geod. Surv., Appendix No. 5: 313–400.
1907. Manual of Tides. Part V. Currents, shallow water tides, meteorological tides and miscellaneous matters. Rep. U. S. Cst. geod. Surv., Appendix No. 6: 213–545.

Proudman, J. and A. T. Doodson
1924. The principal constituent of the tides of the North Sea. Phil. Trans., (A) *224:* 185–219.

Redfield, A. C.
1950. The analysis of tidal phenomena in narrow embayments. Pap. phys. Oceanogr. Meteorol., *11* (4): 1–36.

U. S. Coast and Geodetic Survey
1951. Tide Tables East Coast North and South America for the year 1952. Serial No. 742. Washington, D. C. 249 pp.
1951. Current Tables Atlantic Coast North America for the year 1952. Serial No. 751. Washington, D. C. 174 pp.

THE SIZE OF WATER MASSES CONTAINING PLANKTON BLOOMS[1]

By

HENRY KIERSTEAD[2]

Brown University
Providence, Rhode Island

AND

L. BASIL SLOBODKIN

Bingham Oceanographic Laboratory
Yale University
New Haven, Connecticut

ABSTRACT

If a phytoplankton population is assumed to be increasing logarithmically in a mass of water surrounded by water which is unsuitable for the survival of the population, it can be shown that there is a minimum critical size for the water mass below which no increase in concentration of phytoplankton can occur. In a one-dimensional water mass with leakage at both ends, this size, after a time of the order of $L^2/8\pi^2D$, is given by

$$L_c = \pi\sqrt{\frac{D}{K}},$$

where L_c is the length of the water mass, D the diffusion, and K the rate of increase of the population. The corresponding size in a cylindrical water mass is given by

$$R_c = 2.4048\sqrt{\frac{D}{K}},$$

where R_c is the radius of the water mass.

Any unispecific phytoplankton population can be considered as living in some water mass characterized by suitable values of such properties as temperature, salinity, dissolved oxygen, and dissolved nutrients. If this water mass were completely isolated from the surrounding water it should be possible to analyze the growth of the population in terms of one of the equations which have been developed for laboratory populations (Smith, 1952).

[1] The authors wish to express their gratitude to Mr. Henry Stommel for his advice and encouragement.

[2] Present address: Argonne National Laboratory, P. O. Box 5207, Chicago, Illinois.

As a matter of fact, any mass of physiologically suitable water will mix, at its borders, with unsuitable water. For a species with restricted physiological tolerances it is quite likely that large masses of suitable water will rarely occur. It is of interest, therefore, to determine whether or not there exists a minimum water mass size below which no increase of phytoplankton concentration is possible.

In the simplest analysis the population growth in a diffusing water mass can be expressed as

$$\frac{dN}{dt} = (K - \lambda) N , \tag{1}$$

where K is the growth rate per unit population, λN the rate of loss by diffusion, and N the total number of organisms in the water mass. The simple condition for population increase is $(K > \lambda)$. This does not take into account the size of water mass or the distribution of organisms. A more precise analysis of the leakage λ has been made.

We consider for simplicity the one-dimensional problem of a long narrow body of water limited on the two sides by natural boundaries. We assume further that there is a region of length L and transverse cross-sectional area A in which the effective diffusivity D remains constant. We assume that, outside this region, the diffusivity becomes large or that the water is physiologically unsuitable for the organism. Either condition requires that the concentration of organisms drop to zero at the ends of the region. We can neglect transverse diffusion and consider the concentration c to be a function of the longitudinal position only. Let one end be at $x = 0$ and the other at $x = L$. If the organism did not multiply, we would require the solution of the diffusion equation (Churchill, 1941: 19):

$$\frac{\partial c}{\partial t} = D \frac{\partial^2 c}{\partial x^2} , \tag{2}$$

in which t is time. But reproduction must be accounted for by adding a linear growth term to (2). We have then,

$$\frac{\partial c}{\partial t} = D \frac{\partial^2 c}{\partial x^2} + Kc . \tag{3}$$

We seek solutions of (3) which vanish at $x = 0$ and $X = L$ and which correspond to any given initial distribution of organisms, which we can write as

$$c = g(t) \text{ when } t = 0. \tag{4}$$

If we introduce the new variable,

$$f = ce^{-kt} , \tag{5}$$

we find by substitution in (3) that f must satisfy the equation

$$\frac{\partial f}{\partial x} = D \frac{\partial^2 f}{\partial x^2}, \tag{6}$$

which is the ordinary diffusion equation; f must also satisfy the same initial and boundary conditions as c. The solution of (6) for these boundary conditions is known to be (Churchill, 1941: 104)[3]

$$f = \sum_{n=1}^{\infty} B_n \sin n\pi \frac{x}{L} e^{-n^2\pi^2 D/L^2 t}, \tag{7}$$

where

$$B_n = \frac{2}{L} \int_0^L g(x) \sin n\pi \frac{x}{L} dx. \tag{8}$$

Thus the constants B_n ($n = 1, 2, 3, \ldots$) depend on the form of the initial distribution. Our principal conclusions will not depend on the exact values of these constants. Due to the symmetry properties of the sine functions in (8), the even-numbered terms in (7) will vanish if the initial distribution is symmetric with respect to the plane $x = L/2$; in any event, as we shall see, the values of N and λ will depend only on the odd-numbered terms. Substituting (5) into (7), we obtain an expression for the concentration at any position and time:

$$c = \sum_{n=1}^{\infty} B_n \sin n\pi \frac{x}{L} e^{(k-n^2\pi^2 D/L^2) t}. \tag{9}$$

It should be noted that the different terms in the series have different functional dependence on the time. In particular, the terms for which $(K - n^2\pi^2 D/L^2)$ is negative will decrease with time and will eventually become negligibly small.

The population will then be unable to maintain itself against diffusion unless there is at least one term in the series for which

$$K - n^2\pi^2 \frac{D}{L^2} \geqslant 0. \tag{10}$$

Since the smallest value of n is one,[4] a necessary condition for maintenance of the population is

$$K \geqslant \pi^2 \frac{D}{L^2}. \tag{11}$$

[3] We shall assume that all infinite series used in this paper converge properly for $t > 0$, $0 \leqslant x \leqslant L$. A detailed investigation of their convergence properties shows that this is the case for all situations of physical interest.

[4] This would not be true if $B_1 = 0$. However, $\sin \pi x/L$ is positive throughout the interval $0 > x > L$, and in any real population $g(x)$ cannot be negative and must therefore be greater than zero somewhere. Hence the integral in (8) is necessarily positive.

For given values of D and K, there is a critical length given by

$$L_c = \pi \sqrt{\frac{D}{K}}, \tag{12}$$

such that a population will increase if $L > L_c$, decrease if $L < L_c$, and will remain static if $L = L_c$. Of course the situation is exactly analogous to the situation in a chain-reacting pile.

Going back to equation (9), we can calculate the total number of organisms by integration:

$$N = A \int_0^L c \, dx = \frac{2AL}{\pi} \sum_{n=0}^{\infty} \frac{B_{2n+1}}{2n+1} e^{[k-(2n+1)^2 \pi^2 D/L^2] t}, \tag{13}$$

the terms with even n vanishing on account of their symmetry. The net number of organisms diffusing in the forward direction past any plane in unit time is given by

$$n(x, t) = -AD \frac{\partial c}{\partial x} = -AD \frac{\pi}{L} \sum_{n=1}^{\infty} n B_n \cos n\pi \frac{x}{L} e^{(k-n^2\pi^2 D/L^2) t}. \tag{14}$$

The number lost from the system per unit time by diffusion through the end boundaries $x = 0$ and $x = L$ is

$$n(L, t) - n(0, t) = 2AD \frac{\pi}{L} \sum_{n=0}^{\infty} (2n+1) B_{2n+1} e^{[k-(2n+1)^2 \pi^2 D/L^2] t}. \tag{15}$$

It is useful to define the 'leakage' λ as

$$\lambda = \frac{n(L, t) - n(0, t)}{N}. \tag{16}$$

Then

$$\lambda = \frac{\pi^2 D}{L^2} \frac{\sum_{n=0}^{\infty} (2n+1) B_{(2n+1)} e^{[k-(2n+1)^2 \pi^2 D/L^2] t}}{\sum_{n=0}^{\infty} \frac{B_{2n+1}}{2n+1} e^{[k-(2n+1)^2 \pi^2 D/L^2] t}}. \tag{17}$$

$$= \frac{\pi^2 D}{L^2} \frac{\sum_{n=0}^{\infty} (2n+1) B_{2n+1} e^{-4n(n+1) \pi^2 D/L^2 t}}{\sum_{n=0}^{\infty} \frac{B_{2n+1}}{2n+1} e^{-4n(n+1) \pi^2 D/L^2 t}}. \tag{18}$$

By differentiating (13) with respect to time, we find

$$\frac{1}{N}\frac{dN}{dt} = K - \frac{\pi^2 D}{L^2}\frac{\sum_{n=0}^{\infty}(2n+1)\,B_{2n+1}\,e^{[k-(2n+1)^2\pi^2 D/L^2]\,t}}{\sum_{n=0}^{\infty}\frac{B_{2n+1}}{2n+1}\,e^{[k-(2n+1)^2\pi^2 D/L^2]\,t}}, \quad (19)$$

and, introducing (17),

$$\frac{1}{N}\frac{dN}{dt} = K - \lambda, \quad (20)$$

which is identical to (1). The over-all growth of the population can be described therefore by (1) with λ defined by (18). In general λ will be a function of time, but after a time of the order of magnitude of $L^2/8\pi^2 D$, the first terms in the two series in (18) will be the only ones of importance. We have then

$$\lambda \simeq \pi^2\frac{D}{L^2} \text{ if } t \gg L^2/8\pi^2 D\,. \quad (21)$$

The generality of these results can be seen by considering a different geometrical model. Let the region of constant diffusion coefficient be a cylinder of radius R and depth h bounded on all sides by physiologically unsuitable water; also assume cylindrical symmetry. Equation (2) must then be replaced by

$$\frac{\partial c}{\partial t} = \frac{D}{r}\frac{\partial}{\partial r}\left(\frac{1}{r}\frac{\partial c}{\partial r}\right), \quad (2')$$

and a similar modification must be made in (3) and (6). Solving the modified equations in the same manner as the original ones, we find (Churchill, 1951: 166)

$$c = \sum_{n=1}^{\infty} E_n\,J_0\left(\beta_n\frac{r}{R}\right)e^{(k-\beta_n^2 D/R^2)\,t}, \quad (9')$$

where J_0 is a Bessel function of the first kind and order zero, where the β_n's are the roots of the equation

$$J_0(\beta_n) = 0$$

numbered in order of increasing magnitude, and where

$$E_n = \frac{2}{[R\,J_1(\beta_n)]^2}\int_0^R r\,g(r)\,J_0\left(\beta_n\frac{r}{R}\right)dr\,. \quad (8')$$

J_1 is the Bessel function of order one and $g(r)$ is the initial distribution as before. The first few β_n's and the corresponding values of $J_1(\beta_n)$ are listed in Table I (Jahnke and Emde, 1945: 166) along with the values of $n\pi$ for comparison (for large n_1 B_n approaches $((n - \frac{1}{4})\pi)$. Equations (11), (12), (18), and (21) become

TABLE I.—Comparison of the Coefficients in Series (9) and (9′)

n	$n\pi$	β_n	$J_1(\beta_n)$
1	3.1416	2.4048	+0.5191
2	6.2832	5.5201	—0.3403
3	9.4248	8.6537	+0.2715
4	12.5664	11.7915	—0.2325
5	15.7080	14.9309	+0.2065
6	18.8496	18.0711	—0.1877

$$K \geqq \frac{2 \cdot 4048^2 D}{R^2}, \tag{11′}$$

$$R_c = 2.4048 \sqrt{\frac{D}{K}}, \tag{12′}$$

$$N = 2\pi h \int_0^R rc\, dr = 2\pi h\, R^2 \sum_{n=1}^{\infty} J_1(\beta_n) \frac{E_n}{\beta_n} e^{k - \beta_n^2 D/R^2 t}, \tag{13′}$$

$$\lambda = \frac{D}{R^2} \frac{\sum_{n=1}^{\infty} \beta_n J_1(\beta_n)\, E_n\, e^{(\beta_1^2 - \beta_n^2) D/R^2 t}}{\sum_{n=1}^{\infty} J_1(\beta_n) \frac{E_n}{\beta_n} e^{(\beta_1^2 - \beta_n^2) D/R^2 t}}, \tag{18′}$$

$$\lambda \simeq 2 \cdot 4048^2 \frac{D}{R^2} \text{ if } t \gg \frac{R^2}{25D}, \tag{21′}$$

while equation (20) remains the same.

Solutions for other models are easily derived, but the results are essentially the same as those presented here. The numerical constants in equations (11), (12), and (21) are somewhat different in different models, but they are always of the same order of magnitude.

We conclude, therefore, that a population in a finite region can support itself against diffusion only if its reproductive rate exceeds the leakage, which is of the order of magnitude of the ratio of the diffusivity to the square of the extent of the region in the direction of most rapid diffusion.

REFERENCES

Churchill, R. V.
1941. Fourier series and boundary value problems. McGraw-Hill, Inc., New York. 206 pp.
Jahnke, E. and F. Emde
1945. Tables of functions. 4th Ed. Dover, New York. 306 pp.
Smith, F. E.
1952. Experimental methods in population dynamics, a critique. Ecology, *33* (4): 441–450.

A POSSIBLE INITIAL CONDITION FOR RED TIDES ON THE COAST OF FLORIDA

By

L. BASIL SLOBODKIN

Visiting Investigator at
Bingham Oceanographic Laboratory

ABSTRACT

It seems likely that the occurrence of a discrete mass of water, with a salinity lower than that of normal Gulf of Mexico surface water, is a necessary prerequisite for the occurrence of red tide off the Florida Coast.

On the basis of certain elementary assumptions, it has been shown by Kierstead and Slobodkin (1953) that there is a minimum critical size for a water mass physiologically suitable for the growth of a phytoplankton population which will permit an increase in the concentration of organisms. If the rate of increase of the phytoplankton is given by

$$\frac{dN}{dt} = KN, \tag{1}$$

where N is the total number of organisms in the water mass, then the size of the critical water mass is given by

$$L_c = \pi\sqrt{\frac{D}{K}} \tag{2}$$

in a linear model, where D is the rate of diffusion and L_c is the length of the water mass. For any length less than L_c, the organisms will not increase in concentration.

In a circular model the relation is given by

$$R_c = 2.4048\sqrt{\frac{D}{K}}, \tag{3}$$

where R_c is the radius of the water mass. The order of magnitude of the relation remains unchanged by geometric assumptions.

This relationship is not of particular significance if the phytoplankton species in question is tolerant of a wide range of environmental conditions, but it is important if the physiological requirements and tolerance of the species are highly specialized. The dinoflagellates

responsible for red tide outbreaks (Gunter, et al., 1948; Galtsoff, 1948; Brongersma-Sanders, 1948) are not generally amenable to normal culture techniques (personal communication from Provasoli), and *Gymnodinium brevis*, the species responsible for the 1947 outbreak on the Florida Coast (Davis, 1947) is not normally found in the marine phytoplankton of the region (personal communication from Graham). It can be assumed, therefore, that the physiological requirements of these organisms are specialized and that water masses suitable for their propagation are not common.

On *a priori* grounds it seems reasonable to consider that, if peculiar chemical properties (as yet undefined) are required for propagation of these organisms, small masses of water with the required properties will be more common than large ones. The value of K in (1) can be considered fixed at a first approximation. L will probably be small. Therefore the possibility of a plankton bloom will depend on the value of D in (2) and (3). The likelihood of a bloom will increase with decreasing values of D. D can be considered to vary as A, the coefficient of eddy diffusivity (Riley, 1951), and the conditions which promote the occurrence of a bloom can be considered as identical with those that lower the value of A.

While the precise theory of diffusivity is still unknown, it is apparent that diffusivity is reduced at the junction of water masses of different density (Ichie and Katsumi, 1949) and that it is roughly proportional to current velocity (Riley, 1951). Therefore, red tides might be expected when density differences are liable to permit the persistence of small water masses. Admixture of nonsaline water with sea water in a local area will produce a mass of low density water which may be expected to show a low mixing rate at its boundaries. Therefore, the red tides may be coastal phenomena associated with heavy land drainage. Examination of the rainfall data of the U. S. Weather Bureau during the period immediately preceding red tides on the Florida Coast confirms this expectation (Table I).

In compiling Table I, weather stations in the region of the first recorded outbreak were examined. The values shown are those of the stations with heaviest rainfall. This involves arbitrary selection of data, but in no case does the distance between the weather station and the point of initial reported outbreak preclude the possibility of a water mass moving from one to the other without losing its integrity.

On June 2, 1952 red discoloration of the sea at approximately 84° 30′ W Long. and 28° 30′ N Lat. was found by the U. S. Fish and Wildlife vessel ALASKA. This discoloration was caused by a dense population of a red ciliate, probably *Mesodinium pulex* Noland or a closely related form (Kudo, 1947). The surface salinity at a hydro-

TABLE I(a). DATE AND LOCATION OF RED TIDE OFF THE FLORIDA COAST, AND ASSOCIATED RAINFALL

Year	*Date of Initial Report*	*Location of Red Tide*	*Rainfall (inches), Month; Weather Station*
1844	Unknown (Ingersoll, 1882)	Tampa Bay	15.79, August; Tampa
1854	Unknown (Ingersoll, 1882)	Tampa Bay	15.5, July; Tampa
1878	September (Jefferson, *et al.*, 1878)	Florida Bay	9.40, August; 25.10, September; Miami
1880	August (Ingersoll, 1882)	Tampa Bay	6.40, July; 14.00, August; Tampa
1882	July 20 (Anonymous, 1882)	Mouth of Tampa Bay	5.28, June; 10.44, July; Tampa
1883	Reported by Brongersma-Sanders (1948) from Walker (1884). Reference to Walker's original paper shows that these authors refer to the same 1880 outbreak. Walker's paper was submitted for publication under date of December 21, 1880.		
1885	October (Glennan, 1886)	Egmont Key to Charlotte Harbor	10.64, September; 1.95, October; Tampa 13.68, September; Manatee
1908	Reported by Taylor (1917) as killing sponges, without any mention of dead fish. This is probably an outbreak of sponge blight rather than red tide (Smith, 1941).		
1916	October 3 (Taylor, 1917)	Boca Grande to San Carlos Bay	12.56, July; 8.22, August; 5.34, September; Fort Myers
1946*	November 20 (Gunter, *et al.*, 1948)	Naples	9.23, September; 2.03, October; 9.69, November; Naples
	In October 1946, Fort Meyers, Punta Gorda and the Everglades, Florida were flooded by unusual tides in the wake of a hurricane on October 7–8. Charlotte Harbor and part of the Everglades can be considered as having been thoroughly mixed with sea water, which drained into the Gulf of Mexico in considerable volume. November was warmer by 6.1° than any previous November on record (71.2° mean for Florida). October was 1.1° above normal and warmer than any October in five years for the state as a whole.		
1947*	March (Gunter, *et al.*, 1948)	Florida Bay	10.37, March; Captiva 8.94, March; Fort Meyers Greatest March rainfall on record for state with exception of 1930
1947*†	June 20 (Gunter, *et al.*, 1948)	Bonita Beach (South of Fort Myers)	6.47, May; 12.84, June; Fort Myers (2.69 inches fell after June 20) 3.34, May; 13.33, June; Punta Gorda (.04 inches fell after June 20)
1947*†	July 18 (Gunter, *et al.*, 1948)	Venice to Sarasota	13.06, June; 11.44, July; Sarasota (7.64 inches after July 18) 18.25, July; Punta Gorda (12.72 after July 18) Floods in Okeechobee region during June and July
1952	October 25	Boca Grande and Southwest of Sanibel	12.35, September; 8.34, October; Fort Myers (none after October 25)

* All outbreaks marked with an asterisk are considered by Gunter, *et al.* (1948) as representing a single occurrence. Since discoloration and fish mortality disappeared between each of the listed dates, they are here considered as separate.

† The interval with no fish kills separating these two outbreaks is of the order of two weeks and may or may not indicate separate dinoflagellate populations.

TABLE I(b). Mean Rainfall (inches) by Months at Five Florida Weather Stations

	J	*F*	*M*	*A*	*M*	*J*	*J*	*A*	*S*	*O*	*N*	*D*	*Years*
Belle Glade	1.68	1.48	2.70	2.33	3.60	9.01	6.90	8.06	7.41	4.84	2.90	1.32	1924–1951
Fort Myers	1.76	2.02	1.89	1.89	4.13	8.91	8.16	8.82	7.45	4.48	1.33	1.56	1851–1951
Miami	2.27	2.03	2.63	3.41	7.15	7.07	5.60	5.88	8.65	7.74	3.26	1.98	1855–1951
Punta Gorda	2.24	1.83	2.21	2.20	3.61	7.48	7.54	8.05	8.22	3.97	1.56	1.85	1914–1951
Tampa	2.69	2.56	2.33	2.01	2.99	7.25	7.95	8.18	6.42	3.19	1.72	2.07	1840–1951

graphic station in the discolored water (33.4‰) was lower than that at surrounding stations (34.99, 35.47, 36.17). This would seem to confirm the theory in so far as protista in general are concerned, since the discolored water was approximately 90 miles from the nearest coast.

On the basis of this evidence it can be stated tentatively that red tides require a discrete mass of water of relatively low salinity, but this does not imply that salinity difference is the sole requirement for red tides. The water mass must also satisfy the other physiological requirements of dinoflagellates. It does seem likely, however, that in any newly isolated mass of sea water the nutrient and other requirements of at least one of the algal or protozoan species in the mass will be met and will result in a temporary bloom.

The possible connection between heavy rainfall and fish mortality has been noted by Aggasiz (1890) and by Webb (1886) in their studies of fish mortality on the Florida Coast. Braarud (1951) has found that *Prorocentrum micans*, *Peridinium trochoideum* and *Amphidinium* sp. show maximal reproductive rate at 15–20 ‰ salinity. The salinity optimum for *Exuviaella baltica* is 10 ‰. In July 1952, Riley found a salinity of 24.9–22.7 ‰ in a bloom of *Gonyaulax* sp. in Long Island Sound off New Haven, Connecticut (personal communication from Riley). Ketchum and Keen (1948) have reported a salinity of 33‰ in the 1947 Gulf of Mexico outbreak, which is well below the salinity of normal Gulf of Mexico water (36 ‰).

These reports indicate that the salinity requirements of at least some dinoflagellates are such that a mass of water in the Gulf of Mexico stabilized by low salinity will be physiologically suitable for growth and reproduction. There is some indication that amino acids and vitamins are part of the nutritional requirements of dinoflagellates (personal communication from Provasoli). The possible presence of these compounds in fresh water is indicated by the work of Hutchinson and Setlow (1946).

The excessively high values of total phosphate found in the 1947 outbreak on the Florida Coast can be adequately explained on the hypothesis of Ketchum and Keen (1948), who stated that the excess phosphate "may be the result of terrigenous contamination . . . or may be the result of active swarming of organisms." Both of these

Figure 1. MAP OF SOUTHERN FLORIDA, SHOWING LOCATIONS MENTIONED IN TEXT. 1. Boca Grande, 2. Charlotte Harbor, 3. Egmont Key, 4. Lake Okeechobee, 5. San Carlos Bay, 6. Sanibel Island, 7. Tampa Bay.

TABLE II. Vertical Distribution of *Gonyaulax monilata* During a Red Tide on the East Coast of Florida. Stations *d* and *e* Were not Red but Were in the Same Water Mass as Stations *a*, *b* and *c*.

	Depth (feet)	Millions of *G. monilata*/liter
Red Water Stations		
a	0.5	3.60
	1.5	2.15
	2.6	.90
b	0.7	4.60
	1.2	1.00
c	0	8.20
	1	5.70
	1.5	1.45
	8	.45
Non-red Stations		
d	0.5	.80
	2.0	.17
	5.0	1.19
	8	.94
	9.5	.73
e	0.5	.57
	1.5	.46
	3.3	.07

alternatives are almost certainly true. Samples taken during an outbreak of *Gonyaulax monilata* (Howell, 1953) at Melbourne, Florida in August 1951 showed striking vertical stratification in shallow water (Table II). This outbreak occurred in the inland water way (Indian and Banana rivers). The stations indicated as "not red" were located as close as possible to the edge of discolored areas. It is apparent that a vertical concentration of 10 times in total P by diurnal migration of the organisms is possible.

Conclusions—It is considered likely that red tide outbreaks are initiated by the occurrence of discrete masses of water which differ in salinity and chemical characteristics from the normal water of the Florida Coast. The abnormal nutrient concentrations found in 1947 can be explained on the basis of vertical stratification of the organisms. Upwelling or other purely marine phenomena are superfluous assumptions. Once the nutritional requirements of the dinoflagellates are satisfied, the limiting condition for a bloom is the rate of diffusion of the physiologically suitable water mass. Prediction of red tides will depend on intimate knowledge of coastal drainage and hydrography. Prevention of most red tides may be possible by altering the drainage pattern of the Charlotte Harbor—Calloosahatchee estuary region.

REFERENCES

Agassiz, Alexander

1890. Note on Shaler, 1890. Bull. Mus. comp. Zool. Harv., *16:* 157–158.

Anonymous

1882. Article in Sunland Tribune, Tampa, Florida. Bull. U. S. Fish Comm., *2:* 104.

Braarud, Trygve

1951. Salinity as an ecological factor in marine phytoplankton. Physiol. Plant., *4:* 28–34.

Brongersma-Sanders, M.

1948. The importance of upwelling water to vertebrate paleontology and oil geology. Verh. Akad. Wet. Amst., Afd. Natuurkunde, Tweedie Sect., *45* (4): 112 pp.

Davis, C. C.

1947. *Gymnodinium brevis* n. sp., a cause of discolored water and animal mortality in the Gulf of Mexico. Bot. Gaz., *109:* 358–360.

Galtsoff, P. S.

1948. Red tide. Spec. Sci. Rep. U. S. Fish and Wildl. Serv., No. 46: 44 pp.

Gunter, G., R. H. Williams, C. C. Davis and F. G. W. Smith

1948. Catastrophic mass mortality of marine animals and coincident phytoplankton bloom on the west coast of Florida, November 1946 to August 1947. Ecol. Monogr., *18:* 309–324.

Glennan, A. H.

1886. Fish killed by poisonous water. Bull. U. S. Fish Comm., *6:* 10–11.

Howell, J.

1953. *Gonyaulax monilata,* sp. nov., the causative dinoflagellate of a red tide on the east coast of Florida in August-September, 1951. Trans. Amer. micr. Soc. (in press).

Hutchinson, G. E. and Jane Setlow

1946. Limnological studies in Connecticut. VIII. The niacin cycle in a small inland lake. Ecology, *27:* 13–22.

Ichie, T. and T. Katsumi

1949. On the report of observations of the hydrographical conditions in the Osaka Wan after the heavy rain caused by the typhoon "Della." Pap. Rep. in Oceanography, Kobe Marine Observ., No. 3.

Ingersoll, E.

1882. On the fish mortality in the Gulf of Mexico. Proc. U. S. nat. Mus., *4:* 74–80.

Jefferson, J. P., J. Porter and T. Moore

1878. On the destruction of fish in the vicinity of the Tortugas during the months of September and October, 1878. Proc. U. S. nat. Mus., *1:* 244–245.

Ketchum, B. H. and Jean Keen

1948. Unusual phosphorus concentrations in the Florida "red tide" sea water. J. mar. Res., *7:* 17–21.

Kierstead, Henry and L. B. Slobodkin

1953. The size of water masses containing plankton blooms. J. mar. Res., *12* (1): 141–147.

KUDO, R. R.
1947. Protozoology. 3rd ed., Charles C. Thomas, Springfield, Illinois. 778 pp.
RILEY, G. A.
1951. Parameters of turbulence in the sea. J. mar. Res., *10:* 247–256.
SMITH, F. G. W.
1941. Sponge disease in British Honduras and its transmission by water currents. Ecology, *22:* 415–421.
TAYLOR, H. F.
1917. Mortality of fishes on the west coast of Florida. Rep. Comm. Fish. (1917). Append. 3, 24 pp.
WALKER, S. T.
1884. Fish mortality in the Gulf of Mexico. Proc. U. S. nat. Mus., *6:* 105–109.
WEBB, J. G.
1886. The mortality of fish in the Gulf of Mexico. Bull. U. S. Fish Comm., *6:* 11–13.